การวิเคราะห์เสถียรภาพชั่วครู่โดยคำนึงถึงพารามิเตอร์ที่มีนัยสำคัญ ด้วยระบบอนุมานฟัซซี่โครงข่ายปรับตัวได้

TRANSIENT STABILITY ASSESSMENT CONSIDERING SIGNIFICANT PARAMATERS USING AN ADAPTIVE NEURO-FUZZY INFERENCE SYSTEM

วิศว ภู่ตระกรณ์ชัย
WITSAWA PHOOTRAKORNCHAI

วิทยานิพนธ์นี้เป็นส่วนหนึ่งของการศึกษาตามหลักสูตรปริญญาวิศวกรรมศาสตรดุษฎีบัณฑิต
สาขาวิชาวิศวกรรมไฟฟ้า
คณะวิศวกรรมศาสตร์
สถาบันเทคโนโลยีพระจอมเกล้าเจ้าคุณทหารลาดกระบัง
พ.ศ.2561

KMITL-2018-EN-D-018-115

การวิเคราะห์เสถียรภาพชั่วครู่โดยคำนึงถึงพารามิเตอร์ที่มีนัยสำคัญ ด้วยระบบอนุมานฟัซซี่โครงข่ายปรับตัวได้

TRANSIENT STABILITY ASSESSMENT CONSIDERING SIGNIFICANT PARAMATERS USING AN ADAPTIVE NEURO-FUZZY INFERENCE SYSTEM

วิศว ภู่ตระกรณ์ชัย

WITSAWA PHOOTRAKORNCHAI

วิทยานิพนธ์นี้เป็นส่วนหนึ่งของการศึกษาตามหลักสูตรปริญญาวิศวกรรมศาสตรดุษฎีบัณฑิต

สาขาวิชาวิศวกรรมไฟฟ้า

คณะวิศวกรรมศาสตร์

สถาบันเทคโนโลยีพระจอมเกล้าเจ้าคุณทหารลาดกระบัง

พ.ศ.2561

KMITL-2018-EN-D-018-115

TRANSIENT STABILITY ASSESSMENT CONSIDERING SIGNIFICANT PARAMATERS USING AN ADAPTIVE NEURO-FUZZY INFERENCE SYSTEM

WITSAWA PHOOTRAKORNCHAI

A THESIS SUBMITTED IN PARTIAL FULFILLMENT
OF THE REQUIREMENT FOR THE DEGREE OF
DOCTOR OF ENGINEERING IN ELECTRICAL ENGINEERING
FACULTY OF ENGINEERING
KING MONGKUT'S INSTITUTE OF TECHNOLOGY LADKRABANG
2018

KMITL-2018-EN-D-018-115

THESIS CERTIFICATION
FACULTY OF ENGINEERING
KING MONGKUT'S INSTITUTE OF TECHNOLOGY LADKRABANG

Thesis Title Transient Stability Assessment Considering Significant Parameters using an Adaptive Neuro-fuzzy Inference System
Student Mr. Witsawa Phootrakornchai
Student Id. 55610125
Degree Doctor of Engineering
Program Electrical Engineering
Thesis Advisor Assoc. Prof. Dr. Somchat Jiriwibhakorn
Thesis Reference Number KMITL-2018-EN-D-018-115

EXAMINERS		SIGNATURES
Asst. Prof. Dr. Parnjit	Damrongkulkamjorn	
Asst. Prof. Dr. Nirudh	Jirasuwankul	
Asst. Prof. Dr. Worawat	Nakhaviro	
Dr. Watchara	Chatwiriya	
Assoc. Prof. Dr. Somchat	Jiriwibhakorn	Somchat Jiriwibhakorn

Date 20th July 2018 **Time** 10:00 am – 12:00 pm
Place His Majesty the King's 7th Cycle Birthday Anniversary Building, HM-302

(Assoc. Prof. Dr. Komsan Maleesee)
Dean, Faculty of Engineering
20th July 2018

หัวข้อวิทยานิพนธ์	การวิเคราะห์เสถียรภาพชั่วครู่โดยคำนึงถึงพารามิเตอร์ที่มีนัยสำคัญด้วยระบบอนุมานฟัซซี่โครงข่ายปรับตัวได้
นักศึกษา	นายวิศว ภู่ตระกรณ์ชัย
รหัสประจำตัว	55610125
ปริญญา	วิศวกรรมศาสตรดุษฎีบัณฑิต
สาขาวิชา	วิศวกรรมไฟฟ้า
พ.ศ.	2561
อาจารย์ที่ปรึกษาวิทยานิพนธ์	รศ.ดร.สมชาติ จิริวิภากร

บทคัดย่อ

การประเมินเสถียรภาพชั่วครู่ของระบบไฟฟ้ากำลังโดยทั่วไป พารามิเตอร์พลวัตส่วนใหญ่ของระบบจะถูกละทิ้ง เนื่องจากมีความซับซ้อนและใช้ระยะเวลาในการคำนวณค่อนข้างนาน และยิ่งระบบที่มีขนาดใหญ่ ไม่ใช่เรื่องที่ง่ายที่จะพิจารณาเสถียรภาพชั่วครู่ในลักษณะ Real Time โดยคำนึงถึงพารามิเตอร์พลวัตสำคัญทั้งหมด วิทยานิพนธ์นี้จึงได้มีการค้นคว้าวิธีการต่างๆ เพื่อเพิ่มประสิทธิภาพในด้านความแม่นยำและระยะเวลาที่ใช้ในการคำนวณ โดยงานวิจัยนี้ได้นำเสนอระบบอนุมานนิวโรฟัซซีแบบปรับตัวได้ (Adaptive Neuro Fuzzy Inference System: ANFIS) สำหรับการประเมินเสถียรภาพชั่วครู่ โดยแบบจำลองที่ใช้จะเป็นแบบจำลองแบบละเอียด (Detailed Model) ไม่เพียงแต่พารามิเตอร์พลวัตของเครื่องกำเนิดไฟฟ้าซิงโครนัส (Machine Model) ที่จะนำมาพิจารณา แต่พารามิเตอร์ของระบบควบคุมกังหัน เชื้อเพลิงและความถี่ (Governor) ระบบควบคุมแรงดันอัตโนมัติ (Automatic Voltage Regulator: AVR) และคุณลักษณะเฉพาะของโหลด (Load Characteristic) ก็จะถูกนำมาพิจารณาอย่างละเอียดด้วยเช่นกัน นอกจากนี้เพื่อให้สอดคล้องกับความเป็นจริง แบบจำลองของเครื่องจักรและระบบควบคุมของแต่ละบัสจะมีหลากหลายแบบจำลองซึ่งจะทำให้สมการทางคณิตศาสตร์ซับซ้อนยิ่งขึ้น จุดลัดวงจรในระบบก็จะจำลองหลายๆ ตำแหน่ง ปริมาณโหลดในระบบทดสอบจะปรับเปลี่ยนในแต่ละการจำลองเพื่อให้ครอบคลุมทุกๆ กรณี โดยการประเมินเสถียรภาพชั่วครู่ดังกล่าวจะใช้ค่าช่วงเวลาตัดกระแสวิกฤต (Critical Clearing Time: CCT) มาพิจารณา ระบบที่ใช้ในการทดสอบจะประยุกต์มาจากระบบ IEEE 9 บัส และระบบ IEEE 39 บัส ซึ่งท้ายที่สุดจะเห็นว่าการประเมินเสถียรภาพชั่วครู่โดยคำนึงถึงพารามิเตอร์สำคัญของเครื่องกำเนิดไฟฟ้าซิงโครนัส ระบบควบคุมกังหัน เชื้อเพลิงและความถี่ ระบบควบคุมแรงดันอัตโนมัติ และคุณลักษณะเฉพาะของโหลด ด้วยระบบอนุมานนิวโรฟัซซีแบบปรับตัวได้ เป็นอีกวิธีหนึ่งที่มีประสิทธิผลทั้งด้านความแม่นยำและระยะเวลาในการคำนวณ สามารถนำไปประยุกต์ใช้และพัฒนาต่อได้

Thesis Title	Transient Stability Assessment Considering Significant Parameters Using an Adaptive Neuro-fuzzy Inference System
Student	Mr. Witsawa Phootrakornchai
Student ID.	55610125
Degree	Doctor of Engineering
Program	Electrical Engineering
Year	2018
Thesis Advisor	Assoc. Prof. Dr. Somchat Jiriwibhakorn

ABSTRACT

Normally in power systems, a number of dynamic parameters are ignored for conventional transient stability assessment due to complex equations and a lot of time for computation. Certainly, it is not easy to do the real-time assessment of transient stability of a large power system by considering dynamic impacts in detail. This thesis therefore tries to find any approach to minimize the calculation time and optimize the accuracy of result. Herein, a method, namely an adaptive neuro-fuzzy inference system (ANFIS), is found to overcome the limitation. All significant effects of dynamics can been taken into account; not only the machine model but also the turbine governor model, automatic voltage regulator (AVR) model, and load characteristic are carefully used for transient stability prediction. In addition, the model used for each generation unit is varied in order to be realistic. The assessment of transient stability in this research is evaluated by the means of critical clearing time. The modified IEEE 9-bus system and IEEE 39-bus system are used for the implementation of this study. The locations of fault and loads are varied for each simulation. Eventually, the results of ANFIS can indicate that the application of ANFIS in transient stability prediction considering all significant dynamic effects from machine model, automatic voltage regulator system, turbine governor, and load characteristic is accurate and takes lower computational time. It can be improved and implemented in the real practice.

ACKNOWLEDGEMENT

I would like to thank my advisor, Assoc. Prof. Dr. Somchat Jiriwibhakorn, for the teaching, encouraging, and guiding he has provided throughout my time. Also I would like to thank other teachers and members of King Mongkut's Institute of Technology Ladkrabang who helped, commented, and advised me.

I must express my gratitude to my father, mother, older sister, younger sister, all of my family including my girlfriend for their encouragement, continued support, and love. Certainly, I have today because them. They are everything in my life.

Completion of this research would be more difficult if there were not any supports, experiences, and friendships from my colleagues at B.Grimm Power Public Company Limited, colleagues at ex-companies, my friends and teachers at NIDA, Mahidol University, Bodindecha (Sing Singhaseni) School, Pensmith School, and my friends who are not specified herein.

Finally, I would like to also thank the research fund from Thailand Research Fund (TRF) under the contract no. IRG5780006 and the fund from King Mongkut's Institute of Technology Ladkrabang of the year 2013-2014 for the fund supports.

Witsawa Phootrakornchai

TABLE OF CONTENTS

TABLE OF CONTENTS (CONTINUED)

TABLE OF CONTENTS (CONTINUED)

LIST OF TABLES

LIST OF FIGURES

LIST OF FIGURES (CONTINUED)

Page

CHAPTER 1

INTRODUCTION

1.1 STATEMENT AND SIGNIFICANCE OF THE PROBLEMS

A small disturbance in the power system (i.e., an immediate change in load, short circuit, or loss of generation units) can affect the change in equilibrium in the machine and consequently take an effect of the deviation of voltage, current, frequency, and shaft torque of generator. They can be a cause of the system becoming unstable finally. In the high security of a power system, it should be able to withstand any sudden disturbance and to maintain the system while being disturbed and after the disturbance is over.

The improvement of system enhancement and stability assessment is more interested for researchers. We normally use the critical clearing time (CCT) to be an indicator for the assessment of transient stability. It can indicate how long the system can withstand a disturbance in the system without any instability. There are many constraints and operating conditions when operating the power system. Any configuration of power system always changes. Any results of transient stability study (i.e., CCT), that is done, may not be reliable for the real operation. The study needs to be repeated all the time to have enough ability to control and prevent the power system in case any immediate disturbance happens.

The means used for assessing the CCT conventionally is based on the classical model; most dynamics of a power system (i.e., machine model, excitation system, governor, and load model) are ignored [1, 2]. But in fact, there are many electronic control devices erected in the system for controlling the power system stabilizer (e.g., automatic voltage regulator (AVR) and governor) [3, 4]. If an accurate result is required, the effect of the electronic control device, machine, and loads are to be considered. The dynamic behavior of a power system (i.e., voltage, current, frequency, and rotor angle) after faults is more difficult to be calculated. The evaluation of real-time transient stability is more challenging, as the system is going to be more complex and larger stability [5, 6, 7, 8, 9, 10, 11, 12, 13, 14]. There have been a lot of journals describing various approaches to apply with the assessment of transient [15, 16].

1.2 GOAL AND OBJECTIVE

The focus of this study is we can in real-time evaluate the transient stability with an acceptable accurate result. All the significant effects of dynamics in the system are considered [17, 18, 19, 20, 21]; not only the machine model but also the turbine governor model, AVR model, and load characteristic are taken into account carefully for the CCT estimation.

1.3 HYPOTHESIS TO BE TESTED

The (ANFIS) which is an algorithm applied from NNs and fuzzy logic principles effectively implemented for the real-time estimation of CCT. The estimated CCT by ANFIS proposed in this paper can be real-time computed or the calculation time is within acceptable criteria. Values of all loads in a system can be transferred to ANFIS by a Supervisory control and data acquisition (SCADA) system for the CCT estimation. When any fault occurs in a system, protection relays can be calculating the real-time CCT obtained from ANFIS for an on-line setting of its delay time to avoid any inefficient tripping. The ANFIS results can show that the ANFIS application in CCT prediction by considering effects of all significant dynamic from the machine model, turbine governor, AVR system, and load characteristic is much accurate and significantly takes lower computational time.

1.4 SCOPE OR LIMITATION OF THE STUDY

In this study, the modified IEEE 9-bus or IEEE 9-bus Western System Coordinating Council (WSCC) and Institute of Electrical and Electronics Engineers (IEEE) 39-bus systems are applied for implementation. We simulate the various governor models and AVR models in each system to reflect the realistic practice. The time domain method is used for the simulation in order to get the training and testing data for the ANFIS inputs and outputs. The AVR and governor models simulated in each generation unit of each bus are varied. Fault locations and load levels and are varied for testing.

1.5 PROCESS OF THE STUDY

This thesis is organized as follows: The transient stability principle is shown in Section 2. Section 3 describes the mathematical model used for the simulation. The ANFIS principle is explained in Section 4. Section 5 explains how to simulate the system and implement the ANFIS and results. Section 6 presents conclusion and suggestion of the research.

CHAPTER 2

LITERATURE REVIEW

There have been a number of papers and researches proposing new models and techniques used for the transient stability evaluation. Some researches focused on a decrease in the evaluating computational time to improve the on-line protective devices and other implementations. Some researches focused on modelling and dynamic parameters affecting the accuracy of results to improve the off-line analysis and simulation.

In 1994 [22], Hokuriku Electrical Power Co, Ltd. and Toshiba Corporation Co., Ltd. had proposed an approach to achieve real-time calculation of transient stability through their developed software called Operator Training Simulator (OTS). The conventional approach was used with the algebraic partitioned methods through a multiprocessor to decrease the calculation time. Their computer 'TOSBAC-G8090 Model' was used for their power system simulation system. Up to four processors were supported by the computer. Each processor provided up to 10 MIPS of computing power. With a maximum of 4 processors, the computer system delivered 31 MIPS of computing power. The power system simulation system consisted of 2 computer systems. One computer with 4 processors was applied as a transient stability analysis computer. These processors performed the transient stability analysis in parallel. Another computer with 2 processors was applied as the training control computer. They used a system having 387 Nodes with 60 Generators for their test, they achieved the computational time of transient stability analysis within 1.501 seconds through their parallel processing performed with multiprocessor. However, in their study, some dynamic parameters (e.g., parameters of individual generators and controller having small time constant) needed to be ignored to allow the real-time calculation. Their techniques proposed was applied to the training scenarios for their operators by automatically simulating the actions of power system stabilizing equipment and protective relays.

IN 1997 [23], R.S. Kuruneru and A. Bose had advised that the existing Operator Training Simulator software used for transient analysis at that time did not work, although the first steady state values at the first simulation cycle after the disturbance

were initiated with the corresponding solution obtained with an offline transient stability assessment (TSA) but the trajectories afterwards do not follow properly. The effect of the fault persists for many simulation cycles for some disturbances. The error was much more significant if the fault scenario disturbs the system with larger generator swings over longer times. The Operator Training Simulator without transient stability assessment failed to simulate the correct dynamics that might affect relay operations and operator intervention further during the post disturbance period. It was suspected but probably not as clearly demonstrated as in their tests as follows.

- The transient stability assessment with the Operator Training Simulator on a system gives very promising CPU timing results. The CPU time can be reduced by choosing a larger transient time step without significantly affecting the accuracy. The main factors that determine feasibility were computer performance and power system size.
- There were various different factors to be considered to predict the performance with different computers such as CPU clock speed, type of processor, data throughput, cache memory, compiler technology, etc. It was somewhat difficult to predict the CPU time performances of the OTS with TSA on different computers because of all the above as well as the complexity and size of the Operator Training Simulator software.
- CPU time increases with the size of the power system simulated. The rate of increase of CPU time with the model size was also hard to predict because it depends on the models used for the generators and power plants, the sparsity of the network, and many other physical properties of the system. However, the network solution does take up the bulk of the solution time and so there was a close relationship to the number of buses and CPU times.
- The Operator Training Simulator based on real time transient stability analysis was feasible. Even if very large power systems cannot be simulated yet on control centre computers, the workstations available within a couple of years will be able to handle systems of 1500 to 2000 buses. Much of the

detailed modelling from transient stability studies were ignored in the feasibility study but will need to be incorporated in a production grade Operator Training Simulator.

In 1997 [24], a distributed computing approach had been proposed for real-time transient stability analysis with some detailed model. The public domain Parallel Virtual Machine (PVM) was adopted for implementing the proposed algorithms. The feasibility of real-time transient stability was studied exploiting both domain and functional decompositions, on a homogeneous cluster of eight DEC ALPHA and on an IBM SP2 machine. They tested the functional decomposition with the shifted-picard algorithm under PVM, whereas a scaled domain decomposition was tested running multiple contingencies on different nodes of cluster systems, using the Very Dishonest Newton algorithm (VDNH). The performance of the approaches was assessed through time domain simulations on a realistic-sized network comprising 2,583 buses with 511 generators. However, the tests allowed a fine tuning of the communication model involved in the algorithm. They argued that the bus contention and regular and symmetric communication patterns involved in loosely synchronous algorithms were the main sources of inefficiencies when cluster environments were used. They could achieve the real-time contingency analysis of transient stability analyses on an 8 node IBM SP2 and DEC-ALPHA cluster within 120 seconds and 253 seconds respectively.

In 1999 [25], a novel two-layer fuzzy hyperrectangular composite neural network (FHRCNN) had been proposed for a new method for real-time transient stability prediction using synchronized phasor measurements subject to the generator was modeled by seventh-order differential equations and the loads were modeled as constant impedances. The FHRCNN was a type of classifier that can be constructed off-line from a training set of examples. The FHRCNN was used to classify a transient swing as either stable or unstable on the basis of synchronized phasor measurements. Their simulations were carried out off-line extensively all the time in order to capture the essential features of system behavior. The network building process statistically analyzes this data and constructs a FHRCNN designed to correctly classify new unseen examples. Their simulation programs were developed on a SUN-SPARC II in C++. In their study, they also conducted simulation results on traditional feedforward neural network (FNN) with the same neurons, training set, and test set to compare the results.

The proposed FHRCNN and FNN were trained on the training set using 61 neurous. Their paper says it took a few hundredths of a second to predict the swings in the first second after clearing time for both networks. The FHRCNN has a pretty high classification rate. The FHRCNN has a better performance than traditional FNN. The FHRCNN has the potential to be an on-line tool for real-time transient stability prediction in power systems.

In 2000 [26], Vijay V. studied and advised a detailed description of issues that will impact transient stability analysis and small-signal stability analysis in the restructured utility environment. Several important aspects related to maintaining the reliability and security of the bulk electric systems had been identified and analyzed in his paper as follows.

- Incorporate risk and contingency cases in the analysis for extreme events.
- System size and complexity due to the economy transfers.
- Constraint of complex transfer limits.
- Enormous burden of conceptualizing, building, and maintaining database.
- Stringent requirement of validating model data with measured data.
- Accurate forecast of customer demand.
- Comprehensive incorporation of protective and control systems in studies.
- FACTS elements modeling
- Coordinated protective and control system design
- Coordinated system restoration plans.
- Verifying and validate simulation models.
- Fast techniques to analyze stability.

In 2006 [27], an artificial neural network (ANN) based method for on-line transient stability assessment of power systems had been presented. The proposed methodology was based on an accurate and efficient ANN-based method that allows convenient identification of the system stability. Their output from the ANN is transient stability index to be a robust indicator for an on-line transient stability assessment. Two feature selection methods had been proposed in their study and used for the selection of optimal set of neural network training features. Principal component analysis was used to reduce the selected set of features. Some operating conditions,

ranging from unstressed to very stressed network conditions had been analyzed in their study as well. The correct prediction of transient stability index was obtained for previously unseen cases. They applied with the 39-bus system and the test results were promising. Their study shows that the proposed feature selection algorithm could be seen as an efficient method to cope with the problem of high dimensionality in the design of neural networks and the results obtained indicate the potential of ANN for on-line power system dynamic security assessment. However, they did not show how many seconds the analysis by ANN used for the transient stability prediction.

In 2007 [28], the adequacy of using static load models for transient stability analysis was examined. Model parameters of five static nonlinear load models were derived with multiple sets of on-line measurements, and their performances in modelling real and reactive power behaviours were compared. They summarized their study with respect to the importance of load modelling into five points as follows:

- Static nonlinear load models can be developed to approximate the dynamic behaviors of real power. Hence, static load models can be suitable for transient stability analysis; this development of static load models, however, requires accurate parameter estimation based on multiple measurement data.
- For modelling real power behavior, all five static models under study give similar relative errors. The exponential load model was very promising since it gives reliable and consistently accurate solutions and only had two parameters to be estimated.
- In modelling real power behaviors, third-order induction motor load model gives the most accurate result, first-order induction motor load model and exponential model take the second and third places and the ZIP model give a very slightly worse result. However, the difference of the relative errors between third-order induction motor load model and ZIP model was very small, less than 0.25%.
- In modelling real power behaviors, induction motor load model, does not give much more accurate results than ZIP model and exponential model.

Since transient stability analysis was mainly concerned with real power behaviors of load during and after a disturbance, appropriate static load models were adequate for transient stability analysis.

- Adopting dynamic load models in transient stability analysis increases system dimension and can signifi cantly require computing effort for power system dynamic simulation. This may limit the application of dynamic load models in situations where computation speed was critical.

In 2007 [29], there had been the study regarding the transient stability of wind turbine generator systems analyzed using the six-mass, three-mass and two-mass drive train models for severe network disturbance in two different types of power system models. A detailed transformation methodology from the six-mass to two-mass drive train models was presented in their paper, they can be used in the simulation analysis with reasonable accuracy. By using the transformation procedure, the inertia constants, spring constants, self-dampings of individual masses and mutual-dampings of adjacent masses of the six-mass drive train model can be converted to reduced order models. The effects of drive train parameters such as inertia constants, spring constants and damping constants were examined for the above mentioned three-types of drive train models. Also, the different types of symmetrical and asymmetrical faults were analyzed at different power levels of IG, with or without considering damping constants of six-mass, three-mass and two-mass models. Considering all the simulation results, They concluded in their paper that the wind turbine generator systems can be expressed by the simple two-mass shaft model with reasonable accuracy and that this model was suitable for the transient stability analysis of grid connected wind turbine generator systems.

In 2009 [30], a fuzzy logic-controlled superconducting magnetic energy storage for the enhancement of transient stability in a multi-machine power system had been presented. The control scheme of SMES was based on a pulse width modulation (PWM) voltage source converter (VSC) and a two-quadrant DC–DC chopper using gate-turn-off (GTO) thyristor. Total kinetic energy deviation (TKED) of the synchronous generators was used as the fuzzy input for SMES control. Communication delays introduced in online calculation of the TKED were considered for the actual analysis

of transient stability. Global positioning system (GPS) was proposed for the practical implementation of the calculation of the TKED. Simulation results of balanced fault at different points in a multi-machine power system are shown in their paper that the fuzzy logic-controlled SMES could be an effective device for transient stability enhancement of multi-machine power system.

In 2011 [31], there had been a presentation regarding an artificial neural network controlled superconducting magnetic energy storage (SMES) unit for improvement of transient stability of a power system under various system operating conditions and different fault conditions. The superconducting magnetic energy storage had the capability of storing energy and the stored energy can be supplied or received by controlling the firing angles of the converters of SMES. It can be charged or discharged very rapidly and had flexible control, it can be made use of for power system stabilization. The effectiveness of SMES on power system stabilization depends on its proper control strategy. Power system transient stability being a nonlinear, it was necessary to determine disturbance dependent control. Furthermore, since the nonlinear control was a function of time its on-line realization was problematic. The inputs to the ANN controller were the deviation in rotor angular velocity of the machine connected to faulted-bus and the voltage deviation of the faulted bus and were used for estimating the control variables, the active power, and the reactive power. The teaching data for the learning process of artificial neural network (ANN) may be obtained from the results obtained during transient stability investigations in the presence of proportional type control of SMES (P-SMES) for various initial operating states and different fault conditions of a power system. The system under consideration was single machine connected to infinite bus system and SMES was assumed to be installed at the generator terminal. The set of system variables and the control variables estimated active power and reactive power were made use for the development of ANN control. The results of investigations carried out regarding effectiveness of ANN controlled superconducting magnetic energy storage in improving transient stability of a critically stable two-machine system were compared with proportional type control of superconducting magnetic energy storage.

In 2011 [32], a basic modeling and computational methods of power system dynamic devices for transient stability analysis had been presented. Nonlinear mathematical models of synchronous machine, turbine-governor and exciter system

were successfully modeled using Dynamic Computation for Power Systems (DCPS) software package. The transient stability analysis of IEEE 9-bus test system by using this software had also been presented. The transient stability analysis was carried out to test the response of these devices when subjected to three phase fault at a bus of IEEE 9-bus test system. From this analysis, the fault critical clearing time had been determined. The system will become unstable if the fault clearing time exceeds the critical clearing time limit. It also showed that, the critical clearing time was decreases linearly with increasing load demand. However, the system used for implementation was small to concluded that the decrease in the critical clearing time was linear with the load increase.

In 2011 [33], there has been a simulation of transient stability analysis on Sarawak's Grid data system. The response of transient stability was observed using PSS/E simulation package, based on machine's rotor angle, terminal voltage, speed and also electrical power. Sarawak's Grid data was used to clarify the theory said that the line far from a major generator held a longer critical clearing time (CCT). The study needs tp prove the different result for the same three-phase fault at two different transmission lines; one nearer the generator and another far from the generator but within the same area. The results showed that critical clearing time near the generator was less than the critical clearing time far from the generator.

In 2011 [34], there has been a development of a procedure for multi-machine electrical power systems transient stability analysis using Euclidean ARTMAP neural network. Results were obtained considering an electrical power system corresponding to the south Brazilian region composed of 45 buses with 10 generators. The input stimuli of the neural network were the active and reactive power vectors and data corresponding to the contingencies and configuration of the system. The outputs were the security margins of the system represented by intervals between the maximum and the minimum values. Thus, it was possible to represent the outputs in binary code. The training was executed considering five contingencies (three-phase short-circuit with outage of a transmission line) and three possible configurations of the system. This procedure allows considering several topologies of the electrical network, which was a new proposal not yet, available on the literature. The contingencies were arbitrated as incidents in several points of the electrical network (5 places). Loading levels were randomly arbitrated considering a universe between 80 and 130% of the total load of

the system. For the prediction phase, a scheme that includes new patterns to the memory of the neural network was implemented, thus improving the definition region of the recognition categories and consequently the precision of the results. The obtained results were satisfactory, i.e., the proposed objectives were attained, which were to investigate the application of neural networks for executing diagnosis of electrical power systems transient stability. The Euclidean ARTMAP neural network provides very fast solutions (<1 second with a Pentium IV of 1.8 MHz microcomputer, considering the votation strategy with five repetition training). The solution quality was considered adequate. Concluding, the Euclidean ARTMAP neural network gives very fast answers (there was compatibility with applications on line) and the precision was dependent of implementing an adequate training scheme, with a very well elaborated quantity of input/output data (sufficient quantity and quality). The principal reference of the ARTMAP neural network was the characteristics of plasticity. This property allows conceiving mechanisms that include the continuous training (training reinforcement) without destructing the knowledge extracted previously (in most of the neural networks existent on the specialized literature the training reinforcement needs to reinitialize the process destructing the knowledge previously acquired). Therefore, the neural network was continuously improving the performance to provide more precise solutions according to what was described earlier. The proposed neural network would have a precision increment when the continuous training was intensified. This was the principal proposal of this paper, i.e., a neural network proposal that achieves the improvement as the time passes, including new topologies of the electrical network. From their analysis effectuated considering the topologies provided, the neural network will search the improvement, incremental knowledge acquisition, without overspending the computational costs. Their analysis had computational time compatible for applications in real-time.

In 2011 [35], a methodology for estimating a normalized power system transient stability margin using multi-layered perceptron (MLP) neural network with a fast training approach had been proposed. The nonlinear mapping relation between the normalized power system transient stability margin and operating conditions of the power system was established using the MLP neural network. The potential energy boundary surface method along with a time-domain simulation technique was used to obtain the training set of the neural network. The main objective of the present

investigation was to propose an MLP neural network based approach for online transient stability analysis through estimation of a normalized transient stability margin. The main idea was that for a particular fault scenario, the normalized transient stability margin was a function of only pre-fault system operating point, which can be adequately characterized by a proper set of readily measurable operating conditions (features) in the pre-fault situations. Therefore, an MLP neural network, which was well-known for its universal approximation capabilities, can be employed to approximate the function. Furthermore, based on the examination of generators rotor angles after faults, a method was presented to select the power system operating conditions that most effect the normalized transient stability margin for each fault. This method had been used to reduce the required numbers of features for normalized transient stability margin estimation. The potential energy boundary surface (PEBS) method proposed by Kakimoto et al. was used to quickly obtain the critical energy (V_{cr}) for the particular disturbance under investigation. However, this method may give inaccurate (both over-estimate and underestimate) results. The PEBS method in combination with a TDS technique was employed as a fast tool to obtain the training and/or testing sets for normalized transient stability margin. A fast training method was used for training the proposed MLP NN, and the method was applied to the 10-machine 39-bus New England test power system and the efficiency was examined. Simulation results on the New England 10-machine 39-bus power system demonstrated that the proposed method was capable of estimating normalized transient stability margin with a good degree of accuracy. Furthermore, it was shown that normalized transient stability margin could be estimated fairly accurately by using only the information regarding the advanced machines as the neural networks inputs. The MLP NN requires an iterative procedure for computing the network weights. In this paper, a fast method was used for training the MLP neural network. Their proposed approach looks suitable for online normalized transient stability margin estimation subject to the acceptable accuracy and computational efficiency

In 2011 [15], A GRNN approach to the transient stability evaluation of a sample 9-bus and 39-bus IEEE test systems had been presented. Test set patterns had deliberately been chosen outside the region of the learning set so as to test the generalization and extrapolation capability of the network after learning. Results show that the GRNN gives better performance in terms of transient stability classification.

Thus, the GRNN was a promising neural network technique for the transient stability evaluation of power systems. The major advantage was that the contingencies may be classified very fast with less misclassification rate. The technique could be used to evaluate the transient stability quickly in dynamic stability analysis. However, the primary concern about whether this new concept can become useful as an on-line aid resides on the question of scaling.

In 2012 [36], there had been a presentation regarding an alternative direct method to analyze transient stability having a multi-machine power system. The proposed method was based on transient energy function methods, which can be used to determine transient stability directly without solving the power system equations numerically. However, the method uses integration of swing equations and their corresponding machine energy functions beyond clearing time, but not as long as the time used in simulation of the system using step-by-step integration methods. The method uses the single machine smallest post-fault potential and largest fault clearing kinetic energies which were compared with each other. If the potential energy was greater than the kinetic energy, then the system was considered stable. The proposed method was applied on the IEEE 39-bus power system for several fault cases. The result of performance of the proposed method was verified by comparing it with the numerical method. The proposed method produces a conservative result which was as expected for any direct method. They claimed the proposed method was effective as a screening tool for planning purposes, which was faster than utilization of numerical integration methods with reliance on the integration step size. Also, the proposed method was compared with other direct methods such as, EEAC and critical energy comparison, and numerical methods such as forward Euler numerical integration. The proposed method seems effective in assessing transient stability as well.

In 2013 [37], there had been discussion about methods and techniques for improving computation speed of transient stability analysis with application to the on-line transient stability analysis (TSA). These methods were summarized with their application potential to on-line transient stability analysis. Application examples were presented for some of the methods to show the benefits. These discussions were intended to serve as references when selecting an appropriate method in an on-line transient stability analysis. They can be summarized in the table below:

- Variable step-size integration methods [38] was the best suited for long-term simulations in which integration step size can be made large after the initial fast transients were passed. They had also been successfully used in on-line TSA for which computation speed up to 10 times faster than the fixed step simulations had been reported.
- Direct methods [36] refer to a class of methods that assess the transient stability of a power system, and also give a measure of stability margin, based on partial responses of the system obtained from time-domain simulations. Two main types of such methods had been developed. The methods not only can perform fast stability analysis, they also give valuable information on stability margin and sensitivities, which were very useful in on-line TSA in which identification of system stability for contingencies processed must be done automatically. Such information was also useful in deriving remedial actions for unstable system conditions to prevent the system from losing stability.
- Parallel computation technique [39] may be achieved for part of the computation or for the entire simulation. Parallel computation was very attractive in speeding up TSA as technically it can improve significantly computation speed of simulations while still producing accurate results. Many parallel computation schemes had been proposed for TSA, but actually a few had been used. The main difficulty lies in the fact that an effective parallel code requires implementation of special algorithms and such algorithms in most cases do not run efficiently in the non-parallel mode which was the base for any commercial software. It was obviously not practical for software developers to maintain two sets of code.
- Distributed computation technique [40], the advantage was that very little code changes were necessary for the simulation engine. Only

additional tools need to be developed to manage the distribution of contingencies and data communication between the Client and Server. This makes it possible to use the same commercial code in both distributed and non-distributed mode with minimum amount of work. The efficiency of distributed computation can be very high.

- Early termination method [40], this was an intuitive approach in which conventional simulation was performed up to a time point and a check was then made periodically afterwards at a specified interval, based on a combination of stability indices obtained from the simulation. Very stable or unstable contingencies were terminated as soon as the contingency status can be reliably determined. For contingencies whose stability status cannot be reliably determined prior to the completion of the simulations, full simulations will be performed. Using this method, PJM reported [5] that simulations of 60% to 90% of contingencies in its on-line TSA system can be terminated before reaching the end of the simulations, thus achieving significant saving in terms of computation time.
- Dynamic equivalencing [41], use of the dynamically reduced models for on-line TSA may be required for other reasons. Since on-line TSA was performed for real-time system conditions, the system conditions external to the study area may not be available from SCADA. In such a case, the external system will need to be represented by an equivalent. Time-saving for TSA will be the by-product with this approach.
- Model tuning [37], some of the large interconnected power system models include dynamic model parameters that demand small integration step size in order to maintain numerical stability when using the designated simulation tool. Each simulation can obviously be made faster if a larger step size can be used, while the result accuracy and

numerical stability were maintained. This can be achieved by tuning the critical parameters to eliminate the source of the numerical stability problem.

- Lookup table approach [42], there were possibilities that a real-time system condition cannot be matched with the conditions available in the lookup tables. In such a situation, stability limits will not be available which would restrict the real-time system operation. Stability limits computed from off-line models were often more conservative than those computed directly from the real-time model. This would result in lower transfer capabilities.

In 2013 [21], there had been a presentation of a multi-layer perceptron (MLP) neural network (NN) based approach was proposed for the online transient stability assessment of power systems through estimation of the critical clearing time (CCT) and a transient stability time margin (TM) considering detailed models for the synchronous machines and their automatic voltage regulators (AVRs). The New England 10-machine 39-bus test power system and the IEEE 16-machine 68-bus test power system were used as examples to demonstrate the proposed approach. The software tool PSAT was employed for generating the required training and/or testing patterns using time-domain simulation (TDS) technique. The resilient back-propagation method from MATLAB neural network toolbox was used for fast training the proposed neural network. The proposed neural networks were trained off-line; so the heavy computational burden was avoided in on-line applications. In addition, a neural network based sensitivity method and the principal component analysis (PCA) were used to reduce the dimension of the input data vectors. It was shown that the proposed MLP NNs could estimate the actual CCT and/or TM corresponding to a particular fault scenario with reasonable accuracy at different system operating conditions. They could be employed for quick assessment of the transient stability in a power system control center.

In 2013 [43], A comprehensive technique had been introduced to determine and include transient stability boundary in a transient stability-constrained optimal power flow (TSC-OPF) problem. These approaches use the base dispatch results

provided by the security-constrained unit commitment for a specific hour to evaluate the transient stability within the framework of a TSC-OPF. Two approaches based on maximum relative rotor angle deviations and generators output power had been proposed for this purpose and evaluated using three test systems. The search space for the stability boundary had been significantly reduced by grouping generators with similar transient behavior, i.e. critical and non-critical machines. This makes the application of the proposed method feasible for real power systems. The computation time for TSC-OPF had been significantly reduced compared to the previously proposed methods in the literature. The proposed method accounts here only for one severe contingency and specific hour during a day. However, as an extension, one can similarly derive a transient stability boundary for other credible contingencies and other hours during a day according to the dispatch results provided by security-constrained unit commitment. That may sound cumbersome, but considering that all these calculations were offline, there would be no concerns about required computations. The corresponding transient stability boundary for all contingencies can be stored in a database and recovered later to be used in TSC-OPF. The main contributions of the study were summarized as follows:

- Two approaches were proposed for finding transient stability boundary of a power system, making them suitable for systems with different transient stability requirements and criteria.
- An analytical closed form formula was extracted for the transient stability boundary to be included in any power system study requiring a stability check such as TSC-OPF thus avoiding huge number of discrete differential equations.
- The transient stability analysis and OPF were separated which makes it feasible to use full dynamic models of power systems without increasing TSC-OPF computational time.

Regarding the ANFIS method, it had been used for many applications of power system, for example; designing a static synchronous series compensator based controller for the improvement of transient stability [44], improving the power quality of the power production system of a split shaft micro-turbine [45], power flow analysis

and optimization [46] ,controlling voltage and frequency of a variable-speed wind power generation [47], fault detection in transformers by analyzing dissolved gases [48], monitoring multi-area load frequency [49], design of power system stabilizer with unified power flow controller [50], and designing robust power system stabilizers (PSS) [51].

CHAPTER 3

POWER SYSTEM STABILITY

This chapter describes regarding the general principles of power system stability that are comprised of physical general concept, network type, and relative term. Assessment of configurations of componentry power system by the idealized model method shows a part of fundamental stability parameters of power system [17]. A previous reviews of the contingency of different patterns of stability problems as power systems developed in the related approaches of analysis is also described below. The purpose of this chapter is for explaining the power system stability in overview and for getting a basic of a relative physical rationality. These can help to understand in a detailed resolution of the different views for the topics in next chapters.

3.1 BASIC CONCEPT OF POWER SYSTEM STABILITY

The power system stability is a part of the system that can help the system being in a system equilibrium state under normal operation and to get back an acceptable equilibrium after a disturbance. While the power system instability in a system can happen by various causes relying on the configuration of system and mode of operation at that time. Conventionally, a stability problem is caused by the operation of maintaining synchronous. The power system depends on synchronous generators, a significant condition concerning the acceptable system operation is the whole synchronous generators in the system can stay in the synchronism. The main problem normally comes from the dynamics of generator rotor's angles and relationships of power angle.

The instability may not come from synchronism loss. For instance, a system having a synchronous generator that feeds the power through a transmission and distribution lines to an induction motor load is able to turn into the unstable state due to the voltage collapse at load bus. Thus, to maintain the synchronism state is not an issue in this example, but it is the voltage control and its stability instead. Also

the said instability pattern can happen in the loads that cover some extensive area which is supplied from a large power system.

In the assessment of system stability, mainly the problem is the power system behaviour that is occurred from the transient disturbance. The said transient disturbance could be either small or large. The small disturbance would come from changes of load continually, and the system changes itself to an adjusted condition. The system shall be able to be under the normal operate subject to the changed conditions and keep supplying the demanded amount of load. It must survive any large disturbances from the extreme nature, e.g., a fault from short-circuit occurring on a transmission system, isolation of load, rejection of a generator, or isolation of connection between the connected systems. The response of system to a disturbance will involve and take effects to a number of equipment in the system. For an instance, a short-circuit happening on an important equipment, coming with the isolation of the fault by some protective relay equipment would induce a deviation in power flows, speeds of machine rotor, and voltages at bus. The voltage deviation would induce generators and then voltage regulators of transmission system. The speed deviation will next initiate prime mover governors to operate. The change in connected-line loads can influence the control of power generation. The deviations in frequency and voltage can take an effect of varying degrees of loads in the system, which depends on their equipment and machine characteristics. Moreover, devices used for protection of individual equipment probably responds to deviation in parameters of a system and may take an effect of the performance of systems. In a circumstance, the responses to the limited number of equipment may be significant. Hence, a lot of assumptions are used to make the problems easy and for concentrating on any factors affecting the particular type of stability problem. The understanding of the stability problems is facilitated by the grouping of stability into suitable categories.

The topics below describe various causes of the instability of power system and their basic principles by using simplified configurations of power system.The system analysis applying with idealized models will assist to understand basic parameters of each pattern of the stability and instability problems.

3.1.1 Rotor Angle Stability

The rotor angle stability herein is a capability to keep the synchronism of connected synchronous machines in a power system. The problem of stability relates to power systems' electromechanical swings. A significant part of the problem is the behavior where the power output of synchronous machines varies due to their rotor oscillations. The characteristics of synchronous machine is described below, it will be useful as the 1st step in evolving the relative basic concept.

A. Synchronous machine characteristics

The modeling of synchronous machines and their characteristics are explained in Chapter 3. The explanation below will be only for the basic characteristics relative to the synchronous operation.

There are 2 essential elements for a synchronous machine: 1) armature and 2) field. Generally, the armature is at the stator and the field is at the rotor. The excitation of winding field is normally excited by the DC current. Whenever a turbine prime mover drives the rotor, the field winding's rotating magnetic field will induce the AC voltages into the stator's 3-phase armature windings. The frequency of the induced AC voltages and of the currents flowing in the stator windings subject to being connected load will depend on a speed of the rotor. The stator electricity's frequency will be synchronized with the rotor mechanical speed, normally called synchronizing machine. When 2 or the greater number of synchronous machines are together connected, all machines' stator currents including voltages must be in the same frequency and each's rotor speed is synchronized to the said frequency. Therefore, the rotors of the whole synchronous machines connected to the system shall be in synchronism.

With respect to the physical arrangement of the stator armature windings, the AC current, that flows into the 3-phase winding generates a rotating magnetic field subject to the operational steady-state, will rotate the rotor at the same rotor speed. The rotor field and stator field will respond to each. An electromagnetic torque is from a tendency of the rotor field and stator field. Within a generator, certainly the electromagnetic torque is against the the rotor rotation, thus the mechanical torque need to be driven by the prime mover to maintain the rotation in the same condition. The generator's power output or electrical torque will be changed due to the

adjustment of mechanical torque input by the prime mover. An augmentation in the mechanical torque input will affect the leading of rotor to a new position involved in the stator's rotating magnetic field. On the other hand, the deduction of mechanical torque would slow down the position of rotor. Under an operational conditions of steady-state, the revolving field and the rotor field of a stator are to be in the same frequency. However, there is an separation of angle between revolving field and the rotor field of the stator which it relies on the generator's power output.

The functions of mechanical torque and electrical torque in a synchronous motor will be in the rotation in reverse if compared to generators in the system. The electromagnetic torque keeps the rotation conditions, in the meantime the mechanical load is against the rotation. An increase in the mechanical load will affect retarding the position of rotor in connection to the stator's revolving field.

As abovementioned, the terms of power output and input mechanical torque was exchangeably applied. As the machines' average rotational speed is quite constant although sometimes there would be a small deviation of speed lower and greater than the speed at synchronism temporarily; so for ease in the assessment of power system stability, generally we therefore assume that it is constant. The per unit of power values and torque values are quite the same.

B. Relationship Between Angle and Power

A significant factor of the power system stability is the relation of the power flow and the position of angle of synchronous machines' rotor. Their correlation is quite non-linear. A simplified system illustrated in Figure 3.1 (a), it is comprised of 2 synchronous machines that connect via a transmission system that has one of inductive reactance X_L. The capacitance and resistance can be negligible as they are very small. We assume that the machine no. 1 is a generator that dispatch the load to one of synchronous motor that is symbolized by the machine no. 2.

The load dispatched from the machine no. 1 to the machine no. 2 is an angular separation function (δ) between the 2 machines' rotors. Figure 3.1 (b) illustrates a system's model which is able to be applied to fix the relation of angle and power. The angular separation comprises 3 components, 1) angle that the generator's stator field leading the motor's, 2) the angular deviation between motor

and the generator's terminal voltages and 3) internal generator angle δ_G,. A simplified model that consists of the internal voltage lagging the reactance is applied to be the synchronous machines. The reactance value of used machines relies on the the study objective. For the steady-state index assessment, it is proper to apply the synchronous reactance together with the internal voltage which has the same values as the excitation voltage. The modelling basic and the estimation related to the modelling are described in Chapter 3.

A phasor diagram specifying the relations of the generator and the motor voltages is illustrated in Figure 3.1 (c). The power flowed from the generator to the synchronous motor can be written in the following equations:

$$P = \frac{E_G E_M}{X_T} sin\delta \tag{3.1}$$

$$X_T = X_G + X_L + X_M \tag{3.2}$$

The relation between the angle and corresponding power is illustrated in Figure 3.1 (d). According to the idealized models applied for representation of the synchronous machines, the power would swing as the sinusoidal wave with a high non-linear relation. For the models, that are more precise, used for a machine considering the effects of excitation systems, i.e., automatic voltage regulators (AVR), and other dynamic parameters, the deviation of power and angle will obviously deviated from the sine-curve relation. Nevertheless, the other form is similar. If the angle is 0, it means that there would not be any power transferation. In the meantime if the angle is up more, the power transfer will also up more. After a certain angle, usually ninety degree, an increase in the angle will be the result of the reduction of the transferred power. Therefore, it has a maximum quantity of power at the steady-state which the power from a machine to another machine is able to be dispatched. The quantity of the maximum power will be proportional directly to the machine's internal voltages and inversely proportional to the reactance between the voltages that include the machines' reactances and the reactances of transmission systems connected to the machines.

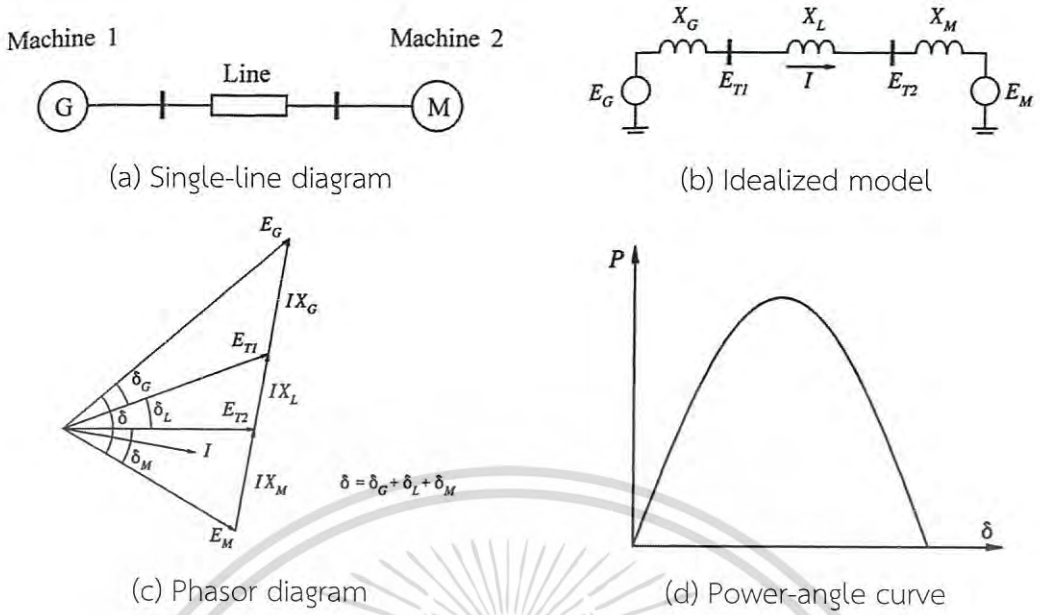

Figure 3.1 Characteristic of power transfer for 2-machine system [17].

In case the system has the number of machines greater than 2 machines, the separation of relative angles will take an effect of the power interchanging in a similar manner. The limited values of the power interchanging and the displacement of relative angles are load distribution and generation functions that are quite complex. The displacement of relative angle at 90° between any 2 machines in itself will have no specific important factor.

C. Stability Characteristic

The equilibrium between opposing forces is the factor of stability condition. The mechanism that is connected to synchronous machines can remain the synchronism with another one via some restoring forces acting when any forces have tendency to decelerate or accelerate one or more machines. Subject to the condition of steady state, the system has equilibrium between the output electrical torque and the input mechanical torque, and the speed of each machine is still constant. In case that the power system disturbance happens, the equilibrium is loss, causing in deceleration or acceleration of the the machines' rotors in compliance with the rules of the rotating body motions. In case that a generator runs temporarily quicker than another one, the rotor angular position that is relative to the slower machine will be

in leading. The angular deviation will transfer some loads from the slower machine to the quicker machine, upon the relationship of power angles. It has to minimize the deviation of speed and then the displacement of relative angles. The relation of the relative power angles as abovementioned, is very non-linear. Other than the certain limitation, an increase in the angle displacement is supplemented by the deduction of the power dispatching. It more ups the angle displacement and can induce the system to instability state. We can say the system stability relies on whether the deviations in rotor angular positions result to sufficient restoring forces or not.

When any synchronous machines lose the synchronism from the residual machines in the system, the rotor will rotate at a lower or higher speed than the needed speed to generate voltages at the synchronous frequency. The displacement between the field of rotor and the field of rotating stator in accordance with synchronous frequency causes the fluctuation largely in the electrical voltage, electrical current, and the power output. It may induce the operation of some protective relays to cut off the unstable machine from the system.

The synchronism loss may happen between a machine and the residual machines in the system or it may happen between machine groups in a system. In the case of the synchronism loss between machine groups, maybe the synchronism within each group is maintained afterwards it is isolated from other groups.

The synchronism of all connected synchronous machines may be comparable to a number of motorcycles that are running in a circular track and they are linked to others by elastic cables. The motorcycles are as the rotors of synchronous machine and the elastic cables are like as the transmission systems. If the whole motorcycles speed symmetrically, the elastic cables will be still in the normal condition. If there is some force acting to a motorcycle running around the circular track and resulting the motorcycle in momentary acceleration, the elastic cables connected the motorcycle with the other motorcycles will extend. Certainly the speed of motorcycle maybe up or down, thus to maintain the overall speed, it has to decrease the speed of the quicker motorcycle and increase the speed of the other motorcycles. A reaction will happen like a chain until all motorcycles come back to run at the same speed. If the pulling force on an elastic cable exceeds its withstanding stress, it will worn out and a motorcycle or more than one will loss from the track.

The change of electrical force of each synchronous machine after the disturbance in the power system can be written in the equation as follows:

$$\Delta T_e = T_S \Delta\delta + T_D \Delta\omega \qquad (3.3)$$

where T_S is the coefficient of synchronous torque. And the $\Delta\delta$ is the change in synchronous torque. Thus the $T_S\Delta\delta$ in the equation epresents the deviation of torque with the displacement of rotor angle. While the T_D is the coefficient of damping torque. And the Delta-w is the change in speed. Thus $T_D\Delta\omega$ in the equation represents the deviation of torque with the speed deviation.

The system stability relies on the being of the two components of torque for each of the synchronous machines. In case that the synchronizing torque is insufficient, the system will be in the state of instability via an abnormal deviation in the rotor angle. In the meantime, if damping torque is insufficient, it will result in the oscillating instability.

For ease in the stability assessment and for more understanding with respect to the normal stability problem, we usually categorize the rotor angle stability characteristic into the two classifications as follows:

(a) Small disturbance stability (or small signal stability) is the capability of the system to stay in steady-state after there are some small disturbances occurring. The disturbance continuously happens in the system due to some small deviations in generation and loads. The disturbances are assumed as not much, the system equations can be linearized for objective of the system assessment. The system instability may be classified into 2 groups: 1) Increase in rotor angle from deficient synchronous torque and 2) Rotor oscillation of rising amplitude from deficient damping torque. The responding character of power systems to a small disturbance relies a lot of components such as the initiating operational conditions, the limitation of transmission and distribution systems, and the models used for generator excitating controlling. For a synchronous generator being synchronized to a large power system, with a fixed field voltage without AVR to control voltage, the instability will happen as the lack of sufficient synchronous torque. It will be the result of the system turning into the instability state via a non-oscillatory mode. For the system having continually

acting excitation controllers, a stability problem of the small disturbances is a point of securing the system oscillations' sufficient damping. The instability is generally via the rising amplitude oscillation.

By now in practical, the small disturbance stability is a main issue of deficient oscillation damping. The following stability types of oscillations have concerns as follows:

- Machine-system mode or local mode is related to the oscillation of generating units at a generating bus connecting to the others in the power systems. The local term is applied as the oscillation is localized at only a small section of the systems of a substation.
- Inter-area mode is related to the oscillation of a number of generators in a group of the system against other generators in other groups. They come from 2 or more groups of close connected generators being weakly connected.
- Control mode is related to generating unit and other device controllers. Inefficient HVDC converter, prime mover governor, static var compensator, and tuned exciter are usually the root cause of these modes' instability.
- Torsional mode is related to the rotating elements of turbine and generator shaft systems. The instability of the torsional mode is from the interaction between prime mover governor, excitation control, series-capacitor-compensated line, and HVDC control.

(b) The transient stability is the capability that the system can remain the synchronism in the system after an extreme transient disturbance happens. The response of system is relative to a signification deviation of generator rotor angles, it is induced by the relationship of non-linear power angle. The stability relies on both of the initial operatonal state and the disturbance severe level. Generally, the system would be adjusted itself to maintain the stability, the post-disturbance at the operation in the post steady state will deviate from the state before the disturbance.

Disturbances of widely changing in severe level and probability of happening may occur in the system. Normally, the system is designed and operated under

stability for some contingency cases. Usually, the contingency cases considered are short-circuits under varied types, such as phase-to-ground short-circuit, or three-phase short-circuit, or phase-to-phase-to-ground short-circuit. Generally, we assume that the fault is occured on a transmission line, but sometimes the faults are assumed at transformer or bus as well. The clearance of fault is assumed by the opening of close circuit breaker to cut off the faulted component from the other parts. In practical, when the fault happens, reclosure relay will be operated automatically.

Figure 3.2 shows the character of a synchronous machine under the unstable situation and stable situation. It illustrates the responses of rotor's angle for two unstable cases and for one stable case.

In the case 1 'stable case', the rotor's angle is increased until a highest value, then decreasing and oscillating by reducing the amplitude until the system comes back to the steady state. In the case 2 'unstable case', the rotor's angle keeps increasing consistently until loss of the synchronism. The instability pattern is relevant to only the 1st swing. The system instability is caused by the deficient synchronous torques. In the case 3 'unstable case', the system can remain the stability in the 1st swing only but afterwards it turns into the unstable state due to an increase in oscillations. The instability pattern normally happens if the steady-state at post-fault condition still have the small disturbance unstable as a the transient disturbance result. For some large power systems, the transient instability may not happen within the 1st swing. It can be the result of several modes' superposition of oscillation inducing the large deviation of rotor's angles after the 1st swing. For the transient stability study, the studying period to be focused is normally within three seconds to five seconds after the disturbance occurs. For a much large power system, the studying period to be focused may be need to extend up to 10 seconds with an oscillation's dominant inter-area mode.

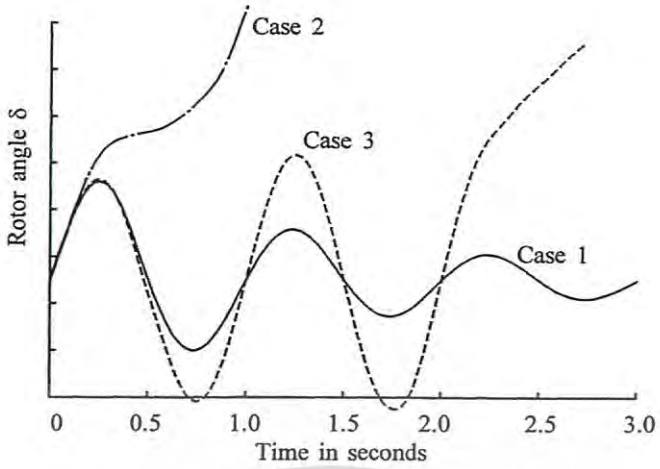

Figure 3.2 Response of rotor angle with transient disturbance [17]

Please note that the dynamic stability term was used in a number of literatures widely to classify the stability coming from the rotor's angle. It was used to illustrate the various aspects of the stability by many authors. For instances, a lot of North American literatures, mostly they were used to signify small-disturbance stability for the response and behavior of the control equipment such as the AVR, how significant difference of the response is from the classical steady-state stability without control devices [52, 53]. In the French and German literatures, they were used to signify what else the transient stability is termed, however, a lot of confusion is from the application of the term dynamic stability, both IEEE and CIGRE have recommended not to use it [54, 55]

3.1.2 Voltage Stability and Voltage Collapse

The voltage stability is the capability that the system can keep all buses with the steady acceptable voltages subject to a normal operational condition after some disturbance has occurred. A system can turn into the state of voltage instability state when augmentation in load demand, changing opertional conditions, or some disturbance causes an uncontrollable and progressive deduction in voltage. The major factor turning the system into the instability state is none of capability of the system to generate or receive the reactive power as demanded. Usually, the main factor of the problem is the voltage deduction occurring during reactive power and active power flowing through transmission and distribution systems' inductive reactances [56, 57, 58].

The voltage stability criteria is that at any operatinal conditions for the whole buses in a power system, the voltage at any buses will be up more if the reactive power flowing into those buses increase. A system's voltages would be unstable if in the system there is a bus or there are more 2 buses getting the voltage decreases but the reactive power flowing into the same bus increases. Or we can say that, the system's voltages will be stable if the V-Q sensitivity at every bus is positive and the system's voltage will be unstable if the V-Q sensitivity at one bus at least is negative.

The gradual deduction in voltages at any buses may be related to the rotor angles displacement going outside of the stability state. For instance, the progressive loss of machines' synchronism coming from the relative rotor angle of 2 machine groups is greater than 180° or about to reach 180° would cause in the too low voltages at the mid points in that network. In despite, the type of voltage drop permanently relative to the voltage instability will happen when the rotor angle stability does not relate to the issues.

The voltage instability is a significant local event. Nevertheless, its consequences probably induce a large effect to the power system. The collapse of voltage is more complicated than the simple instability of voltage and usually it causes a sequence of events involving the instability voltages, which lead to a low-voltage profile in the power system significantly.

The voltage instability could happen from a lot of various causes. In the simplified configuration, we may describe it with a model having 2 networks at the end of each terminal [56]. It is comprised of a voltage source (E_S), which its value is fixed. The power is supplied through an impedance (Z_{LN}) to the terminal load (Z_{LD}). The configuration can represent a basic radial feeding power to a load. Also it can represent a load area is supplied through a transmission system from the source of large system. The equation of the configuration can be written as follows:

$$\tilde{I} = \frac{E_S}{Z_{LN} + Z_{LD}} \tag{3.4}$$

$$Z_{LN} = Z_{LN}\angle\theta \; Z_{LD} = Z_{LD}\angle\phi \tag{3.5}$$

where $\tilde{I}$ and E_S are phasor.

3.2 TRANSIENT STABILITY

The transient stability is the capability that the system can stay in the synchronism after some extreme temporary disturbances such as rejection of generation, rejection of large loads, or some fault at transmission systems. The system response to the disturbance relates to the significant deviations of generator rotor angle, bus voltage, power transfer, and other system's parameters. The stability in the system is relative to the system's non-linear characteristics. Whenever that the relative angle displacement between a machine and other machines in the system is still in the acceptable boundary, it means the system's synchronism is still maintained. However, the synchronism loss due to the transient instability, it would normally be apparent in two to three seconds after the disturbance occurs.

3.2.1 Elementary View of Transient Stability

Considering the network illustrated in Figure 3.3, comprising a generator dispatching the load through 2 circuits to a connected large system, symbolized by an infinite bus. The fixed frequency and fixed voltage are assumed for source for the large system [52, 53, 54].

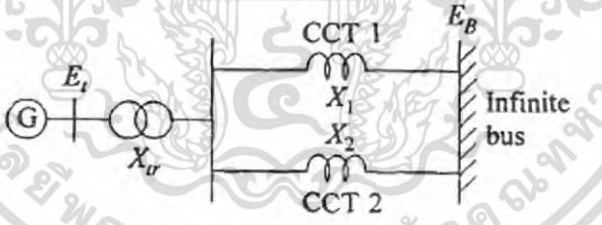

Figure 3.3 Single machine infinite bus system [17].

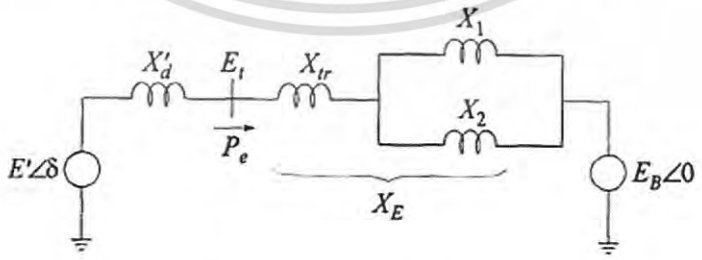

(a) Equivalent circuit

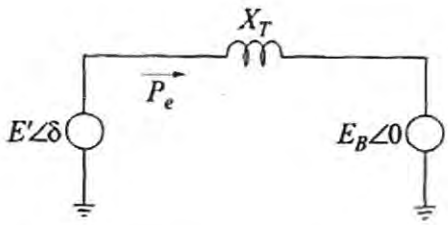

(b) Simplified equivalent circuit

Figure 3.4 Classical model representing the system **[17]**

A transient stability's basic principle and concept used for analysis of the response for a large disturbance will be described. We simulate the generator model as the classical model. Figure 3.4 (a) illustrates the representation of the said system. We normally neglect the effects of prime mover governor. Also, we ignore any resistances for such analysis. The voltage lagging the transient reactance ($X_d^{'}$) is symbolized by E'. The angle between E_B and E' is symbolized by the rotor angle δ. It is assumed that the E' magnitude value remains unchanged before the disturbance. After a disturbance occurs in the system, the δ would deviate that is caused by the change of the generator rotor speed from the synchronzing speed at w_s.

The network modelling could be simplified to a simple configuration illustrated as Figure 3.4 (b). The simplified approaches could be used for the analysis. It would help us for understanding fundamentally the behavior of transient stability. From the Figure 3.4 (b), the generating power output can be written in the following equation:

$$P_e = \frac{E'E_B}{X_T} sin\delta = P_{max} sin\delta \qquad (3.5)$$

where

$$P_{max} = \frac{E'E_B}{X_T} \qquad (3.6)$$

As the stator resistance has been ignored. The terminal or air-gap powers is symbolized by P. Pm symbolizes an input mechanical power, at the steady state, an output electrical power Pe is the same value as the input mechanical power. Each point on the graph represents its operational conditios. The curve of relative power angle for the two transmission circuits in service (I/S) is shown as graph no.1 in Figure

3.6. In case that a circuit of that is not in service (O/S), causing the reactance X_T value is increased. Figure 3.5 illustrates the curve of relative power angle subject to the circuit 2 is not in service as the graph no. 2. It can be seen that the power at maximum has been lower. At an input mechanical power P_m, the relative rotor angle changes to δ_b, in accordance with the operational point of b on the graph no. 2; with an increase in reactance, the rotor angle increases so that it keeps the system in the steady state.

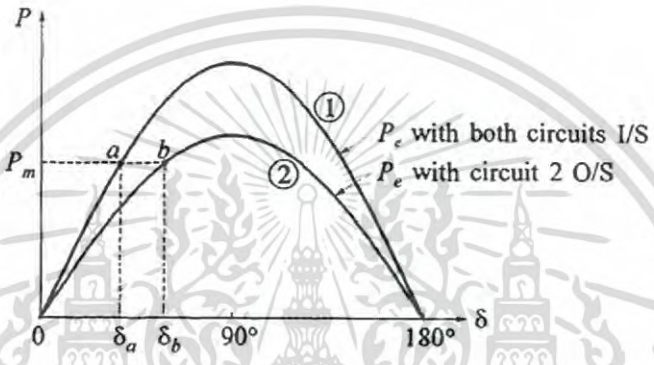

Figure 3.5 Relative Power Angle [17]

While some disturbance occurs in the system, the oscillating swing δ is added on the synchronizing speed ω_0, however, the change in speed $\left(\Delta\omega_r = d\delta / dt\right)$ is quite smaller than the ω_0. Hence, in practical the generator speed is the same value as the value of synchronizing speed ω_0. The per unit (pu) of air-gap torque can be deemed that it is the same value as the value of per unit (pu) of air-gap power. Thus the torque and power will be interchangeably used for reference of the equation of motion.

We can write the swing equation as the following equation:

$$\frac{2H}{\omega_0}\frac{d^2\delta}{dt^2} = P_m - P_{max}sin\delta \qquad (3.7)$$

where

t is time, in second

δ is inertia constant in MW:s/MVA

P_{max} is output maximum electrical power in per unit

P_m is input mechanical power in per unit

3.2.2 Response to Step Change in Mechanical Power

In this section, we will explain the transient characteristic for the classical system subject to the two circuits are available, taking into account that the input mechanical power immediately increases from a starting point at P_{m0} to P_{m1} as illustrated in Figure 3.6 (a). As the rotor inertia, the relative rotor angle would be unable to suddenly change from the starting value from δ_0 to δ_1 in the same value to a new equilibrium value at b that $p_e = P_{m1}$ certainly. The input mechanical power presently is greater than the output electrical power. An torque being accelerated induces an acceleration of rotor from the starting operational point, to a new equilibrium value at b, routing the $p_e - \delta$ graph with a rate fixed by the equation of motion. An accelerating power is represented by the deviation from P_{m1} to P_e at any momentary point.

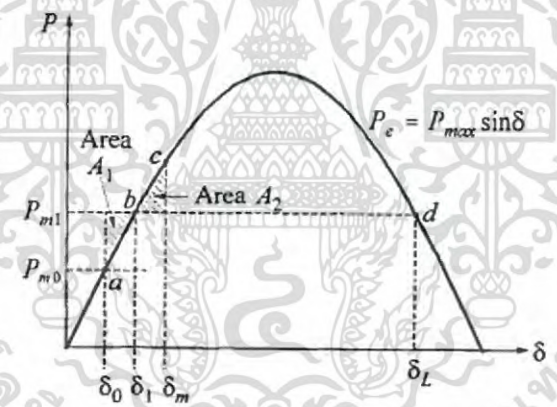

(a) Change in power angle

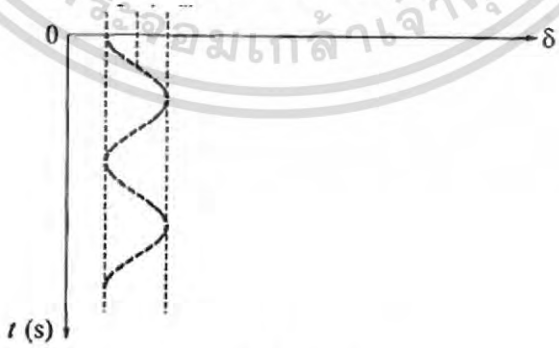

(b) Response of rotor angle time

Figure 3.6 Responding for a step change of input mechanical power [17]

Whenever the system reaches the point b, the change in power will be 0. However, the synchronizing speed ω_0 in accordance with the infinite bus's frequency is still lower than the disturbed machine's rotor speed. The machine's rotor angle must therefore keep increasing to reach the synchronizing speed ω_0. If the value of δ_0 is greater than δ_1, P_e will become more than the value of P_{m1} and the rotor would be decelerated. In the case of the value δ_m is at a peak, the machine's rotor speed comes back to the synchronizing speed ω_0, while P_e is greater than P_{m1}, The machine's rotor will keep decelerating with a reduction of speeding below the synchronizing speed ω_0. The operational point would return to the $P_e - \delta$ graph from c to b and next to a. The rotor angle here will swing around the new equilibrium angle δ_1 indefinitely, with an amplitude having constant value, as illustrated by δ in Figure 3.7 (b).

In the analysis of the power system abovementioned, please note that the whole resistances are ignored. We use the classical model for the system simulation. The model, it ignores most damping parameters. Hence, oscillation of rotor may be continually increased followed by a disturbance. Practically, it has a lot of positive damping sources as well as rotor amortisseur circuits and field flux variations to be considered.

3.2.3 Equal-Area Critetion Method

For the system model considered above, it does not need to officially resolve the equation of motion to resolve if the rotor angle is indefinitely increased or out of equilibrium point or not. We can use the power angle diagram shown in Figure 3.7 to get the limitation of stability and the information with respect to the angle displacement at a maximum value (δ_m). Even though the approach cannot be applied to a multimachine system with detailed modelling for some synchronous machines, but it can help in the basic understanding of any factors that influence the power transient stability.

From Equation 2.7, we have the following relationship between an accelerating power and a rotor angle:

$$\frac{d^2\delta}{dt^2} = \frac{\omega_0}{2H}\left(P_m - P_e\right) \tag{3.8}$$

Now P_e, is a non-linear function of δ

$$2\frac{d\delta}{dt}\frac{d^2\delta}{dt^2}=\frac{\omega_{0(P_m-P_e)}}{H}\frac{d\delta}{dt} \tag{3.9}$$

or

$$\frac{d}{dt}\left[\frac{d\delta}{dt}\right]^2=\frac{\omega_0\left(P_m-P_e\right)}{H}\frac{d\delta}{dt} \tag{3.10}$$

Integrating gives

$$\left[\frac{d\delta}{dt}\right]^2=\int\frac{\omega_0\left(P_m-P_e\right)}{H}d\delta \tag{3.11}$$

The change in speed $d\delta/dt$ is initial by 0. It will change from the disturbances. For the condition of operational stability, the change in angle shall be limited in boundary, going until a highest value and then change in a direction. It requires the change in speed $d\delta/dt$ to become 0 for a time after the disturbance. Therefore, from Equation 2.11, as a criterion for stability we may write

$$\int_{\delta_0}^{\delta_m}\frac{\omega_0}{H}\left(P_m-P_e\right)d\delta=0 \tag{3.12}$$

where δ_0 is the rotor angle at initial state, δ_m is the rotor angle at maximum value, as illustrated in Figure 3.7. Hence, the area subject to the function of P_m-P_e plotted and it shall be zero once the system becomes to the stable condition. In Figure 3.7, It would be accepted if the area A_1 has the same area value as the area A_2. Kinetic energy is increased by the accelerating rotor where δ is changed from δ_0 to δ_1. The increased energy can be written as the following equation:

$$E_1=\int_{\delta_1}^{\delta_1}\left(P_m-P_e\right)d\delta=area\ A_1 \tag{3.13}$$

The energy lost while being decelerated where it is changed from δ_1 to δ_m can be written in the following equation:

$$E_2 = \int_{\delta_0}^{\delta_1} (P_e - P_m)\, d\delta = area\, A_2 \qquad (3.14)$$

Due to the losses are not considered in the method, the increased energy therefore has the same value as the lost energy. Hence in this case, the area A_1 will have the same area as the area A_2. These are a basic of the approach of equal-area criterion. We are able to use it for determining the maximum δ of the oscillation, also we can use it for assessing the power system's stability regardless of computation of the responding time via the conventional solution by the equation of motion.

The said criteria means is able to be applied for a power system for the determination of an allowable maximum augmentation in the P_m of Figure 3.4. The stability will be able to be remained subject to an area A_2 at least having the same value as an area A_1, can stay over the P_{m1}. If the area A_1 is more than the area A_2, then $\delta_m > \delta_L$ and the system stability will be gone. This is due to P_{m1} is greater than P_e (for $\delta > \delta_L$), also the net torque is speeding up rather than speeding down.

We will examine the mechanism of transient instability by considering next the system response to a fault by short-circuit on a transmission line, which is the common form of a disturbance considered in transient stability studies.

3.2.4 Transient Stability Factors

From the described above, we can summarize that the generator's transient stability depends on the points as follows:

a) Fault clearing time

b) Fault type and its location

c) Generator electrical output during the fault

d) Heavily each generator is loaded

e) Reactance of postfault transmission system

f) Internal voltage magnitude (E') of each generator (The voltage will rely on the excitation of field)

g) Reactance of each generator. (The lower reactance will help in decrease in initial rotor angle and increase in the peak power)

h) Infinite bus's voltage magnitude (E_B)

i) Generator's moment inertia (The higher moment inertia, it can slow the deviation rate in rotor angle. This can be the result of the decrease in the kinetic energy increased during the fault)

As the approaches for fundamental principles, we took into account a system that have an easy networks and described by a simplified configuration. It enables the stability analysis by applying a curve method. Even though the plots of relative rotor angle as a time function are illustrated in Figure 3.7 and Figure 3.8, they have not been computed actually, thus we have not defined any timescales for those plots. Practically, the network structures in a power system is very complicated. The precise assessment of the transient stability needs detailed models for all machines, all generators, load characteristics, and other control devices, more detail will be described in Chapter 3. Nowadays, the well-known practical method used for analyzing the transient stability is the time domain method where the non-linear differential equations are resolved by applying the step-by-step numerical integration techniques. This leads us to the next section in which some of the commonly used numerical integration methods are explained.

CHAPTER 4

SYSTEM MATHEMATICAL MODELLING

4.1 SIMULATION OF POWER SYSTEM DYNAMIC RESPONSE

4.1.1 Structure of Power System Model

The transient stability assessment of a power system would be regarding the calculation of the nonlinear dynamic response from large disturbances, normally it would be a fault at transmission system, followed by the isolating the faulted part by nearby protection relays.

Figure 4.1 depicts the general structure of the power system model which is applicable to the assessment of transient stability. However, for transient stability analysis, nonlinear equations are solved. Moreover, large discontinuities caused by network switching and faults, as well as small discontinuities caused by some limitation of system variables, are shown in the model. Line flows, bus voltages, and protection performance have interest, also the fundamental information relative to the system stability. The representation of overall power system are comprised of models for the individual elements as follows:

- Inductive and synchronous motor loads
- Connecting transmission networks including their static loads
- Synchronous generators and their control devices
- Other devices i.e. SVCs, HVDC converters, and other devices

The models applied for any element should be suitable for assessment of transient stability. Their equations shall be organized in an appropriate pattern for the applying numerical approach. It can be seen in what follows, the complete system model comprises large sparse algebraic equations and a large set of differential equations. The assessment of transient stability is therefore the problem involving the differential algebraic initiating-values.

4.1.2 Representation of Synchronous Machine

To describe the implementing a generator modelling for the assessment of transient stability [59], the models with one d-axis and two q-axis is represented for the generator in the network.

The equations below are for synchronous machines, they are a group of the 1st-order-differential equations, having units of rotor angle δ in radian, time t in second, and other quantities in per unit.

$$p\Delta\omega_r = \frac{1}{2H}\left(T_m - T_e - K_D\Delta\omega_r\right) \tag{4.1}$$

$$p\delta = \omega_0\Delta\omega_r \tag{4.2}$$

where

ω_0 is synchronous speed, rad/s,

$\Delta\omega_r$ is deviation in rotor speed

p is derivative operator d'dt

A. Equations of Rotor Circuit

The rotor's current described in terms of a rotor and mutual flux linkages the rotor circuit dynamic can be written in the equations as follows:

$$p\psi_{fd} = \omega_0\left[e_{fd} + \frac{\left(\psi_{ad} - \psi_{fd}\right)R_{fd}}{L_{fd}}\right] \tag{4.3}$$

where

$$p\psi_{1d} = \omega_0\left(\frac{\psi_{ad} - \psi_{1d}}{L_{1d}}\right)R_{1d} \tag{4.4}$$

$$p\psi_{1q} = \omega_0\left(\frac{\psi_{aq} - \psi_{1q}}{L_{1q}}\right)R_{1q} \tag{4.5}$$

$$p\psi_{2q} = \omega_0\left(\frac{\psi_{aq} - \psi_{2q}}{L_{2q}}\right)R_{2q} \tag{4.6}$$

The q-axis and d-axis mutual flux linkages are as follows:

$$\psi_{ad} = -L_{ads}i_d + L_{ads}i_{fd} + L_{ads}i_{1d} \tag{4.7}$$

$$\psi_{ad} = L^n_{ads}\left(-i_d + \frac{\psi_{fd}}{L_{fd}} + \frac{\psi_{1d}}{L_{1d}}\right) \tag{4.8}$$

$$\psi_{ad} = L^n_{aqs}\left(-i_q + \frac{\psi_{1q}}{L_{1q}} + \frac{\psi_{2q}}{L_{2q}}\right) \tag{4.9}$$

where

$$L^n_{ads} = \frac{1}{\frac{1}{L_{ads}} + \frac{1}{L_{fd}} + \frac{1}{L_{1d}}} \tag{4.10}$$

$$L^n_{ads} = \frac{1}{\frac{1}{L_{aqs}} + \frac{1}{L_{1q}} + \frac{1}{L_{2q}}} \tag{4.11}$$

Where L_{ads} and L_{aqs} are the saturated values of the q-axis and d-axis mutual inductances as follows:

$$L_{ads} = K_{sd} L_{adu} \tag{4.12}$$

$$L_{aqs} = K_{sq} L_{aqu} \tag{4.13}$$

and K_{sd} and K_{sq} are computed as a function of the air-gap flux linkage ψ_{at} r.

B. Stator Voltage Equations

The stator voltage may be written in the equations below (the speed variations (ω/ω_0) and the stator transients ($p\psi_d, p\psi_q$) are neglected):

$$e_d = -R_a i_d + \left(\underline{\omega} L^n_q\right) i_q + E^n_d \tag{4.14}$$

$$e_q = -R_a i_q - \left(\underline{\omega} L^n_d\right) i_d + E^n_q \tag{4.15}$$

with

$$E^n_d = -\underline{\omega} L^n_{aqs}\left(\frac{\psi_{1q}}{L_{1q}} + \frac{\psi_{2q}}{L_{2q}}\right) \tag{4.14}$$

$$E^n_q = \underline{\omega} L^n_{ads}\left(\frac{\psi_{fd}}{L_{fd}} + \frac{\psi_{1d}}{L_{1d}}\right) \tag{4.15}$$

$$L^n_d = L_l + L^n_{ads} \tag{4.16}$$

$$L^n_q = L_l + L^n_{aqs} \tag{4.17}$$

As we have neglected the impact of deviation in speed on the stator voltage, $\underline{\omega}=\omega/\omega_0=1.0$ in the equations above. Thus, $\underline{\omega}L_d^n = X_d^n$ and $\underline{\omega}L_q^n = X_q^n$. The equations above are for the d-q reference frame of individual machine which runs with the machine rotor. For the result of the connectted transmission system equations, a rotating synchronously common R-I reference is applied. The relations are applied to convert variables from a reference frame to the others. The R-axis of the common reference frame also serves as the reference to measure the rotor's angle δ of any machine.

$$e_d = E_R sin\delta - E_I cos\delta \tag{4.18}$$

$$e_q = E_I sin\delta + E_R cos\delta \tag{4.19}$$

$$E_R = e_d sin\delta + e_q cos\delta \tag{4.20}$$

$$E_I = e_q sin\delta - e_d cos\delta \tag{4.21}$$

For convenience in the organizing a complete set of algebraic equations, the stator voltage equations are described in the common R-I reference frame. Use of Equations 4.21 to transform the stator voltage equations 4.17 yields:

$$\begin{bmatrix} E_R \\ E_I \end{bmatrix} \begin{bmatrix} -R_{RR} & X_{RI} \\ -X_{IR} & -R_{II} \end{bmatrix} \begin{bmatrix} I_R \\ I_I \end{bmatrix} + \begin{bmatrix} E_R'' \\ E_I'' \end{bmatrix} \tag{4.22}$$

The components of the impedance matrix are as follows:

$$R_{RR} = \left(X_d'' - X_q''\right) sin\delta cos\delta + R_a \tag{4.23}$$

$$R_{II} = \left(X_q'' - X_d''\right) sin\delta cos\delta + R_a \tag{4.24}$$

$$X_{RI} = X_d'' cos^2\delta + X_q'' sin^2\delta \tag{4.25}$$

$$X_{IR} = X_d'' sin^2\delta + X_q'' cos^2\delta \tag{4.26}$$

As noted earlier, $\underline{\omega}$ is assumed to be equal to 1.0 pu. The internal voltage elements are as follows:

$$E_R'' = E_d'' sin\delta + E_q'' cos\delta \tag{4.27}$$

$$E_I'' = E_q'' sin\delta - E_d'' cos\delta \tag{4.28}$$

If subtransient saliency is negligible, $L_d'' = L_q''$ Then

$$R_{RR} = R_{II} = R_a \tag{4.29}$$

$$X_{RI} = X_{IR} = \underline{\omega} L_d'' = X_d'' = X_q'' = X'' \tag{4.30}$$

In this case, $E_R'' + E_I''$ represents the voltage behind the subtransient impedance $R_a + JX''$. For network solution, the generator may be represented by either of the simple equivalent circuit.

$$E'' = E_R'' + JE_I'' \tag{4.31}$$

$$I'' = Y'' E'' \tag{4.32}$$

$$Z'' = R_a + JX'' \tag{4.33}$$

$$Y'' = 1/Z'' \tag{4.34}$$

Variations in L_{ads} and L_{aqs} due to saturation may introduce a small amount of subtransient saliency during a transient condition. This is usually insignificant and may be ignored, if it is desired to take advantage of the computational simplicity offered by the above equivalent circuits.

Active power and reactive power at the generator stator terminals are

$$P_t = e_d i_d + e_q i_q \tag{4.35}$$

$$Q_t = e_q i_d - e_d i_q \tag{4.36}$$

The air-gap torque needed for the solution of the equation of motion (13.22) is:

$$T_e = \psi_d i_q - \psi_q i_d \tag{4.37}$$

$$T_e = \psi_{ad} i_q - \psi_{aq} i_d \tag{4.38}$$

Since we have assumed $\underline{\omega} = \omega / \omega_0 = 1.0$ pu in the stator voltage equations, in pu the air-gap torque has the same value as the air-gap power. Thus,

$$T_e = P_e = P_t + R_a I_t^2 \tag{4.39}$$

The field current in the reciprocal pu system is given by

$$i_{fd} = \frac{\psi_{fd} - \psi_{ad}}{L_{fd}} \tag{4.40}$$

The pu exciter output current I_{fd} is

$$I_{fd} = L_{adu} i_{fd} \tag{4.41}$$

Here we have considered a generator model with two q-axis and one d-axis amortisseur circuits. For models with a different number of rotor circuits, changes to the above formulation of machine equations are straightforward. However, we have assumed equal mutual inductances between the armature and rotor circuits in each axis. Reference [59] provides a description of the implementation of a model with unequal mutual inductances for stability analysis, using the above general approach.

C. Initial Values of Generator Variables

As mentioned above, the assessment of transient stability relates to the resulting of a large set of differential equations and algebraic equations with some initiating value. The pre-fault power flow assessment would provide the initiating value of variables, as well as the reactive power and active power outputs including voltages at the generator terminals.

D. Classical Generator Model and Infinite Bus

For the machine that is modelled by the classical model, which the $X_{RI} = X_{IR} = X_d^{'}$ and the E'' is overwritten by E' instead. The rotor angle is an angle that the E' leading the R-axis. The E' magnitude is fixed along the solution. The I and R elements of E' are changed with δ, as determined by the solution of the equation of motion.

For a node related to the infinite bus, both of angle and magnitude of the node voltage are still constant.

4.1.3 Overall System Equations

In Sections 13.3.2 and 13.3.3 we described the organization of synchronous generator and excitation system equations. Treatment of these models is similar to that of the excitation system.

Each of the generating units and other dynamic devices can be described in the following equations:

$$x_d = f_d\left(x_d, V_d\right) \tag{4.42}$$

$$I_d = g_d\left(x_d, V_d\right) \tag{4.43}$$

where

V_d is bus voltage's I and R elements

I_d is I and R elements of current injection from a device into the network

x_d is individual device's state vector

The equations of overall system, comprised of the differential equations (4.42) for all the control equipment and the combined algebraic equations for the devices (4.43) and the network are described in the general form as follows, including a set of the 1st –order-differential equations:

$$x = f\left(x, V\right) \tag{4.44}$$

and a set of algebraic equations

$$I\left(x, V\right) = Y_N V \tag{4.45}$$

with a set of initial conditions (x_0, V_0), where

I is current injection vector

V is bus voltage vector

x is system state vector

Time t does not appear explicitly in the above equations. A large range of methods has been presented in the literatures for resolving the equations, relying on the numerical approaches and used modelling detail. Reference [60] provides some

reviews of these approaches. A lot of potential schemes for the solution of Equation 3.44 and Equation 3.45 are classified by the following factors:

(a) The characteristic of interfacing between the differential equations 3.44 and the algebraic equations 3.45. Either a partitioned method or a simultaneous method may be applied.

(b) The integration approaches applied, such as an explicit approach or an implicit approach.

(c) The approach applied for resolving the algebraic equations. As in the case of assessment of power flow, an approach of the following approaches could be applied: 1) Gauss Seidal approach based on formulation of admittance matrix, 2) Direct solution applying the factorization of sparsity oriented triangular, and 3) literative solution applying the Newton-Raphson approach.

All of the above approaches are successfully applied in transient stability programs. In the next section, two basic solution schemes are described. One scheme uses a partitioned solution and an explicit integration method, and the other uses a simultaneous solution with an implicit integration method.

4.1.4 Solution of Overall System Equations

A. Partitioned Solution with Explicit integration

In this approach, the algebraic and differential equations are solved separately. Initially, at t=0", the values of the state variables x and the network variables V and I are known, and they form a consistent set; that is, the system is in steady state and the time derivatives f(x, V) are equal to zero.

Following a disturbance, usually a network fault, the state variables x cannot change instantly. The algebraic equations 3.45 are solved first to give V and I, and the corresponding power flows and other non-state variables of interest at t=0*. Then the time derivatives f(x, V) are computed by using the known values of x and V in Equations 3.44. These then can be used to initiate the solution of the state variables x by using any of the explicit integration methods.

We will illustrate this by considering Gill's version of the fourth order R-K method. There are four stages (j=1 to 4) per time step At. Using the values of f(x, V) computed at the beginning of a time step, ki, x,, and q, are computed according to

Equations 13.17 with j=1. Then the algebraic equations 13.54 are solved with $x=x_1$ to compute V_1 and I_1. These are in turn used in Equations 13.17 to compute k_2, x_2), and 42. This process, involving alternating solutions of algebraic and differential equations, is applied successively with x_4 representing the solution at the end of each time step. During a switching operation, the network variables change instantly, but not the state variables.

Since the solution of differential equations requires values of network and state variables only from the previous step/stage, the differential equations may be partitioned in any way desired. For example, differential equations associated with each device may be solved independently. This offers considerable programming flexibility.

For solution of networks associated with large interconnected systems, the most efficient method is to use sparsity-oriented triangular factorization.

The partitioned approach with explicit integration is the traditional approach used widely in production-grade stability programs. Its advantages are programming flexibility and simplicity, reliability, and robustness. Its principal disadvantage is susceptibility to numerical instability. For a stiff system, a small time step is required throughout the solution period, as dictated by the smallest time constant (or eigenvalue).

B. Simultaneous Solution with implicit integration

In this approach [61], the state variables and the network variables are solved simultaneously. We will illustrate this using the trapezoidal rule.

With $x = x_n$ and $V = V_n$ at $t=t_n$, the solution of x at $t = t_{n+1}=t_n + \Delta t$ is given by applying the trapezoidal rule to solve Equation 3.44:

$$x_{n+1} = x_n + \frac{\Delta t}{2}\left[f\left(x_{n+1}, V_{n+1}\right) + f\left(x_n, V_n\right)\right] \tag{4.46}$$

From Equation 3.45, the solution of V at $t = t_{n+1}$ is:

$$I\left(x_{n+1}, V_{n+1}\right) = Y_N V_{n+1} \tag{4.47}$$

The vectors x_{n+1} and V_{n+1} are unknown. Let

$$F\left(x_{n+1},V_{n+1}\right)=x_{n+1}-x_n-\frac{\Delta t}{2}\left[f\left(x_{n+1},V_{n+1}\right)+f\left(x_n,V_n\right)\right] \tag{4.48}$$

and

$$G\left(x_{n+1},V_{n+1}\right)=Y_N V_{n+1}-I\left(x_{+1},V_{n+1}\right) \tag{4.49}$$

At solution,

$$F\left(x_{n+1},V_{n+1}\right)=0 \tag{4.50}$$

$$G\left(x_{n+1},V_{n+1}\right)=0 \tag{4.51}$$

Equations 3.50 and 3.51 are both nonlinear algebraic equations. Thus the differential equations have been made algebraic by using an implicit formula. These equations are very sparse; for computational efficiency it is necessary to take advantage of their special structure. Applying the Newton method to solve Equations 3.50 and 3.51, we may write for the $(k+1)^{st}$ iteration

$$\begin{bmatrix} x_{n+1}^{k+1} \\ V_{n+1}^{k+1} \end{bmatrix}=\begin{bmatrix} x_{n+1}^{k} \\ V_{n+1}^{k} \end{bmatrix}+\begin{bmatrix} \Delta x_{n+1}^{k} \\ \Delta V_{n+1}^{k} \end{bmatrix} \tag{4.52}$$

The following equation is solved to obtain Δx_{n+1}^{k} and ΔV_{n+1}^{k}:

$$\begin{bmatrix} -F\left(x_{n+1}^{k},V_{n+1}^{k}\right) \\ -G\left(x_{n+1}^{k},V_{n+1}^{k}\right) \end{bmatrix}=\begin{bmatrix} \dfrac{\partial F}{\partial x} & \dfrac{\partial F}{\partial V} \\ \dfrac{\partial G}{\partial x} & \dfrac{\partial G}{\partial V} \end{bmatrix}\begin{bmatrix} \Delta x_{n+1}^{k} \\ \Delta V_{n+1}^{k} \end{bmatrix} \tag{4.53}$$

The Jacobian in the above equation is computed at $x=x_{n+1}^{k}$ and $V=V_{n+1}^{k}$. It has the following structure:

$$J=\begin{bmatrix} \dfrac{\partial F}{\partial x} & \dfrac{\partial F}{\partial V} \\ \dfrac{\partial G}{\partial x} & \dfrac{\partial G}{\partial V} \end{bmatrix}=\begin{bmatrix} A_D & B_D \\ C_D & \left(Y_N+Y_D\right) \end{bmatrix} \tag{4.54}$$

The matrices A_D, B_D, C_D and Y_D are associated with the models for the dynamic devices and nonlinear static loads. For a system with m such devices, they have the following structures:

$$A_D = \begin{bmatrix} A_{d1} & 0 & \cdots & 0 \\ 0 & A_{d2} & \cdots & 0 \\ \vdots & \vdots & \ddots & \vdots \\ 0 & 0 & \cdots & A_{dm} \end{bmatrix} \quad B_D = \begin{bmatrix} B_{d1} \\ B_{d2} \\ \vdots \\ B_{dm} \end{bmatrix} \quad Y_D = \begin{bmatrix} Y_{d1} & 0 & \cdots & 0 \\ 0 & Y_{d2} & \cdots & 0 \\ \vdots & \vdots & \ddots & \vdots \\ 0 & 0 & \cdots & Y_{dm} \end{bmatrix}$$

$$CD = \begin{bmatrix} C_{d1} & C_{d2} & \cdots & C_{dm} \end{bmatrix}$$

The solutions of Equations 13.50 and 13.61 are given in terms of the above matrices by

$$A_D \Delta x_{n+1}^k + B_D \Delta V_{n+1}^k = -F\left(x_{n+1}^k, V_{n+1}^k\right) \square -F_{n+1}^k \tag{4.55}$$

$$C_D \Delta x_{n+1}^k + \left(Y_N + Y_D\right) \Delta V_{n+1}^k = -G\left(x_{n+1}^k, V_{n+1}^k\right) \square -G_{n+1}^k \tag{4.56}$$

In the above equations, k is the iteration counter and good starting values (x_{n+1}^0, V_{n+1}^0) are established by extrapolation. Also F_{n+1}^k and G_{n+1}^k are the residue vectors of the states and current injections, respectively.

From Equation 13.64, Δx_{n+1}^k can be expressed as a function of ΔV_{n+1}^k:

$$\Delta x_{n+1}^k = -A_D^{-1}\left[F_{n+1}^k + B_D \Delta V_{n+1}^k\right] \tag{4.57}$$

Substitution of Equation 13.66 into Equation 13.65 yields

$$\left(Y_N + Y_D - C_D A_D^{-1} B_D\right) \Delta V_{n+1}^k = -G_{n+1}^k + C_D A_D^{-1} F_{n+1}^K \tag{4.58}$$

Now ΔV_{n+1}^k and Δx_{n+1}^k can be calculated by solving Equations 3.57 and 3.58. Then x_{n+1}^{k+1} and V_{n+1}^{k+1} are obtained from Equation 3.52.

4.1.5 Treatment of discontinuities

Equations 3.55 and 3.56 are valid only when the functions given by Equations 3.48 and 3.49 are continuous and differentiable. At points of discontinuity, such as

network switching or limits on state variables, the exact formulation by the Newton method or any method requiring derivatives would be complicated [62]. This problem is dealt with in reference [61] as follows:

• For large network discontinuities, such as a network fault or switching operations, the integration method is temporarily changed to the fourth order Runge-Kutta method for one step at the point of discontinuity. This time step has a zero step size and is used only for the calculation of the postfault network conditions (the state vector is not updated). After this, the normal trapezoidal integration is resumed.

• For local non-differentiable functions, such as limits associated with controllers, the device Jacobians are computed by neglecting their effect. This is acceptable since they have only local impact and the overall convergence will not be significantly affected.

4.2 EQUATIONS OF MOTION

The equations of central importance in power system stability analysis are the rotational inertia equations describing the effect of unbalance between the electromagnetic torque and the mechanical torque of the individual machines. In this section, we will develop these equations in per unit form and define parameters that are used to represent mechanical characteristics of synchronous machines in stability studies.

4.2.1 Review of Mechanics of Motion

Before we develop the equations of motion of a synchronous machine, it is useful to review the quantities and relationships associated with the mechanics of motion. These are summarized in Table 4.1. Since it is easier to visualize quantities associated with rotation by analogy with those associated with the more familiar linear motion, the latter are also included in the table.

4.2.2 Swing Equation

As we are introducing new per unit equations and parameters, once again we temporarily resort to the use of superbars to identify per unit quantities.

When there is an unbalance between the torques acting on the rotor, the net torque causing acceleration (or deceleration) is

$$T_a = T_m - T_e \tag{4.59}$$

where

T_a = accelerating torque in N•m

T_m = mechanical torque in N•m

T_e = electromagnetic torque in N.m

In the above equation, T_m and T_e are positive for a generator and negative for a motor.

The combined inertia of the generator and prime mover is accelerated by the unbalance in the applied torques. Hence, the equation of motion is

$$J\frac{d\omega_m}{dt} = T_a = T_m - T_e \tag{4.60}$$

where

J = combined moment of inertia of generator and turbine, kg•m_2

ω_m = angular velocity of the rotor, mech. rad/s

t = time, s

Table 4.1 Summary of Lenear Motion and Rotation [17]

Linear Motion			Rotation		
Length	s	meter (m)	Angular displacement	θ	radian (rad)
Mass	M	kilogram (kg)	Moment of inertia	$J = \int r^2 dm$	kg-m^2
Velocity	$v = ds / dt$	meter/second (m/s)	Angular velocity	$\omega = d\theta / dt$	rad/s
Acceleration	$a = dv / dt$	m/s^2	Angular acceleration	$\alpha = d\omega / dt$	rad/s^2

Linear Motion			Rotation		
Force	$F = ma$	newton (N)	Torque	$T = J\alpha$	newton-meter (N-m) or J/rad
Work	$W = \int Fds$	joule (J)	Work	$W = \int Td\theta$	J, or W•s
Power	$p = \frac{dW}{dt} = Fv$	watt (W)	Power	$p = \frac{dW}{dt} = T\omega$	W

The above equation can be normalized in terms of per unit inertia constant H, defined as the kinetic energy in watt-seconds at rated speed divided by the VA base. Using Wom to denote rated angular velocity in mechanical radians per second, the inertia constant is:

$$H = \frac{1}{2}\frac{J\omega_{0m}^2}{VA_{base}} \tag{4.61}$$

The moment of inertia J in terms of H is

$$J = \frac{2H}{\omega_{0m}^2}VA_{base} \tag{4.62}$$

Substituting the above in Equation 3.60 gives

$$\frac{2H}{\omega_{0m}^2}VA_{base}\frac{d\omega_m}{dt} = T_m - T_e \tag{4.63}$$

Rearranging yields

$$2H\frac{d}{dt}\left(\frac{\omega_m}{\omega_{0m}}\right) = \frac{T_m - T_e}{VA_{base/\omega_{0m}}} \tag{4.64}$$

Noting that Tbase = VAbase/Wom, the equation of motion in per unit form is

$$2H\frac{d\omega_r}{dt} = T_m - T_e \tag{4.65}$$

In the above equation,

$$\bar{\omega}_r = \frac{\omega_M}{\omega_{0m}} = \frac{\omega_r / p_f}{\omega_0 / p_f} = \frac{\omega_r}{\omega_0} \tag{4.66}$$

where ω_r is angular velocity of the rotor in electrical rad/s, ω_0 is its rated value, and p_f is number of field poles.

If δ is the angular position of the rotor in electrical radians with respect to a synchronously rotating reference and δ_0 is its value at t=0,

$$\delta = \omega_r t - \omega_0 t + \delta_0 \tag{4.67}$$

Taking the time derivative, we have:

$$\frac{d\delta}{dt} = \omega_r - \omega_0 = \Delta\omega_r \tag{4.68}$$

and

$$\frac{d^2\delta}{dt^2} = \frac{d\omega_r}{dt} = \frac{d(\Delta\omega_r)}{dt} \tag{4.69}$$

$$\frac{d^2\delta}{dt^2} = \omega_0 \frac{d\bar{\omega}_r}{dt} = \omega_0 \frac{d(\Delta\bar{\omega}_r)}{dt} \tag{4.70}$$

Substituting for $d\omega_t / dt$ given by the above equation in Equation 3.65, we get:

$$\frac{2Hd^2\delta}{\omega_0 dt^2} = \bar{T}_m - \bar{T}_e \tag{4.71}$$

It is often desirable to include a component of damping torque, not accounted for in the calculation of T_e separately. This is accomplished by adding a term proportional to speed deviation in the above equation as follows:

$$\frac{2Hd^2\delta}{\omega_0 dt^2} = \bar{T}_m - \bar{T}_e - K_D \Delta\bar{\omega}_r \tag{4.72}$$

From Equation 3.68,

$$\Delta\omega_r = \frac{\Delta\omega_r}{\omega_0} = \frac{1}{\omega_0}\frac{d\delta}{dt} \tag{4.73}$$

Equation 3.72 represents the equation of motion of a synchronous machine. It is commonly referred to as the swing equation because it represents swings in rotor angle during disturbances.

4.2.3 Per Unit Moment of Inertia

Substituting in Equation 3.73 gives:

$$\frac{2H}{\omega_0}\frac{d^2\delta}{d\bar{t}^2} = \bar{T}_m - \bar{T}_e - \frac{K_D}{\omega_0}\frac{d\delta}{dt} \tag{4.74}$$

In Equations 3.73 and 3.74, K_D is the damping factor or coefficient in pu torque/pu speed deviation.

If it is desired to use per unit value of time $\underline{t}$, Equation 3.74 becomes

$$2H\omega_0\frac{d^2\delta}{d\bar{t}^2} = \bar{T}_m - \bar{T}_e - K_D\frac{d\delta}{d\bar{t}} \tag{4.75}$$

Some authors for example, reference 19] refer to $2H\omega_0$ as the per unit moment of inertia $\underline{J}$.

4.2.4 Mechanical Starting Time

From the equation 3.68 we can write as:

$$\frac{d\omega_r}{dt} = \frac{1}{2H}\bar{T}_a \tag{4.76}$$

Integrating with respect to time gives

$$\bar{\omega}_r = \frac{1}{2H}\int_0^t \bar{T}_a dt \tag{4.77}$$

Let T_M be the time required for rated torque to accelerate the rotor from standstill to rated speed. From Equation 3.206, with $\bar{\omega}_r$ = 1.0, $\bar{T}_a$ = 1.0 and with the starting value of $\bar{\omega}_r = 0$, we have:

$$1.0 = \frac{1}{2H}\int_0^{T_M} 1.0\,dt = \frac{T_M}{2H} \tag{4.78}$$

Therefore,

$$T_M = 2H \tag{4.79}$$

and T_M is called the mechanical starting time. The symbol M is also used in the literature to denote this time.

4.2.5 Calculation of Inertia Constant

The inertia constant is given by:

$$H = \frac{stored\ energy\ at\ rated\ speed\ in\ MW \cdot s}{MVA\ rating} \tag{4.80}$$

Calculation of H from moment of inertia in MKS units

Stored energy = kinetic energy

$$H = \frac{1}{2} J \omega_{0m}^2 \ \text{W•s} \tag{4.81}$$

$$H = \frac{1}{2} J \omega_{0m}^2 \times 10^{-6} \ \text{MW•s} \tag{4.82}$$

where

J = moment of inertia in kg•m2 wom

ω_{0m} = rated speed in mech. rad/s

$$H = 2\pi \frac{RPM}{60} \tag{4.83}$$

Therefore,

$$H = \frac{1}{2}\frac{J\omega_{0m}^2 \times 10^{-6}}{MVArating} \tag{4.84}$$

$$H = \frac{1}{2}\frac{J\left(2\pi RPM / 60\right)^2 \times 10^{-6}}{MVArating} \tag{4.85}$$

$$H = 5.48\times10^{-9}\frac{J\left(RPM\right)^2}{MVArating} \tag{4.86}$$

Sometimes the moment of inertia of the rotor is given in terms of WR^2, which is equal to the weight of rotating parts multiplied by the square of radians of gyration in lb•ft2. Then, moment of inertia in slug•ft^2-WR^2/32.2.

The following relationship between MKS units and English units is useful in converting WR^2 to J:

1 m = 3.281 ft

1 kg = 2.205 lb (mass)

1 slug•ft2 $= \frac{1}{0.0685\times3.281^2} = 1.356\ kg\cdot m^2$

The moment of inertia J in kg•m2 is related to WR^2 as follows:

$$J = \frac{WR^2}{32.2}\times1.356 \tag{4.87}$$

Substituting the above expression for J in Equation 3.86 gives

$$H = \frac{5.48\times10^{-9}\times1.356\left(WR^2\right)\left(RPM\right)^2}{MVArating\times32.2} \tag{4.88}$$

$$H = \frac{2.31\times10^{-10}\left(WR^2\right)\left(RPM\right)^2}{MVArating} \text{ in MW•s/MVA} \tag{4.89}$$

Table 4.2 gives the normal range within which the inertia constant H lies, for thermal and hydraulic generating units. The values of H given are in MW:s per MVA rating of the generator, and represent the combined inertia of the generator and the turbine.

Table 4.2 Normal range within which the inertia constant H lies

Type of generating unit	H
Thermal unit	
(a) 3600 r/min (2-pole)	*2.5* to 6.0
(b) 1800 r/min (4-pole)	4.0 to 10.0
Hydraulic unit	2.0 to 4.0

4.3 REPRESENTATION IN SYSTEM STUDIES

For analysis of power system dynamic performance, the component models are expressed in the state-space form or the block diagram form.

The state-space form requires the component models to be expressed as a set of first order differential equations. The swing equation 3.203, expressed as two first order differential equations, becomes

$$\frac{d\Delta\bar{\omega}_r}{dt} = \frac{1}{2H}(\bar{T}_m - \bar{T}_e - K_D\Delta\bar{\omega}_r \tag{4.90}$$

$$\frac{d\delta}{dt} = \omega_0\Delta\bar{\omega}_r \tag{4.91}$$

In the above equations, time t is in seconds, rotor angle δ is in electrical radians, and ω_0 is equal to $2\pi f$. When we use the above equations we will not use superbars to identify per unit quantities. We will assume the variables $\Delta\omega_r$, T_m and T_e to be in per unit. However, t will be expressed in seconds and ω_0 in electrical radians per second. While two-axis machine model used in the detail model in this research can be written as follows:

$$\frac{d\delta_i}{dt} = \omega_i - \omega_s \tag{4.92}$$

where δ_i is rotor angle of machine, ω_i is rotor speed of machine, and ω_s is rotor synchronous speed of machine

$$\frac{d\omega_i}{dt} = \frac{1}{M_i}[P_{mi} - (E'_{qi} - X'_{di}I_{di})I_{qi} - (E'_{di} + X'_{qi}I_{qi})I_{di} - D_i(\frac{d\delta_i}{dt})] \quad (4.93)$$

$$\frac{dE'_{qi}}{dt} = \frac{1}{T'_{doi}}[E_{fdi} - E'_{qi} - (X_{di} + X'_{di})I_{di}] \quad (4.94)$$

$$\frac{dE'_{di}}{dt} = \frac{1}{T'_{qoi}}[-E_{fdi} + (X_{qi} + X'_{qi})I_{qi}] \quad (4.95)$$

where M_i is moment of inertia of the machine, P_{mi} is machine mechanical power input, P_{mi} is machine mechanical power input, E'_{qi} is q-axis transient voltage, E'_{di} is d-axis transient voltage, I'_{qi} is q-axis transient current, I'_{di} is d-axis transient current, X_{qi} is q-axis synchronous reactance, X_{di} is d-axis synchronous reactance, X'_{qi} is q-axis transient reactance, and X'_{di} is d-axis transient reactance, T'_{qoi} is q-axis open-circuit time constant, and T'_{doi} is d-axis open-circuit time constant

$$E'_{qi} = V_i \cos(\delta_i - \theta_i) + R_{si}I_{qi} + X'_{di}I_{di} \quad (4.96)$$

$$E'_{di} = V_i \cos(\delta_i - \theta_i) + R_{si}I_{di} - X'_{qi}I_{qi}, \quad (4.97)$$

where V_i is machine terminal voltage, θ_i is machine angle, R_{si} is machine armature resistance, E'_{qi} is q-axis transient voltage, E'_{di} is d-axis transient voltage, I'_{qi} is q-axis transient current, I'_{di} is d-axis transient current, X'_{qi} is q-axis transient reactance, and X'_{di} is d-axis transient reactance.

CHAPTER 5

ADAPTIVE NEURO-FUZZY INTERFERENCE SYSTEM

5.1 ARTIFICIAL NEURAL NETWORKS

The artificial neural network (ANN) is a system that was improved to use for the data computation, the methodology is similar to the biological systems. It was designed like a brain of human that is able to process the information that is nonlinear and complex. It was developed to construct the systems of human brain like the architectural structure, operating techniques, and learning techniques. It is able to in parallel work, i.e., distributed, adaption, and local processin together. It is the reason why ANN is being adopted widely by researchers. Its ability and accuracy to develop any complicated nonlinear models and can be applied to resolve many large functions, particularly in the field of weather and climate. The sections below will explain the ANN and ANFIS capabilities, i.e., structure, modeling, and learning step [63].

5.1.1 Neuron Modeling

These neurons work as a tool, which is able to perform the information processing of human senses. It is explained that there are a lot of neurons that are connected to another one in the human brain. The system comprises one cell body [64], which the cell membrane covered the circumstances (Figure 5.1). There are many branches, dendrites namely, connected to each cell.

The dendritic functions as the information receiver and transmiting it into the cell body via the axon. The axon does function as transmitting signals from the cell body to neurons and next neurons. Its physical looks like a fiber. An interfacing point from the neurons to next neurons is in a small area between the axons and dendrites, it is called synapse. The synapse gap is used for receiving and transmitting the whole data. Any coming data would be computed in the pattern of electrical signal. The whole signals transmitting to the synapses would be calculated and counted. If the signals are unable to be separated, the synapses will be slowed down. The slowing synapses may be a result of connection problem between neurons. If electrical

signals coming without the limitation defined in the synapse, it will respond to another input electrical signal to be used for the next neurons.

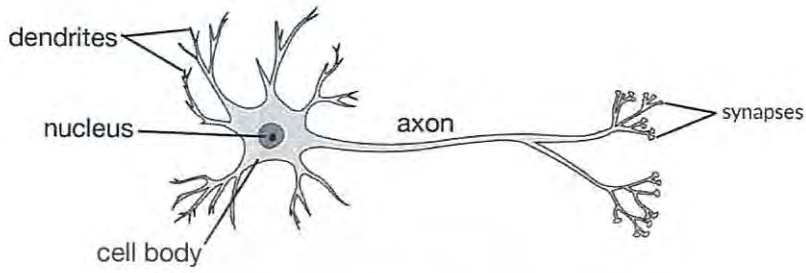

Figure 5.1 Schematic diagrams of biological neurons [64]

In reference with the biological neuron model, [65] proposed a neuron model, which has the transmission and receipt characteristics of information process similar to the step happening in the biological neuron. The neurons' mathematical models that are generally used for the ANN is shown in Figure 5.2. The neuron model becomes a reference for the ANN improvement right now. A neuron will take role for operating the network and determining the function. The modeling based on Figure 5.2 can be described by the following mathematical equation:

$$u_{(k)} = \sum_{j=1}^{n} w_{ki} x_i \text{ and } y_{(k)} = \varphi(u_{(k)}) + b_{(k)} \qquad (5.2)$$

where $u_{(k)}$ is the output obtained from the function model, w_{kj} is the weighted value in synapse path j to k neuron, x_j is input signal on path synapse j, and $y_{(k)}$ is the neuron out, depending on the function of activation $\varphi(\cdot)$ and the bias $b_{(k)}$. There are a lot of types of activation functions, which are used in the neuron modelling, some are sigmoid function, linear function, bipolar sigmoid function, and limiter function [66, 67].

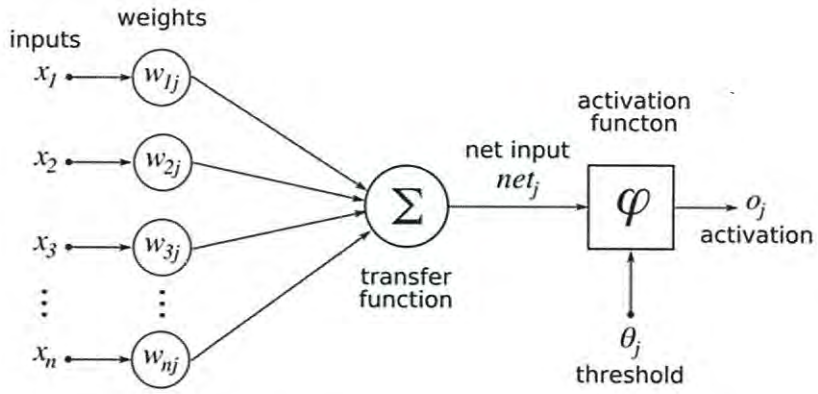

Figure 5.2 Neuron mathematical modeling

5.1.2 Architecture

The interconnections from neuron to other neurons are in a layer form. The architecture of ANN generally comprises 3 layers. The 1st layer, we call it as the layer of input. It is like an input or data receiver from the outside boundary. The amount of neurons in the layer is perhaps greater than once. The income data will be transmitted into the subsequent layer. It has no related rules to determine the amount of neurons. The amount relies on the amount of input in that network. The subsequent layer, we call it as hidden layer. There can be one or more neurons in the hidden layer, it is up to the complexity and suitability of each case. The hidden layer comprises neurons, which is able to get electrical signal or data than the input layer. The electrical signal or data that transmits to the layers will be computed with available functions available, i.e., mathematics and arithmetic, etc. The layer's processing results are next transmitted to the output layer. The output layer will be determining the data validity, which are computed based on the limitation that is existing in activation functions. The layer's output may be used as a the outcome determinant.

Refer to the form of interconnections of neurons in the ANN, generally its architecture can be mainly classified into 2 types, i.e., 1) feedback neural network (NN) and 2) feed-forward NN [68, 64].

The feedback NN is a type of ANN. Its architectural has feedbacks coming from the before layer. The electrical signals or data that are permitted to feedback and propagate forward are able to be the neurons' input. The network is normally used

for the dynamic applications, i.e., adaptive control. Jordan network, Elman network, and Hopfield networks are in the part of ANNs applying with the feedback NN.

An architecture other than above is the feed-forward NN. The feed-forward NN is a type of ANN. The design is similar to the feedback NN architecture. Nevertheless, there is no additional feedback in the architecture like as the feed-forward NN. The incoming signals or data are permitted just to transmit in only once direction, none of feedback. The each layer's output will not affect the before layer. Normally, we can improve the architecture by applying multiple layers or only a single layer into the structure. Generally, the multi-layer element comprises 3 layers, i.e., 1) the input layer, 2) the output layer, and 3) the hidden layer as mentioned above. The hidden layer element In any multi-layer will do an increasing in the ability of calculating power. The radial basis function, multi-layer perceptron, and one-layer perceptron are a part of ANN types applying the feed-forward NNs.

5.1.3 Algorithm of Learning

The ANN algorithm for learning is like the process of the value and parameter modifications in the network. The learning algorithm application allows ANN to assembly themselves to get the compatible responses for the network's input. During the process of learning, in the network the weights and parameters of synapses will be adjusted. It is a response feeding to the input inducement to the output generated according to the needed output. The learning level will end once the final output becomes steady subject to the needed output.

There are five steps required to do for the preliminary design of algorithm of learning as follows [68].

1) Learning paradigm: It is with respect to a process that the designer have to select the process of learning in compliance with the circumstances of data.

2) Learning algorithm: It is with respect to the learning rule, which is applied with the modification of synapse weights and variables in the ANN series.

3) To evaluate how many networks can be learned.

4) To evaluate how many sets of sample are needed for the training.

5) To evaluate how fast the system can learn.

With reference to the learning type in the ANN, there are 2 types of learning processes adopted widely, called the supervised learning and the unsupervised

learning. Apparent differences between the supervised learning and the unsupervised learning depends on the data transmitted from that network. Generally for the supervised learning, the data provided to it is in the pattern of sample sets that have already been labeled or marked. But the unsupervised learning, it is opposite. Hence, for the unsupervised learning, it works randomly.

In the unsupervised learning, it has no target output or guidelines within the algorithm of learning. The network would just receive a number of sampling inputs, and putting the samples to category or classes. The characteristics of producting class response will be similar to the input stimulus when the stimulus is determined and sent into the input layer. In opposite, the network will newly create a coding that is led to a new category or class [64].

On the other hand, the supervised learning, any patterns which are determined and sent to the network, are as their output. Each of incoming signals sent to a single neuron would keep spreading along the whole structure until the the final layer's last neuron. The pattern of output in the output layer would be produced and be compared to the needed output pattern. It depends on an error signal in that comparison process between the patterns of output produced by patterns of the needed output. The process needs to be adopt and the weights of network need to be adjusted in order that the actual output will be in line with the needed output.

5.2 ADAPTIVE NEURO-FUZZY INTERFERENCE SYSTEM

The modification of ANFIS is a merging approach from 2 methods of fuzzy logic and ANN [69, 70]. The fuzzy logic is capable of changing the qualitative parameters based on human's experience and knowledge, as well as the human's understanding to the accurate quantitative analysis process. Nevertheless, there is no specified approach used for a fixed guideline for the transformation process and human for the rule base fuzzy inference system, as well as in addition, the adjustment of membership functions takes a long time. While the ANN approach has a greater ability in the learning and adjusting its structure to the suitable conditions. Hence, the ANN will be applied for automatical adjustment of the membership functions and to decrease the error rate in the rule determination in the fuzzy logic. The ANN and

fuzzy logic is therefore combined into the ANFIS. This section will describe the ANFIS architecture, the fuzzy inference system, flexibility, and basic learning algorithm.

5.2.1 Fuzzy Interference System

The ANFIS is developed based on 3 elements mainly, called 'basic rule'. Firstly, we need to choose the fuzzy logic rule for the fuzzy membership's functions and fuzzy inference techniques for the basic rule to obtain the result. The mentioned rule is comprises of a conditional statement 'If-Then' and fuzzy logical operators. The basic rule can be built from either automatic generation or a human. There are a lot of types of fuzzy interference system, i.e. Takagi-Sugeno, Mamdani, and Tsukamoto. However, the fuzzy inference system using the Takagi–Sugeno model is widely used in the application of ANFIS method. The fuzzy inference system would operate when the input containing the real value is transformed to the fuzzy values by the process, in which it is in the range of from zero to one. A part of the accuracy depends on databases and basic rule that come from the human's knowledge, understanding, and experience, in which both are significant parts for the making decision. Generally, the databases comprise definitions, i.e., the data on fuzzy parameters with functions, which have been specified for all existing linguistic parameters. The database improvement typically comprises definition of a universe, determination of the amount of linguistic values for each linguistic variable, and establishment of a membership function.

5.2.2 Adjustable Network

The adjustable network is an instance for the feed-forward NN having multi-layers as shown in Figure 5.3. The NN usually used is the supervised learning algorithm for the learning algorithm. Moreover, the network's architectural characteristic comprise many direct connected adaptive nodes with none of weight values. Each node has various tasks and functions in the network, its output relies on the input values and variables inside of that node. A rule applied for the learning can significantly take an effect of parameter adjustment and also able to reduce the error happening at the adjustable network's final result [69].

In the basic learning, normally the gradient descent or the back propagation with chain rule is used for the adjustable network. All of this learning process was

presented by [69, 63]. Up to now, the learning process by both of back propagation and gradient descent are still generally used in any adjustable network. Although, some weaknesse was found in the back propagation and can decrease in the decision capacity and result's precision. The convergence slowly and stucking in a local area frequently are the main troubles of the learning algorithm using back propagation. However, a method, called hybrid algorithm, proposed for the ANFIS learning process was presented [69]. It can obviously give us a greater capability. It can speed the convergence of final result and avoid stucking in a local area significantly.

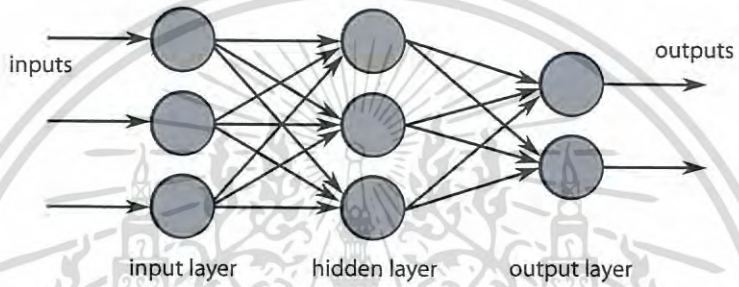

Figure 5.3 adjustable network [63]

5.2.3 ANFIS Architecture

We can see the mechanism for the architecture of ANFIS and the Takagi–Sugeno model as Figure 5.4. The ANFIS is deemed as an adjustable network, for which the supervised learning is applied for its algorithm. The system has main functions like as the'Takagi-Sugeno' fuzzy inference system. To be ease, assuming that the structure has 1 output named f and only 2 inputs, named x and y. Only 2 rules are applied in the base rule:

Rule no.1: If x is A_1 and y is B_1 Then $f_1 = p_1x+q_1x+r_1$

Rule no.2: If x is A_2 and y is B_2 Then $f_2 = p_2y+q_2y+r_2$

where A_1, A_2 and B_1, B_2 are the each input's membership functions and p_1, q_1, r_1 and p_2, q_2, r_2 are the linear parameters in the consequent part.

With reference to the Figure 5.4, the structure of ANFIS consists of totally 5 layers. The 1st layer and the 4th layer comprise only one adaptive node. Each of all

remaining four layers comprise one fixed node. The each layer's description are briefed as follows:

Layer 1: All nodes of the layer are comprised of function parameters. The output of each node is like as the membership value degree, which comes from the membership function input. For instance, the membership function can be the Gaussian as Equation 4.2 or the generalized bell as Equation 4.3, or other.

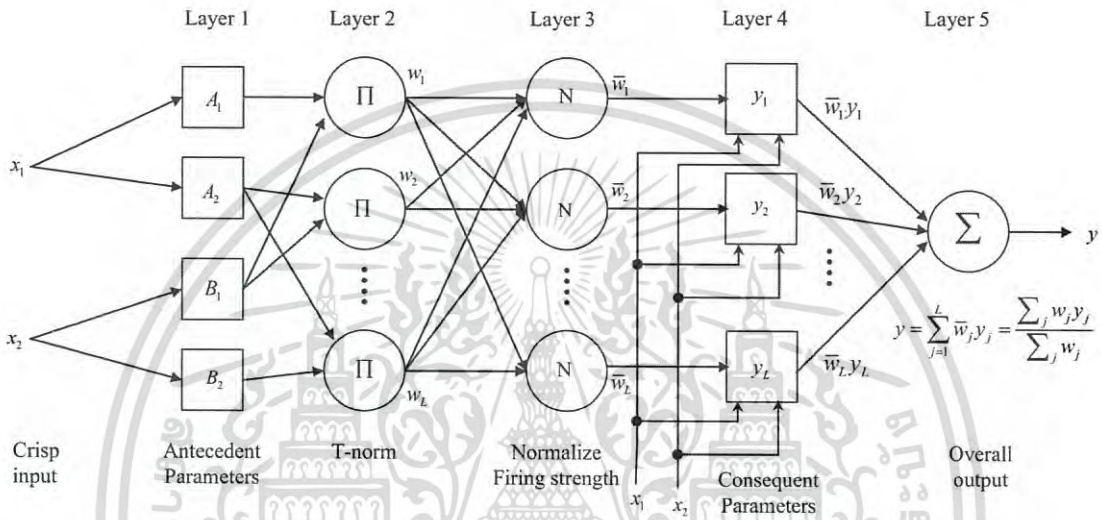

Figure 5.4 (a) Fuzzy interference system and fuzzy logic mechanism of Sugeno. (b) Architecture of ANFIS **[63]**

$$\mu_{Ai}(x) = \exp\left[-\left(\frac{x-c_i}{2a_i}\right)\right] \tag{5.2}$$

$$\mu_{Ai}(x) = \frac{1}{1+\left|\frac{x-c_i}{a_i}\right|^{2b}} \tag{5.3}$$

where $\{a_i, b_i, c_i\}$ are the membership function's parameters which is able to change the function shape. The said parameters are mentioned as premise parameters and μ_{Ai} and μ_{Bi-2} are the membership function's degrees for the fuzzy sets of A_i and B_i, respectively.

$$O_{1,i} = \mu_{Ai}(x) \; i = 1,2 \tag{5.4}$$

$$O_{1,i} = \mu_{Bi-2}(y) \; i = 3,4 \tag{5.5}$$

Layer 2 : All nodes here are fixed. Each node of the layer sends the output called the firing strength for each rule. In this layer, the T-norm operator with normal performance, as '&', is used to get the output. The output comes from the multiplying of signals inputting into the node and sent out to the subsequent nodes.

$$O_{2i} = w_i = \mu_{Ai}(x) * \mu_{Bi}(y) \; i = 1,2 \tag{5.6}$$

where w_i is the firing strength output.

Layer 3: All nodes of the layer are nonadaptive. The output of this layer is called normalized firing strength. Each node's output is the ratios between the rule's firing strength and the summation of all firing strengths of the whole rules.

$$O_{3i} = \overline{w}_i = \frac{w_i}{\sum_i w_i} \tag{5.7}$$

Layer 4: All nodes of the layer are adaptive nodes having a node function defined n in equation as:

$$O_{4i} = \overline{w}_i f_i = \overline{w}_i (p_i x + q_i y + r_i) \tag{5.8}$$

where ($p_i x + q_i y + r_i$) is a parameter of the node. The parameters of the layer are mentioned as the consequent parameters. $\overline{w}_i$ is the normalized firing strength obtained from the previous layer.

Layer 5: All single nodes here are nonadaptive, which calculates from the summation of every input signals coming from the before node.

$$O_{5i} = \sum_i \overline{w}_i f_i = \frac{\sum_i w_i f_i}{\sum_i w_i} \tag{5.9}$$

5.2.4 Hybrid Learning Algorithm

The 1st layer and the 4th layer are comprised of parameters which are able to be modified all the time. As described above, there is the nonlinear premises parameter in the 1st layer and there are linear consequent parameters in the 4th layer. A hybrid algorithm presented here would be applied in this research for training the parameters. For adjusting both of the parameters during the learning process that is capable of training both of the parameters and adjust to its circumstance, we apply this hybrid algorithm due to the back-propagation algorithm applied for training the parameters exists in the adjustable network particularly discovered in a convergence of result slowly and be stucking in a local area.

It has two sections of the hybrid algorithm, one is called backward path and another one is called forward path. For the forward path, parameters of the premises in the 1st layer are to be consistent. We use a recursive least square estimator (RLSE) to fix the consequent parameter in the 4th layer. Due to the consequent parameters are linear, the RLSE method is, thus, able to be used for speeding the rate of convergence and process of hybrid learning. Afterward we get the consequent parameters, the input data will be sent back to the input of adjustable network, and the output produced from the network will be compared to the real result.

In the other hand, while the backward path is running, the consequent parameters are to be constant. The errors happened during the comparison between the output produced with the actual output is propagated back to the first layer. In the mean time, the premises parameter in the 1st layer are adjusted using the learning methods of back propagation or gradient descent method. With the application of hybrid learning algorithm combining RSLE and the gradient descent approaches, it can guarantee that the convergence rate is quicker due to it is able to deduct the space of dimensional searching in the original approach of back-propagation [63]. Table 5.1 briefly shows a hybrid learning process in the ANFIS.

Table 5.1 Hybrid learning process for each type

Type	Path forwards	Path backwards
Signal	Node of Output	Error rate
Consequent Parameter	RSLE	Fixed
Premise Parameter	Fixed	Gradient Descent

5.2.5 Back Propagation Learning

The premise parameters in the Equation 4.3 and Equation 4.4 are adjustable parameters, which they could get trained to obtain the parameter values according to their circumstance. If to have an adjustable network, in which the network comprises totally 5 layers and there is total of N(L) node in the layer-L, the amount of square error in the layer L to p data is $1 \le p \le N$. It can be written as the following equation [69, 63]:

$$E_p = \sum_{k=1}^{N(L)} d_k - X_{k,p}^L \tag{5.10}$$

where d_k is the k-th the vector component of the needed output, while $X_{k,p}^L$ is k-th the vector component of real output produced by adjustable network with input obtained from the input vector *p*. The objective of adaptive learning system is mainly to decrease errors occurring in the Equation 4.10.

The early learning stage starts from the calculation of output's error rate *i-th* node and *L* layer, as the following equation:

$$\varepsilon_{L,i} = \frac{\partial E_P}{\partial_{i,p}^L} = -2\left(d_{i,p} - X_{i,p}^L\right) \tag{5.11}$$

For the nodes inside of the layer l at the position *i*, the rate of error could be computed applying the Chain Rule as the equation below:

$$\frac{\partial E_p}{\partial X_{l,i}} = \sum_{m=1}^{N(l+1)} \frac{\partial E_p}{\partial X_{m,p}^{l+1}} \frac{\partial x^*}{\partial \alpha} \tag{5.12}$$

with $0 \le l \le L-1$. The internal error is explained as a linear combination of the rate of error in the $l(l+1)$ layer node. The equation 4.12 is applied to compute the error signal at the layer node *i-th* to $l(l < L)$, while the use of equation 4.12 to reach the final layer. It can be written in the following equation:

$$\frac{\partial E_P}{\partial \alpha} = \sum_{x^* \in S} \frac{\partial E_P}{\partial x^*} \frac{\partial x^*}{\partial \alpha} \tag{5.13}$$

where S is the set of nodes comprising the parameter a, thus that the whole issues of measurement error can be written as the equation below:

$$\frac{\partial E}{\partial \alpha} = \sum_{p=1}^{p} \frac{\partial E_P}{\partial \alpha} \tag{5.14}$$

with the approach of steepest gradient descent, the equation for repairing parameter a can be written as follows:

$$\Delta\alpha = -\eta \frac{\partial E}{\partial \alpha} \tag{5.15}$$

with η is the learning rate and it can be written in the following equation:

$$\eta = \frac{k}{\sqrt{\sum \alpha \left(\frac{\partial E}{\partial \alpha} \right)^2}} \tag{5.16}$$

and k is the size of step that can be adjusted to speed up the rate of result convergence in the adjustable network.

5.2.6 Learning to Parameter Consequent RSLE

When the premises parameter become constant, all output obtained from the consequent parameters can be described in the following combined linear equation [69]:

$$\begin{aligned} f &= \overline{w}_1 f_1 + \overline{w}_2 f_2 \qquad (5.17) \\ &= \overline{w}_1 (p_1 x + q_1 y + r_1) + \overline{w}_2 (p_2 x + q_2 y + r_2) \\ &= (\overline{w}_1 x) p_1 + (\overline{w}_1 y) q_1 + (\overline{w}_1) r_1 + (\overline{w}_2 x) p_2 + (\overline{w}_2 y) q_2) + (\overline{w}_2) r_2 \end{aligned}$$

When N training data is sent to equation 4.17, the equation will be obtained as follows:

$$\begin{aligned}(\overline{w}_1 x)_1 p_1 + (\overline{w}_1 y)_1 q_1 + (\overline{w}_1)_1 r_1 + (\overline{w}_2 x)_2 p_2 + (\overline{w}_2 y)_2 q_2 + (\overline{w}_2)_2 r_2 = f_1 \qquad (5.18)\\ \vdots \\ \vdots \\ (\overline{w}_n x)_n p_n + (\overline{w}_n y)_n q_n + (\overline{w}_n)_n r_n + (\overline{w}_n x)_n p_n + (\overline{w}_n y)_n q_n + (\overline{w}_n)_n r_n = f_n\end{aligned}$$

The equation 2.18 can be simplified in the matrix as the following equation:

$$f \quad A\theta = y \qquad (5.19)$$

where θ is the vector M × 1. M refers to the amount of components, which are the set of consequent parameter. While A is the vector P × M, in which P is the amount of N data training provided for the adjustable network and y is the vector P × 1 of output, their elements are N number of output data. Generally, the number of training data will be bigger than the amount of consequent parameters, thus the best solution for θ is to minimize the squared error $\|A\theta = y^2\|$ By the least squares estimator (LSE), the equation for θ can be written as the following:

$$f \quad \theta^* = \left(A^T A\right)^{-1} A^T y \qquad (5.20)$$

where A^T is the inverse of A and if not singular, $(A^T A^{-1})$ is its the pseudo-inverse. To use the RLSE method, It can be written in the following equation:

$$f \left.\begin{aligned} \theta_{i+1} &= \theta_i + P_{i+1} a_{i+1} \left(y_{i+1}^T - a_{i+1}^T \theta_i\right) \\ P_{i+1} &= P_i - \frac{P_i + a_i + 1 a_{i+1}^T P_i}{1 + a_{i+1}^T P_i a_{i+1}}, \qquad i = 0,1...,P-1 \end{aligned}\right\} \qquad (5.21)$$

where a_i^T is a row vector of the matrix A in the equation 4.19, y_i is i-th element of y. P_i, is a covariance matrix. It can be written in the following equation:

$$f\ \theta^* = \left(A^T A\right)^{-1} A^T y \qquad (5.22)$$

5.2.7 Linear Regression

Generally, the regression is an approach that is able to give us the data regarding the relationships between variables. In the regression approach, the variables can be divided into 2 types: 1) dependent variables, the variables impacted by other variables, generally represented by Y, and 2) predictor variables, they are called as independent variables that does not get effects from other variables, generally they are represented by X [63].

The main objective of the regression analysis is for creating a mathematical model, which is able to be used for forecasting the dependent variable values based on any variables values The regression analysis is separated into 2 simple linear and multiple linear regressions. The analysis of simple regression is a relationship between two variables that are independent and the dependent variables. For the analysis of multiple linear regression, the relationship is discovered between 3 or more variables containing at least one dependent variable and 2 independent variables.

For the multiple linear regressions, the equation comprising 2 or more variables can be written as follows:

$$f\ Y = \beta_0 + \beta_1 X_1 + \beta_2 X_2 + \beta_m X_m, \quad m = 1, 2, 3, ..., n \qquad (5.23)$$

where β_0 is a cut-off and $\beta_1 ... \beta_m$ are the coefficients of regression and the regression coefficient in equation 4.23. The least squares method is frequently used to obtain the values of the intercept [63].

CHAPTER 6

IMPLEMENTATION

6.1 IMPLEMENTATION

In this study, the critical clearing time (CCT) is focused as it is an important factor in maintaining the system stability. As we have described in the previous section, there are many methods to resolve the CCT (e.g. time domain simulation, transient energy function, and equal-area criterion). But the time-domain method is taken into account as the most precise result, and it is also able to be applied with unlimited models of machines, generators, turbines, controllers, and loads. Nevertheless, the obtained result using the time domain method is quite complicated and takes a long time to compute, as there are many multiple nonlinear differential-algebraic equations (DAEs).

In this implementation, we start with the transient simulation subject to various models to see what difference happen. Conventionally, the method used for evaluating the CCT is the classical model approach, wherein most dynamics of a power system are ignored. However, in reality, there are many electronic control devices installed in the system (e.g. AVR and governor). If an accurate result is required, the effect of the electronic control device, machine, and load is to be taken into account. How much the transient evaluation impacts results can be determined using the following approaches:

- Classical model
- Detailed model considering machine model and AVR
- Detailed model considering models of machine, AVR, and governor
- Detailed model considering models of machine, AVR, governor, and load characteristic

We apply the three-phase balanced fault to the bus 3 in the IEEE 39-bus system at t = 1 second and the fault elimination is done at t = 1.180 second. These faults are applied to the four approaches subject to the same conditions. The generators' rotor angle relative to the slack bus's angle for the four approaches are plotted in Figure 6.1 to 6.4, respectively.

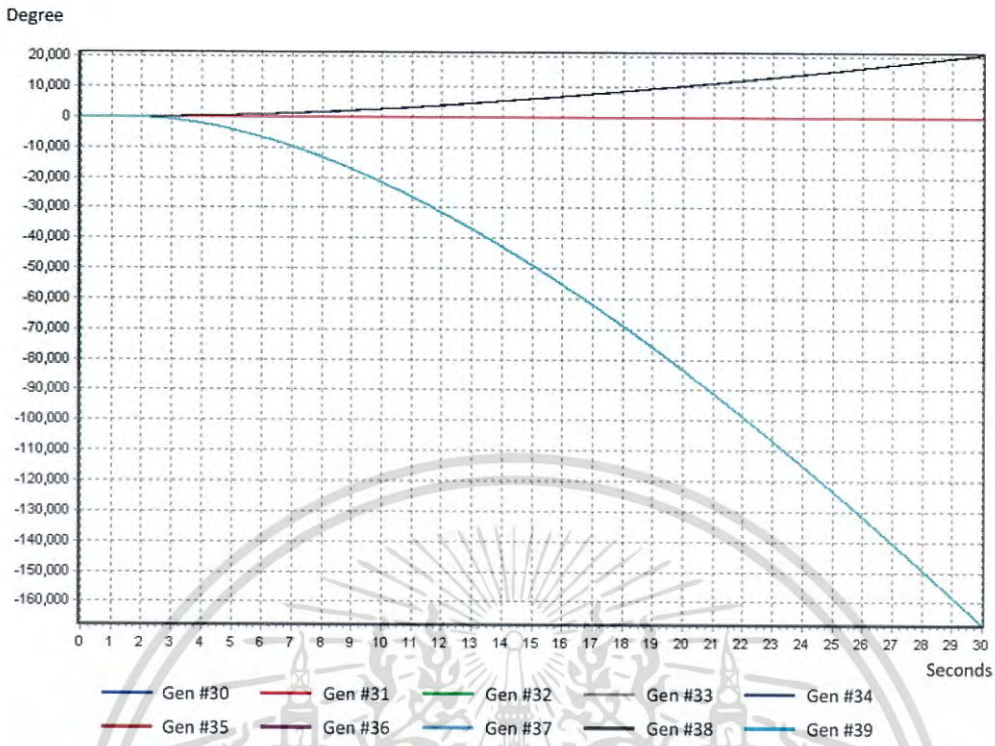

Figure 6.1 Rotor angles: classical model

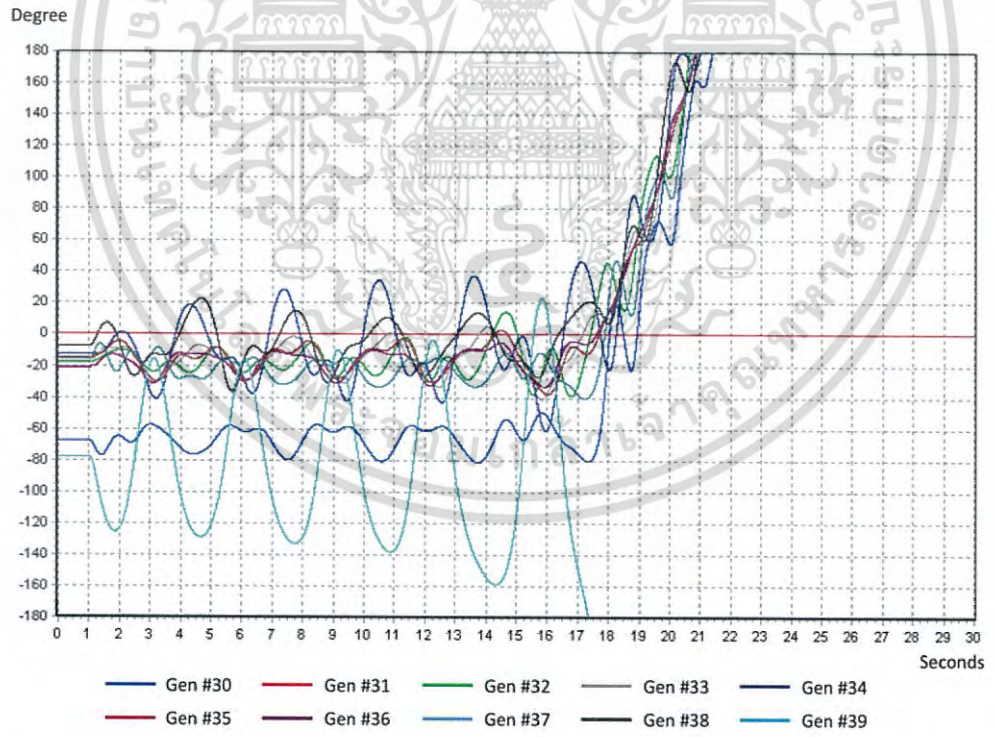

Figure 6.2 Rotor angles: detailed model considering the machine model and AVR

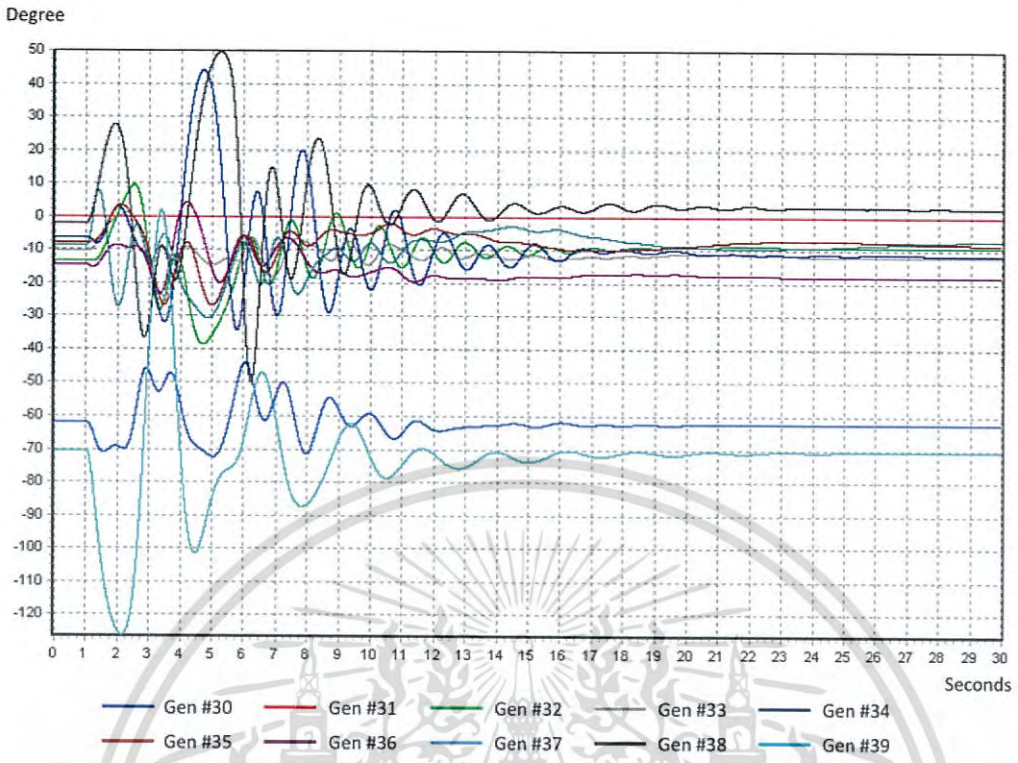

Figure 6.3 Rotor angles: detailed model considering the machine model, AVR, and governor

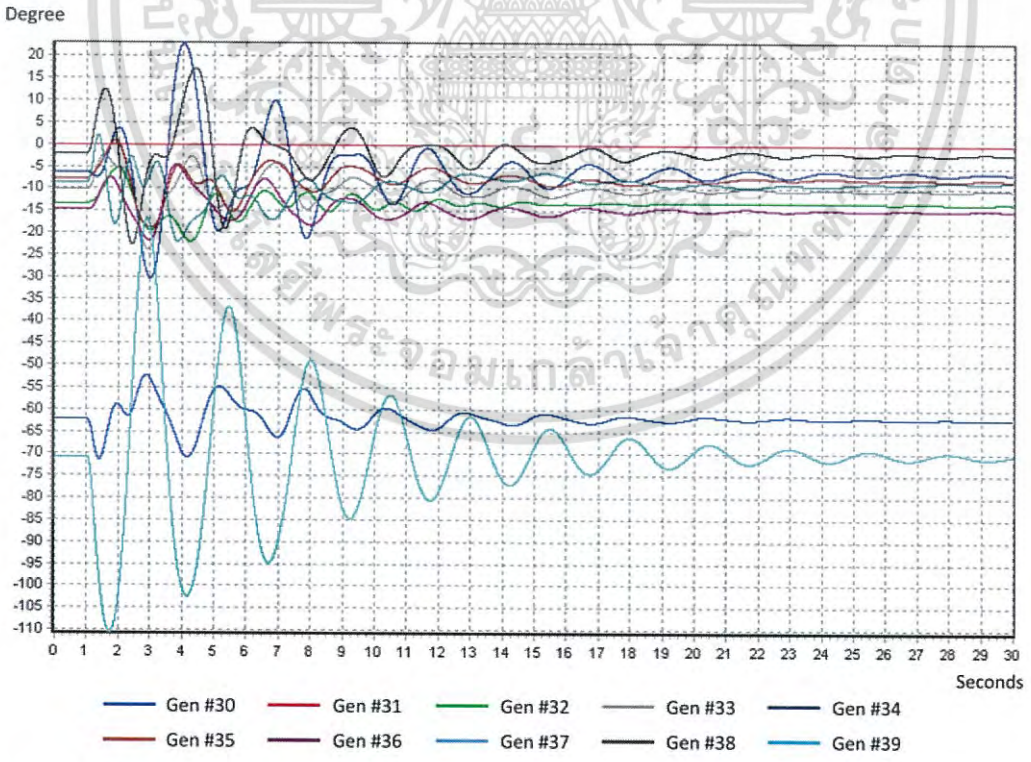

Figure 6.4 Rotor angles: detailed model considering the machine model, AVR, governor, and load characteristic

From the plotted curves, we can see that if the power dynamic system is simulated using the classical model, the power system becomes unstable; all generators' rotor angles are quickly divergent. However, the classical representative for the power system illustrated in the Figure 6.1 is valid for only 2-3 seconds after the transient initiation. If simulated using a detailed model by considering only the machine behavior and AVR, all generators' rotor angles are divergent at approximate 17 s. If simulating using a detailed model considering the machine behavior, AVR, and governor, we can see that the power system can settle back smoothly to the steady-state condition. However, if simulating using a detailed model considering the machine behavior, AVR, governor, and load characteristic, we can see the power system can settle back to the steady state also but takes more time than the detailed model considering only the machine model, AVR, and governor. The CCT of each case is shown in the Table 6.1. Obviously, it shows that the factors of governor and load characteristic significantly affect the different results for transient assessment in this case.

Table 6.1 Difference of CCT from simulation considering each model

Case	Modeling	CCT
1	Classical model	131 ms
2	Machine model, AVR	169 ms
3	Machine model, AVR, governor	291 ms
4	Machine model, AVR, governor, load	180 ms

Thus in this study, we take into account all the significant effects of dynamic factors; not only the machine behavior but also the AVR, turbine governor, and load characteristic are considered for the prediction of CCT in detail. In addition, we apply various types of AVR model and governor model in each bus of systems as well. The solution using time domain for such systems is applied with the detailed model and having various models for each bus. Certainly, the equation would be very complicated and would take much time for calculation. Figure 6.5 illustrates the process of implementation in this study.

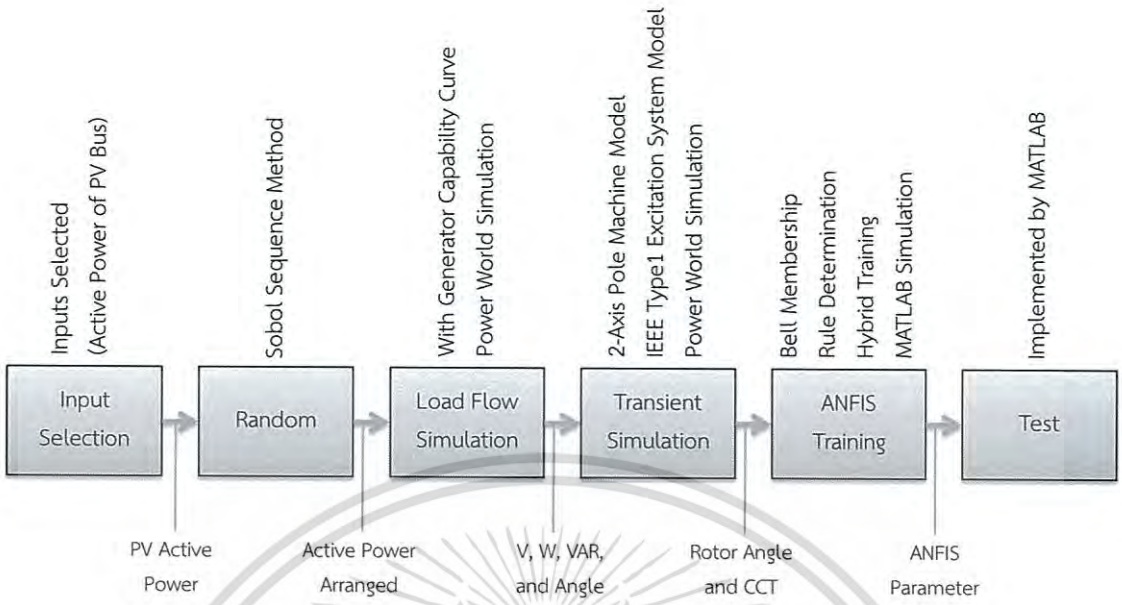

Figure 6.5 Implementation process

In the first step of implementation, the appropriated inputs shall be selected for the system. Herein, the active power and reactive power of all PV buses are considered to be the inputs for CCT prediction. Since practically, all power plants connected to the national gird, there would normally be the signals sending the analog data of active power and reactive power to the national grid control center through SCADA system. On the other hand, it is not easy to obtain all updated accurate statuses of loads in the system in real-time as well as all dynamic parameters. Thus, we selected the values of active power and reactive power of all PV buses to be as the ANFIS inputs and we get the CCT as the ANFIS output as the outline shown in Figure 6.6. Hence, we could use those signals for the prediction practically.

The second step: as we know, there shall be at least a bus in the system running the synchronous machines in the frequency mode acting as the slack bus to balance the generation system with the loads and losses. Also, the active power and reactive power at the slack bus shall be set free, not fixed. Also the reactive power of each PV bus will not fixed as it would affect the system voltage, especially the bus having large synchronous machine connected. Thus, the active power of slack bus and the reactive power of all PV buses shall be generated

from the exact calculation. This step, we random of active power of all PV bus, except the active power at the slack bus.

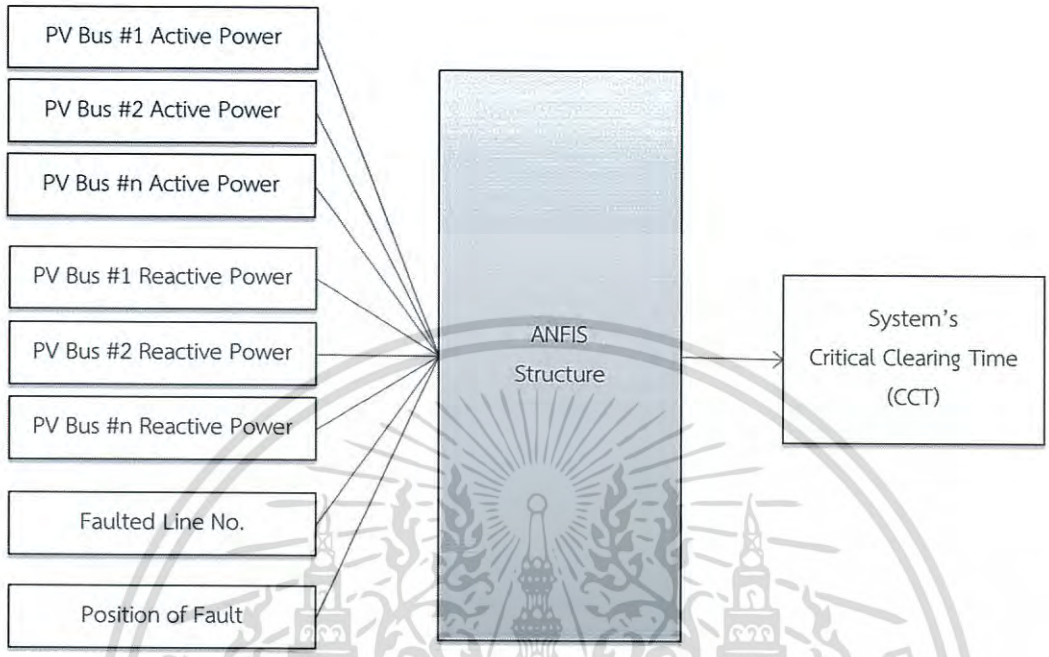

Figure 6.6 Input and Output Structure

The ANFIS structure will be more effective if the learning quality is good. The learning quality depends on the training data applied to the ANFIS. The ANFIS training should cover all areas that may occurs for all cases. Herein, the quality of input and output distribution are a main factor and shall be considered. However, since the active power of slack bus and the reactive power of all PV buses that to be the ANFIS inputs shall come from the calculation, thus the distribution of these input may be unable to be directly controlled. But the distribution of the remaining inputs can be controlled through a mathematical approach.

In this research, we use the sobol sequences for the ANFIS input random. Generally, a sample randomly would be created by a pseudo-random generator that is provided from a lot of software [71]. A sample is distributed randomly in a specified interval. The sobol sequences are for producing a sample being distributed over the unit cube uniformly [72, 73, 74]. The sobol sequence belongs to the family of quasi-random sequences. The quasi-random sequences are

developed to produce the sampling points of multiple parameters over the multi-dimensional parameter space uniformly as much as possible. The significant difference of the pseudo-random numbers is that the sampling values are selected under consideration of the previous sampling points to avoid the happening of any gap and cluster. The sobol sequences' sampling is developed to produce samples subject to the low discrepancy. The sampling points generated by the sobol sequences' sampling are distributed more evenly than the sampling points generated by the other sampling techniques. The discrepancy in the multi-dimensional space is quite better if compared to the other sampling methods. The variance and mean can be computed in the similar manner as the other sampling methods. Figure 6.7 shows some samples of distribution of inputs that are random by Sobol Sequence technique for 39 bus implementation in this study.

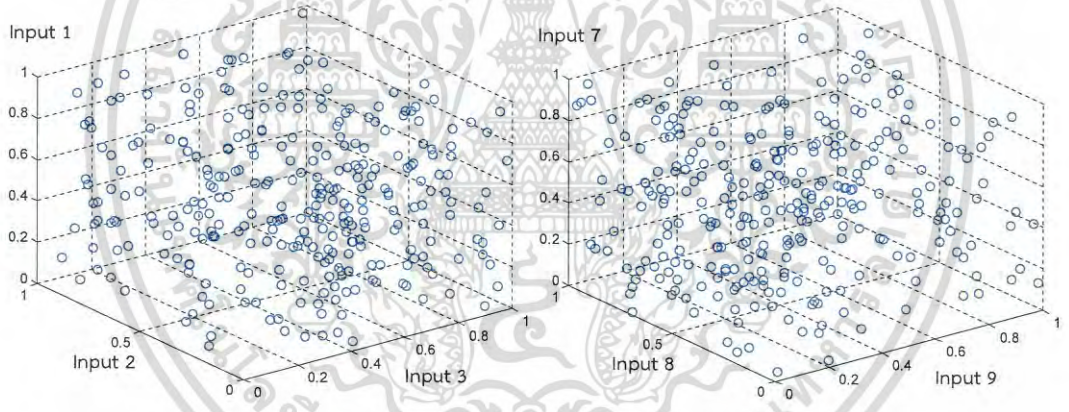

Figure 6.7 Inputs Distribution Random by Sobol Sequence of This Study

In this step, we will have inputs of active power at all PV buses, except the active power at the slack bus. We take the said inputs for the power flow simulation to solve the active power at the slack bus and all reactive power at all PV buses. In this process, the dynamic parameters are not used. Only load, voltage, active power, reactive power, impedance, and angle of all synchronous machines, buses, transmission lines, distribution systems, loads, and some equipment are considered. Also the active power and reactive power at the load buses in the study areas are varied by Sobol Sequence between 70% - 110% of the base load to have various case covering all learning. The power factor of all

generators is set as free so the reactive power would not depend on the active power. The power world simulation software Version 17 [75] will be used for the load flow simulation.

However, other than the considered parameters mentioned, to be realistic in this study, we also considered the transmission line constraint, i.e., current capability and power flow limitation. Also, the generator capability curve, i.e., stator heating limit, rotor heating limit, stability limit, zero field current limit, and core end heating limit are also considered in this study. Table 6.2 shows an example of results difference in this study for the case considering the generator capability curve and not considering the generator capability curve. Certainly, the equation relation will be more complex with a lot of further constrain equations.

Table 6.2 Difference of results regardless of generator capability curve

No.	Description	Unit	No Cap. Curve	Cap. Curve
1	Active Power (Gen32)	MW	712.9	712.9
2	Reactive Power (Gen32)	MVar	223.2	205.5
3	PV Bus Voltage (Bus32)	kV	13.6	13.4
4	Power Factor (Gen32)	-	0.95	0.97
5	Generator Rotor Angle (Gen32)	Deg	55.84	55.62
6	Critical Clearing Time	Sec	0.102	0.089

After the power flow simulation above, we have obtained the active power at the slack bus further and reactive power at all PV buses. Thus in this step, we have had all inputs to be used for the ANFIS.

Next step, the transient system will be simulated. In the transient simulation, the significant effects of dynamic parameters are taken into account, not only the machine model but also the AVR model, turbine governor model, and load characteristic are considered in detail for the prediction of CCT. In addition, the models of AVR and governor applied with each generation unit are varied for each bus. However, the stabilizer and its parameter are ignored. The relation of models used in this study can be seen in the Figure 6.8, the model and parameters shown as dash line are ignored in this study.

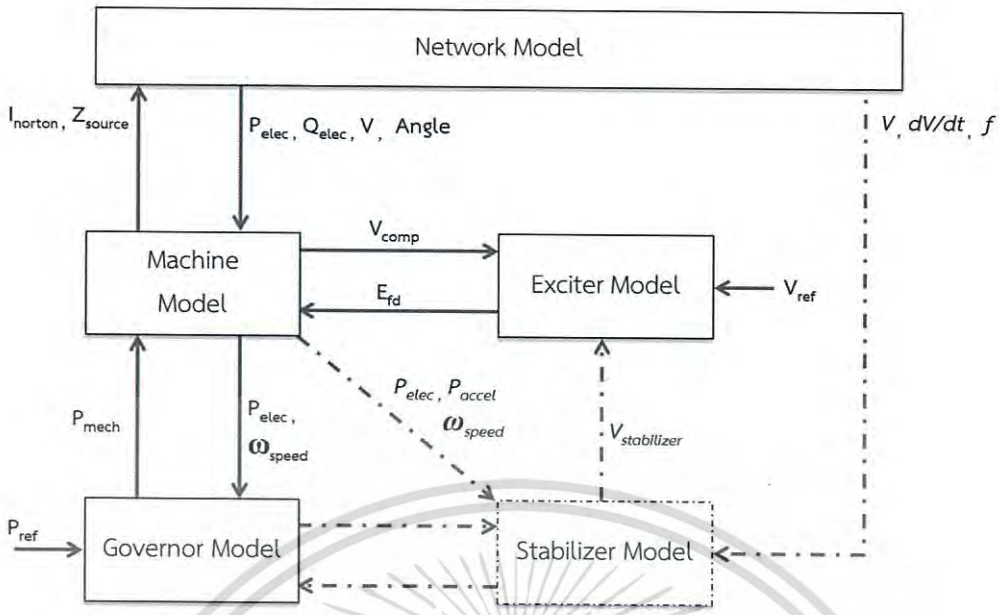

Figure 6.8 Relation of each model and their parameters

Next, a fault by the 3-phase short-circuit is simulated to the system and cleared by disconnection of the line having fault by isolating nearby circuit breakers at the ends of the line. In the various cases having different loads, the 3-phase balanced short-circuit is applied at either a transmission line or a bus. The position of the short-circuit applied is varied along the transmission line (0–100% of transmission length). After the 3-phase short-circuit clearance, if the terminal voltage is able to retrieve and the generator's rotor angle related to the slack bus angle can be back to steady state, then this indicates the system stability can be maintained. However, if the relative rotor angle is divergent, that indicates the system becomes in the unstable state.

To solve the CCT of each pattern, we do the trial and error by decrease and increase in the step-time (Δt) of fault clearing time by 0.001s and checking the plotted rotor angle curve until the system became unstable. The maximum fault clearing time during which a disturbance can be applied without the system losing its stability is the CCT.

Next step, we take all inputs above and the CCT as the output to the ANFIS training, the data set are divided into two sets, one is for training and another one is for testing. In this paper, 90% data of the data set are chosen for training and 10% of the data set are chosen for testing.

The ANFIS structure is to be designed. The shape membership function will be determined here by trial and error. Its optimal structure and rules can be found by means of trial and error. We use MATLAB version 2014B for ANFIS application [76, 77].

The variables used for ANFIS inputs comprise of the active power, reactive power, faulted line no., and position of fault at the line. Whereas the training and testing output of ANFIS use the CCT values. The input of fault position on the transmission line is represented by the percentage of the transmission length between nearby buses. For instance, in case a fault happens at 5-7 line, the input will be 3. The position of fault is at 30% of line length from the bus 5, and the numerical input will be 30.

Figure 6.9 shows the flow chart for the implementation of this study. The IEEE 9-bus and the IEEE 39-bus systems are used in this study.

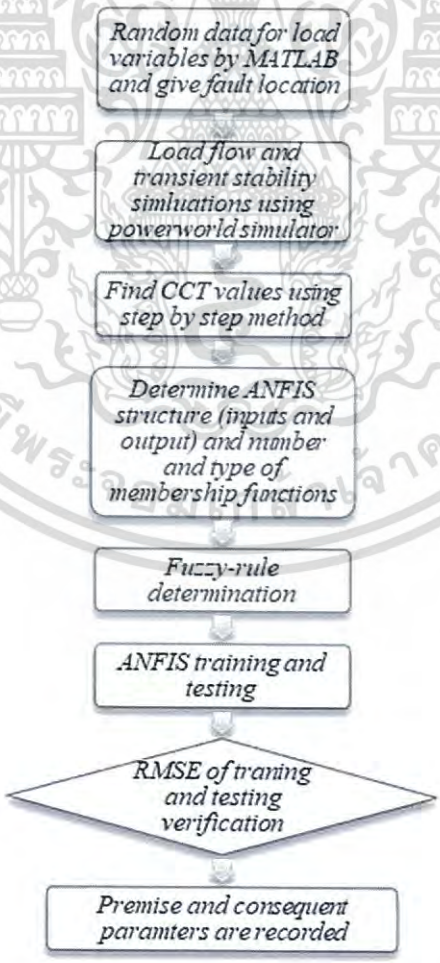

Figure 6.9 Flow chart of implementation steps

The ANFIS performance index can be assessed by the root mean square error (RMSE) between the actual CCT acquired by the time domain method and the predicted CCT acquired by the ANFIS method. The RMSE equation can be written as follows:

$$RMSE = \sqrt{\frac{\sum_{i=1}^{n}(O_i - F_i)^2}{n}} \tag{6.1}$$

where O_i is the actual CCT, F_i is the predicted CCT acquired by the ANFIS method, and n is the number of training set

6.2 ANFIS IMPLEMENTATION

6.2.1 IEEE 9-Bus System Implementation

The prediction of CCT is carried out in the IEEE 9-bus as illustrated in Figure 6.10. The first step, we start with the selection of the appropriated inputs. Herein, the active power and reactive power of all PV buses, comprised of the generator bus 1, generator bus 2, and generator bus 2, are selected to be as the inputs for CCT prediction as Figure 6.11.

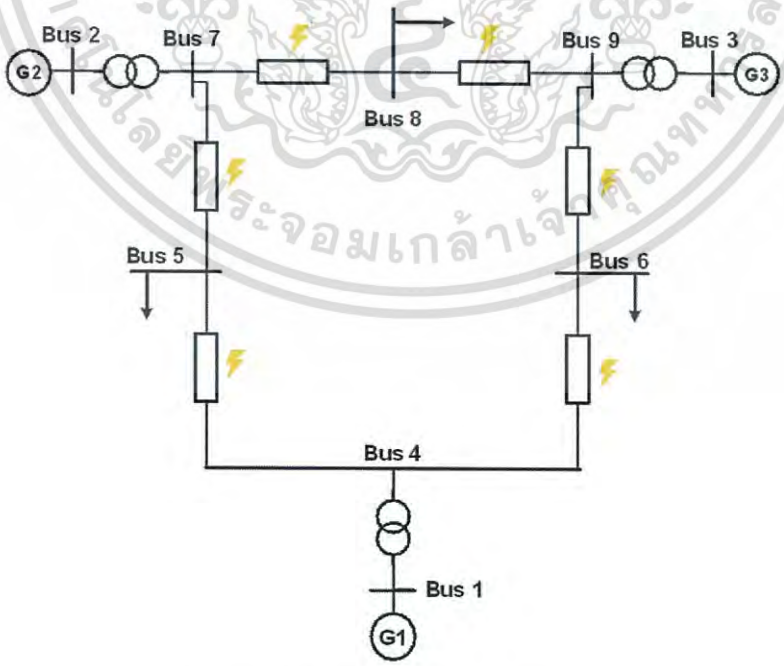

Figure 6.10 IEEE 9-bus system

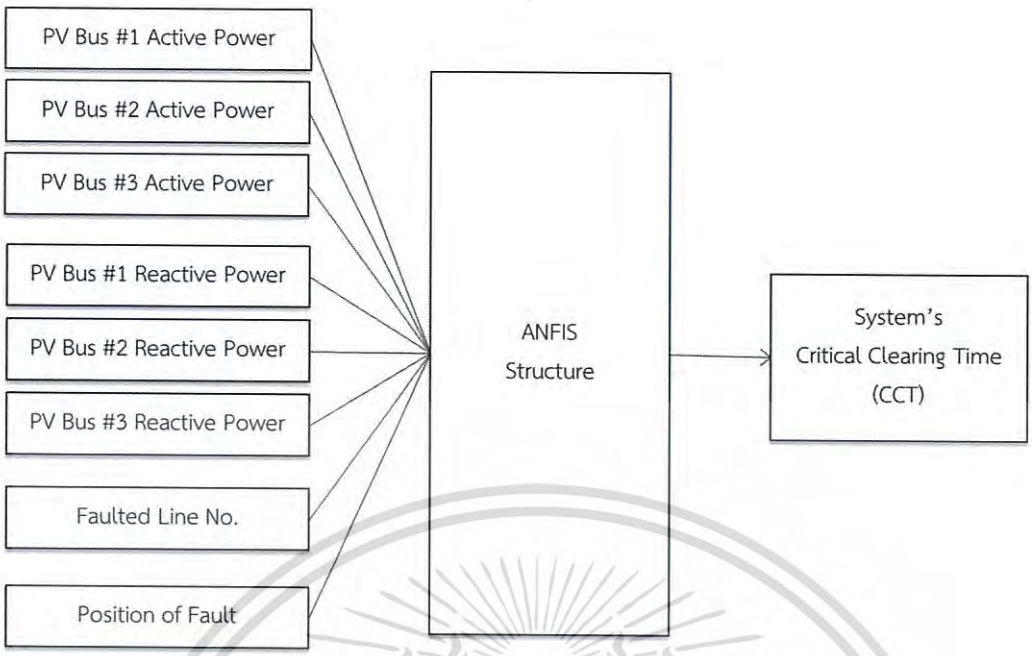

Figure 6.11 Input and Output Structure

The next step as described above, there shall be at least a bus in the system running the synchronous machines in the frequency mode acting as the slack bus to balance the generation system with the loads and losses. Herein, the active power and reactive power at the slack bus is set free. Also the reactive power of each PV bus are not fixed as it would affect the system voltage. The bus 1 having a big generator are selected as the slack bus. This step, we would random of active power of all PV bus, except the active power at the bus 1 using the sobol sequences.

After the input random above, we would have the inputs of active power at all PV buses, except the active power at the bus 1. We use the available inputs generated from the sobol sequence for the power flow simulation to solve the active power at the slack bus and all reactive power at all PV buses. The power world simulation software Version 17 [75] is used for the load flow simulation. In this process, the dynamic parameters are not used. Only the load, voltage, active power, reactive power, impedance, and angle of all synchronous machines, buses, transmission lines, distribution systems, loads, and some equipment are considered here. We input the data regarding the transmission line constraint, i.e., current capability and power flow limitation in the simulation. The constraint of

generator capability curve, i.e., stator heating limit, rotor heating limit, stability limit, zero field current limit, and core end heating limit are also created in the simulation. The active power and reactive power at the load buses in the study areas are varied by Sobol Sequence between 70% - 110% of the base load to have various case covering all learning. The power factor of all generators is set free so the reactive power would not depend on the active power.

After the power flow simulation above, we have obtained the active power at the slack bus further and reactive power at all PV buses. By now we have had all inputs to be used for the ANFIS.

Next step, we simulate the transient system to solve the CCT. In the transient simulation, the significant effects of dynamic parameters are taken into account, not only the machine model but also the AVR model, turbine governor model, and load characteristic are considered in detail for the prediction of CCT. In addition, the models of AVR and governor applied with each generation unit are varied for each bus. However, the stabilizer and its parameter are ignored.

All machines are modeled with a detailed model by considering the machine model, AVR models, turbine governor models, and load characteristic model. The two-axis model is applied for machines at bus 1 to 3. The load characteristics at bus 5, 6, and 8 are modeled with the CLOD complex load model. The AVR model "IEEE 421.5 2005 AC8B" and the turbine governor model "GGOV1" are applied to the generation unit at bus 1. The models "IEEE type 2" and "IEEEG1" are applied to the generation unit at bus 2. The models "IEEEX1" and "TGOV3" are applied to the generation unit at bus 3. The types of the AVR model and the turbine governor model applied to each generation unit are summarized in the Table 6.3.

Table 6.3 Type of AVR model and the turbine governor model applied to IEEE the 9-bus

Bus	Machine	Excitation	Governor
1	Two-axis model	AC8B	GGOV1
2	Two-axis model	IEEET2	IEEEG1
3	Two-axis model	IEEEX1	TGOV3

The training and testing data (i.e. loads and CCT values) are obtained from the simulation using the Power World software. The CCT values are obtained by the time-domain means. In the simulation, the active power of all generators, except the generator at slack bus (bus 2), is fixed. The power factor of all generators is set as free so the reactive power would not depend on the active power. In the various cases having different loads, the 3-phase balanced short-circuit is applied at either a transmission line or a bus. The position of the short-circuit applied is varied along the transmission line (0–100% of transmission length). The fault clearance is by isloating two nearby circuit breakers.

The rotor angles relative to slack bus's angle are plotted for the first 30 s subject to 0.001 s of the time-step (Δt). To resolve the CCT of each case, the fault clearing time is gradually increased with a step-time of 0.001 s until the system becomes unstable. There is a total of 600 sets of data generated from the simulation for ANFIS implementation. The whole sets of data produced from the simulation are random for the training sets for 90% and for the testing sets for 10%. The 540 sets of data are used for training and the 60 sets of data are used for testing.

The CCT value is chosen as the ANFIS output. The variables used for ANFIS inputs are composed of

- Active Power at PV Bus;
- Reactive Power at PV Bus;
- Faulted transmission line; and
- Position of fault.

The active and reactive power of PV bus are inputted in units of MW and MVAR, respectively. The input of fault position on the transmission line is represented by the percentage of the transmission length between nearby buses. For instance, in case a fault happens at 5-7 line, the input will be 3. The position of fault is at 30% of line length from the bus 5, and the numerical input will be 30.

Next, we need to design the ANFIS structure. Its optimal structure can be found by means of trial and error. We discover that Layer 1 should have structure of 2-2-2-2-2-2-3-3, meaning there are 2 membership functions for bus 1 active

load input, bus 1 reactive load input, bus 2 active load input, bus 2 reactive load input, bus 3 active load input, and bus 3 reactive load input, and there are 3 membership functions for input of faulted transmission line number and the position of fault. All membership functions should be bell shaped with 64 fuzzy rules set.

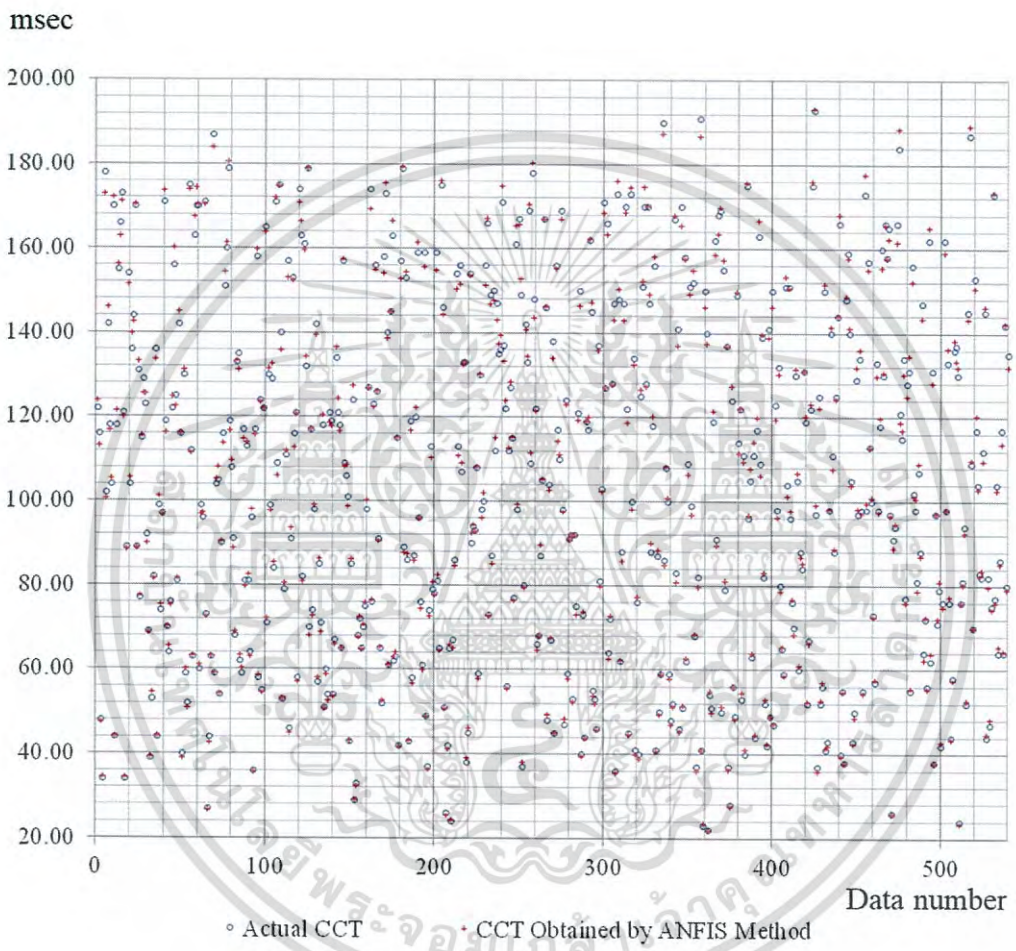

Figure 6.12 ANFIS outputs and target outputs: training data for IEEE 9-bus

We obtain the RMSE of 2.025 for training. The actual CCT obtained by the time-domain means and the estimated CCT acquired by the ANFIS method are plotted in Figure. 6.12 for the training data sets.

6.2.2 IEEE 39-Bus System Implementation

In this section, the IEEE 39-bus system as Figure 6.13 is briefly explained because the approach used for the IEEE 39-bus system is similar to the 9-bus

system. All machines in the IEEE 39-bus system are also modeled with a detailed model considering the machine model, AVR models, turbine governor models, and load characteristic model. The 2-axis model is applied for all machines. The load characteristics of all PQ buses are modeled with the CLOD complex load model. The type of AVR model and the turbine governor model applied to each generation unit are shown in Table 6.4.

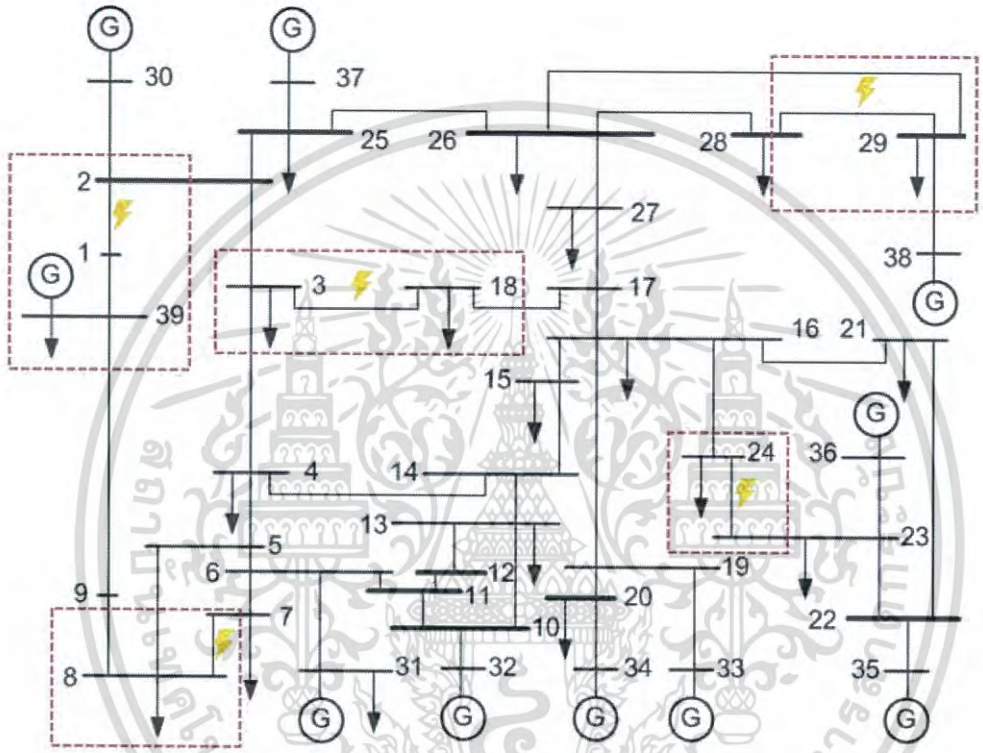

Figure 6.13 IEEE 39-bus system

The first step, we start with the selection of the appropriated inputs. Herein, the active power and reactive power of all PV buses, comprised of the generator bus no. 1 to bus no. 10 are selected to be as the inputs for CCT prediction as Figure 6.14.

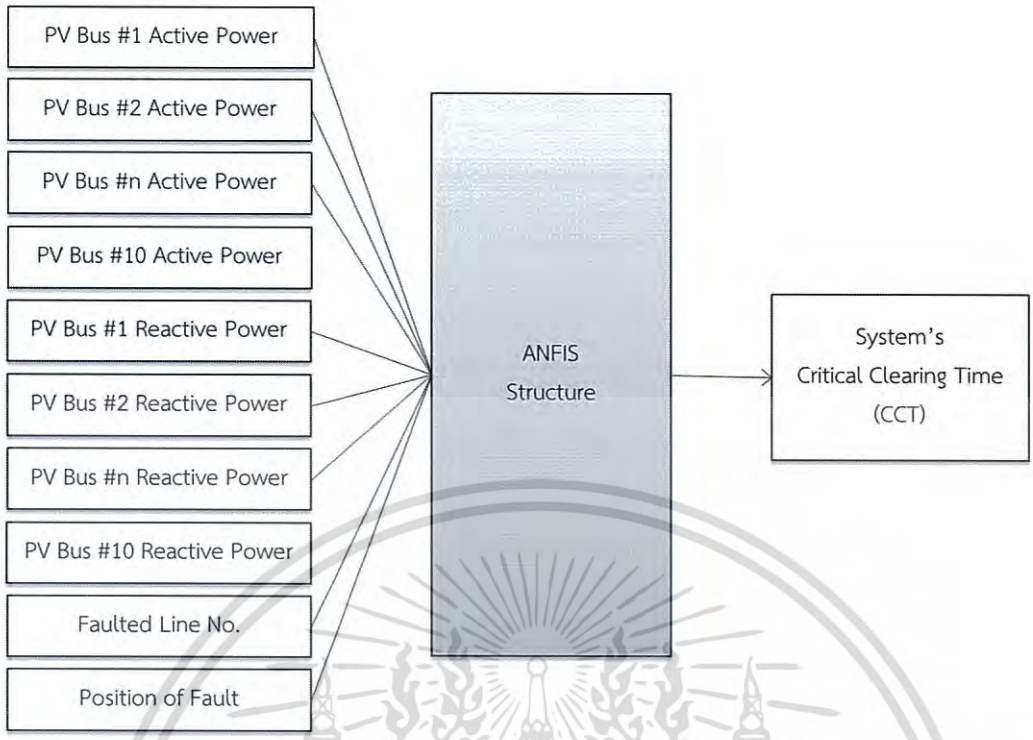

Figure 6.14 Input and Output Structure

The next step as described above, there shall be at least a bus in the system running the synchronous machines in the frequency mode acting as the slack bus to balance the generation system with the loads and losses. Herein, the active power and reactive power at the slack bus is set free. Also the reactive power of each PV bus are not fixed as it would affect the system voltage. The bus 2 having a big generator are selected as the slack bus. This step, we would random of active power of all PV bus, except the active power at the bus 1 using the sobol sequences.

After the input random above, we would have the inputs of active power at all PV buses, except the active power at the bus 2. We use the available inputs generated from the sobol sequence for the power flow simulation to solve the active power at the slack bus and all reactive power at all PV buses. The power world simulation software Version 17 is used for the load flow simulation. In this process, the dynamic parameters are not used. Only the load, voltage, active power, reactive power, impedance, and angle of all synchronous machines, buses, transmission lines, distribution systems, loads, and some equipment are considered here. The active power of all generators, except the generator at slack

bus (bus 2), is fixed. We input the data regarding the transmission line constraint, i.e., current capability and power flow limitation in the simulation. The constraint of generator capability curve, i.e., stator heating limit, rotor heating limit, stability limit, zero field current limit, and core end heating limit are also created in the simulation. As the system is quite large, the study area is determined to be less the number of input, training data, and computation time. The study area is in the dashed line, as illustrated in Figure 6.13. The active power and reactive power at the load buses in the study areas (i.e. bus 3, 8, 18, 24, 29, and 39) are varied by Sobol Sequence between 70% - 110% of the base load to have various case covering all learning. The power factor of all generators is set free so the reactive power would not depend on the active power.

After the power flow simulation above, we have obtained the active power at the slack bus further and reactive power at all PV buses. By now we have had all inputs to be used for the ANFIS. Next step, we simulate the transient system to solve the CCT. In the transient simulation, the significant effects of dynamic parameters are taken into account, not only the machine model but also the AVR model, turbine governor model, and load characteristic are considered in detail for the prediction of CCT. In addition, the models of AVR and governor applied with each generation unit are varied for each bus. However, the stabilizer and its parameter are ignored. The figures 6.15 – 6.28 illustrate an example of some dynamic curves affected from the transient fault.

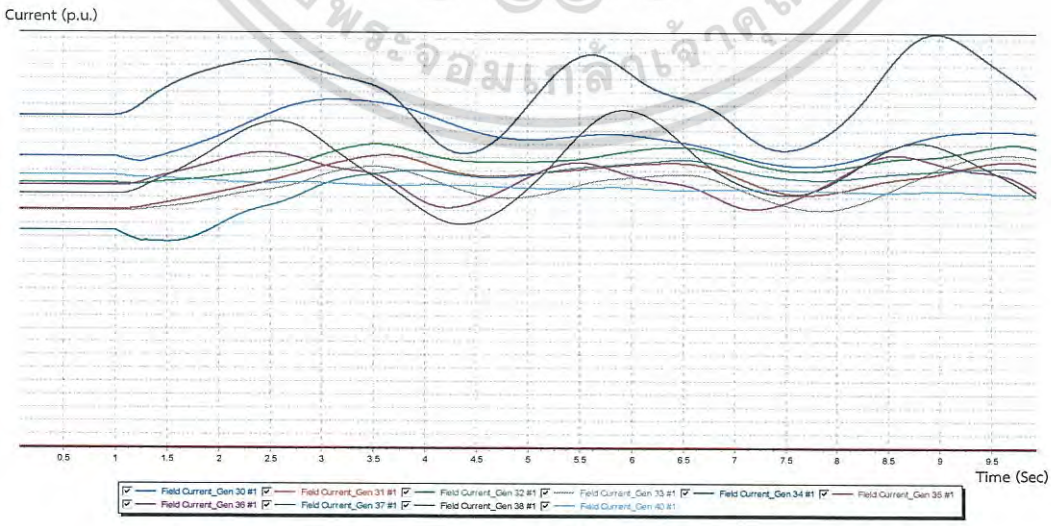

Figure 6.15 Field Current Curve After Fault Clearance at CCT

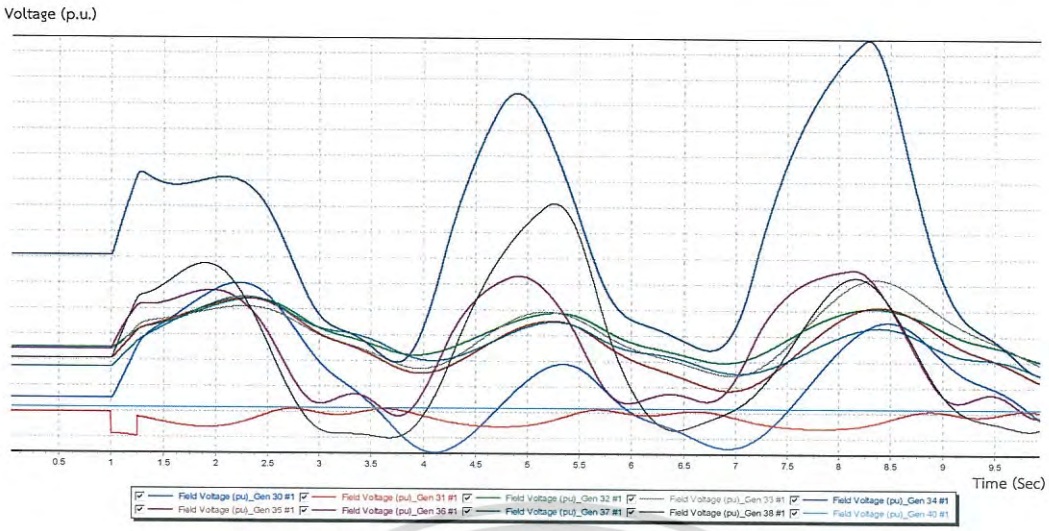

Figure 6.16 Field Voltage Curve After Fault Clearance at CCT

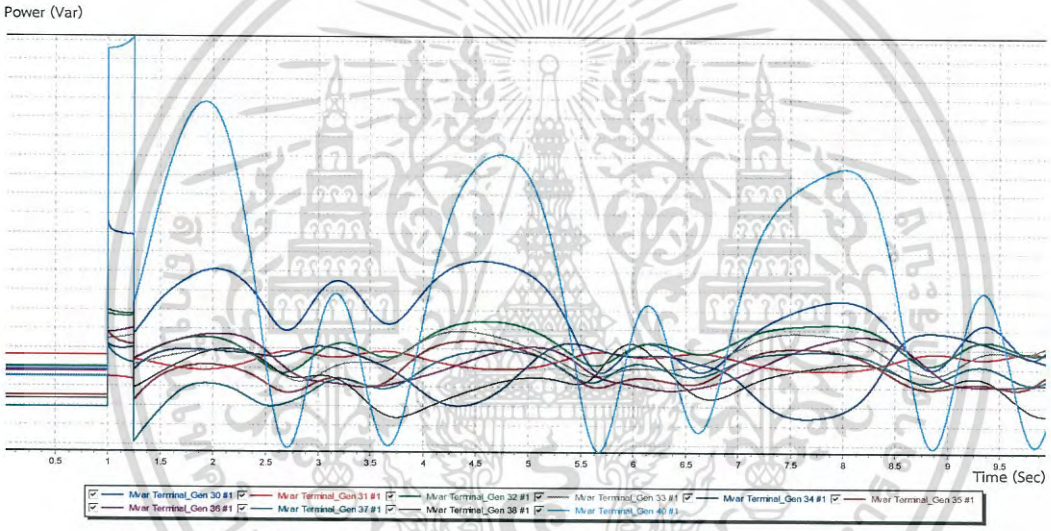

Figure 6.17 Reactive Power Curve After Fault Clearance at CCT

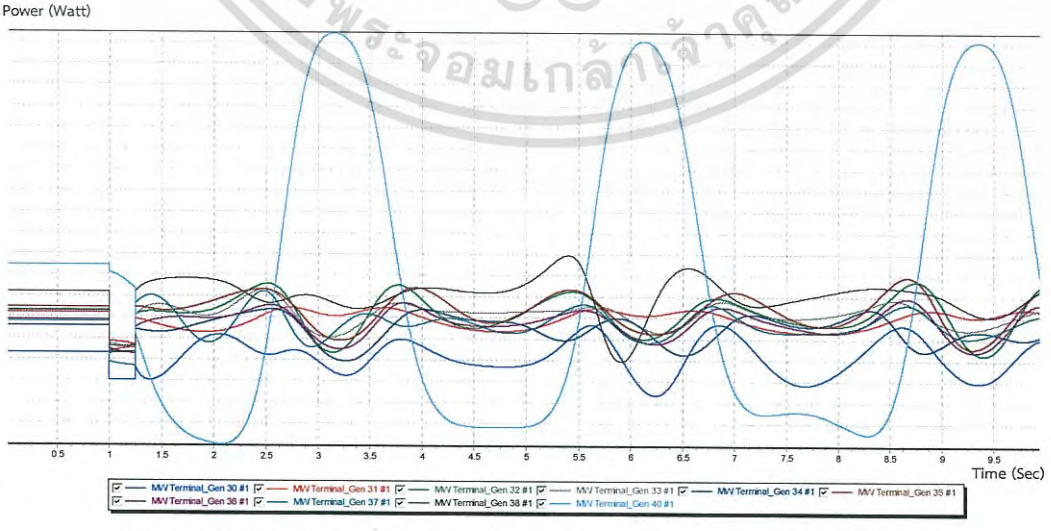

Figure 6.18 Active Power Curve After Fault Clearance at CCT

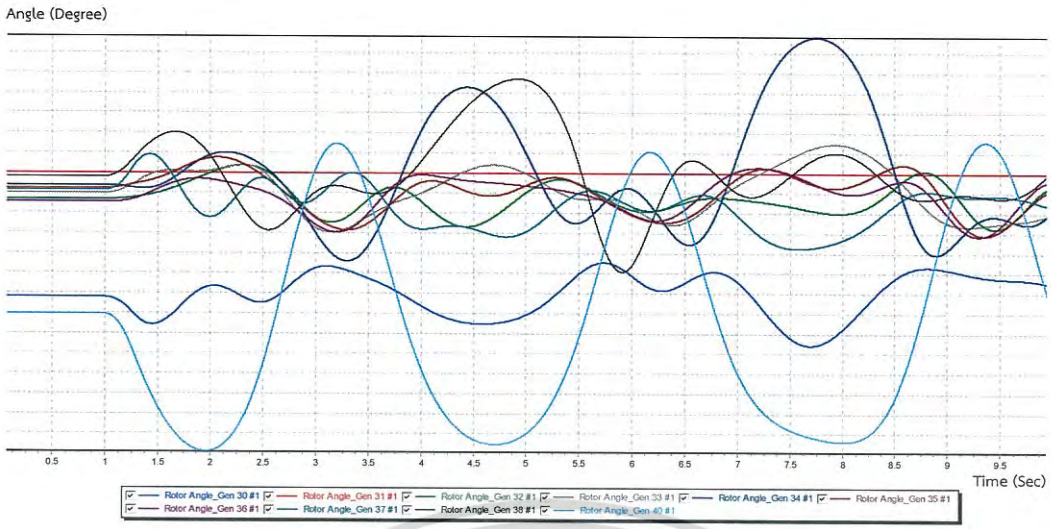

Figure 6.19 Rotor Angle Curve After Fault Clearance at CCT

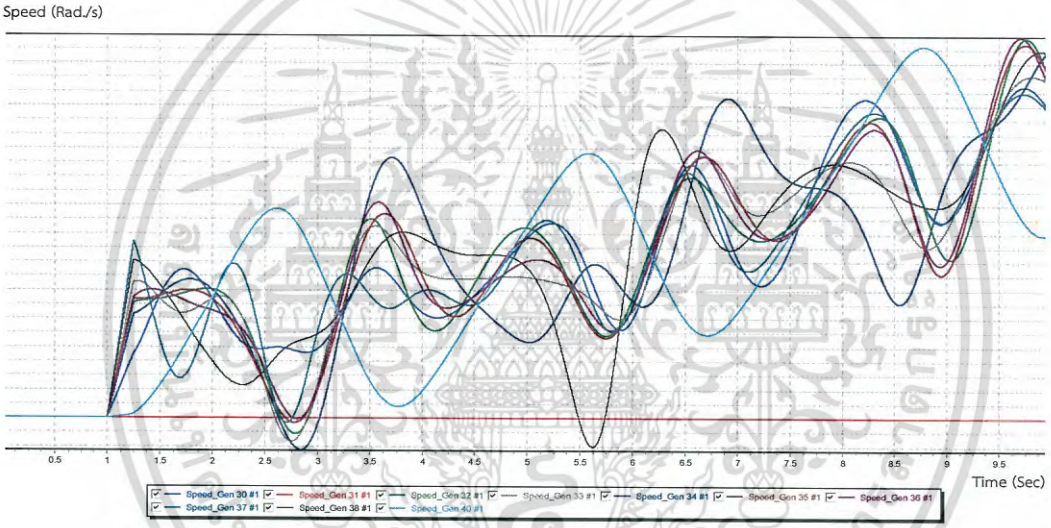

Figure 6.20 Generator Speed Curve After Fault Clearance at CCT

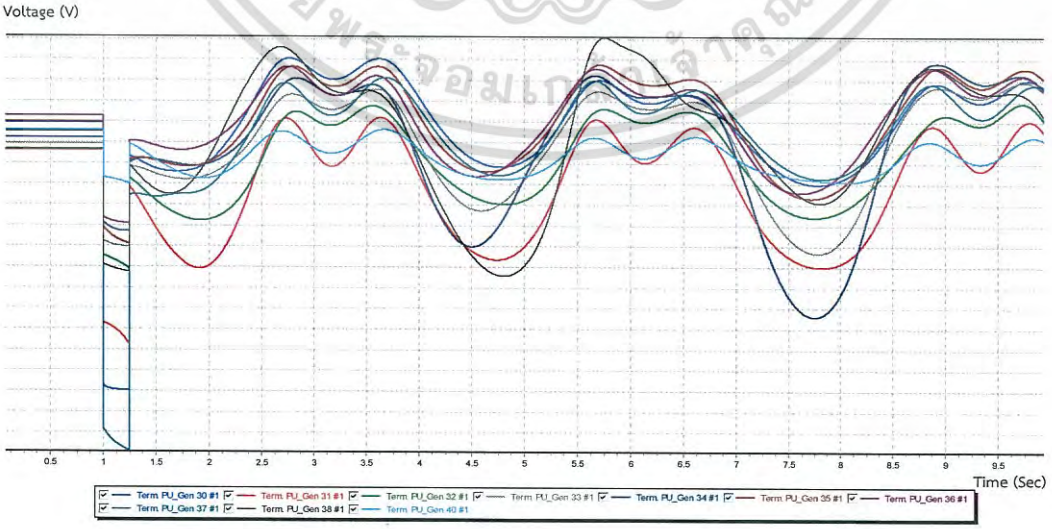

Figure 6.21 Terminal Voltage Curve After Fault Clearance at CCT

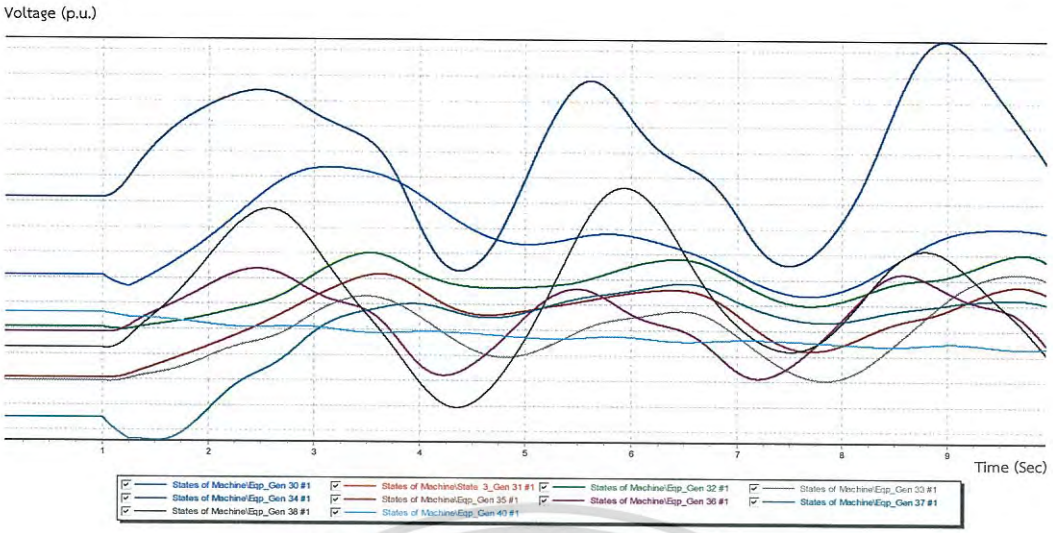

Figure 6.22 Eq Curve After Fault Clearance at CCT

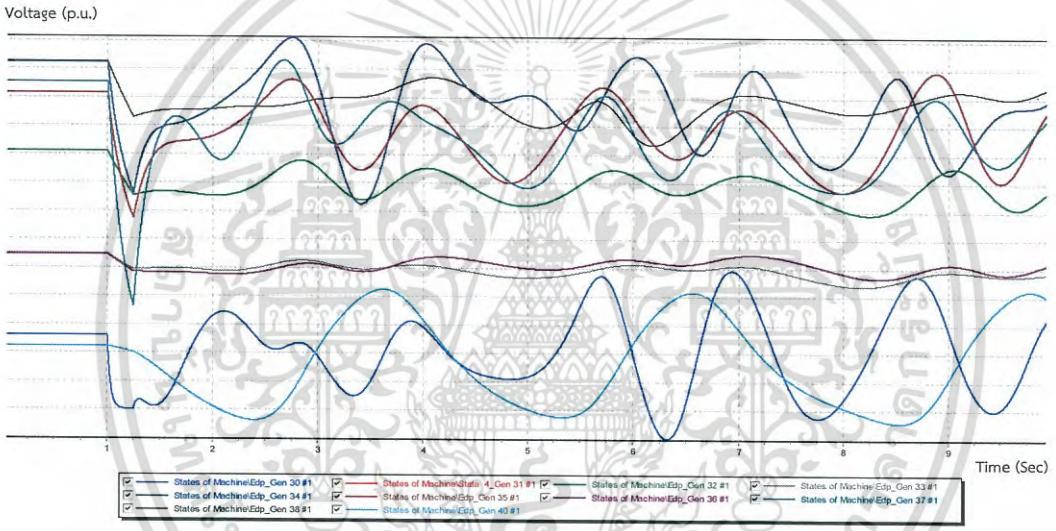

Figure 6.23 Ed Curve After Fault Clearance at CCT

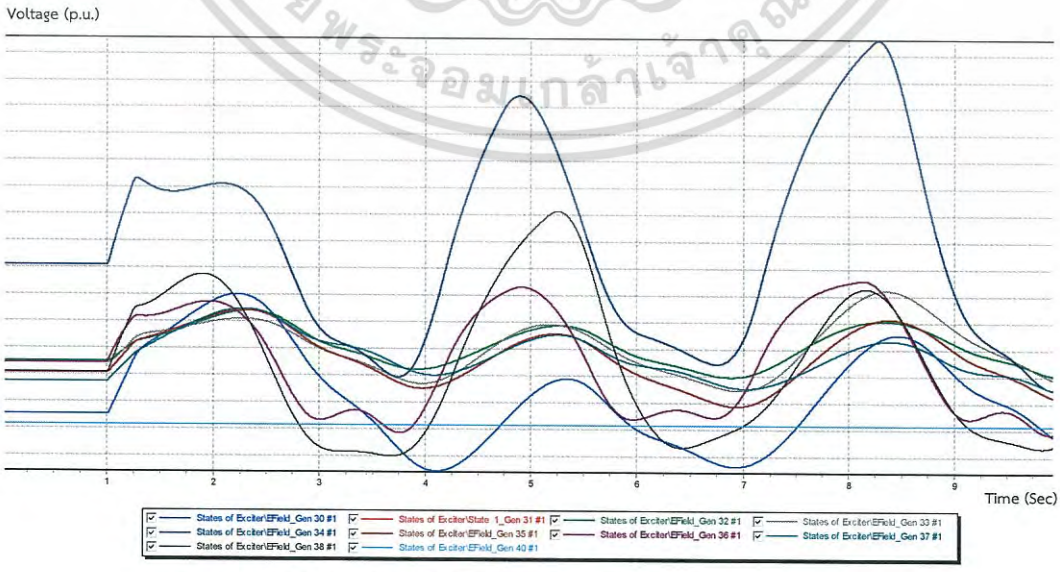

Figure 6.24 Exciter Ef Curve After Fault Clearance at CCT

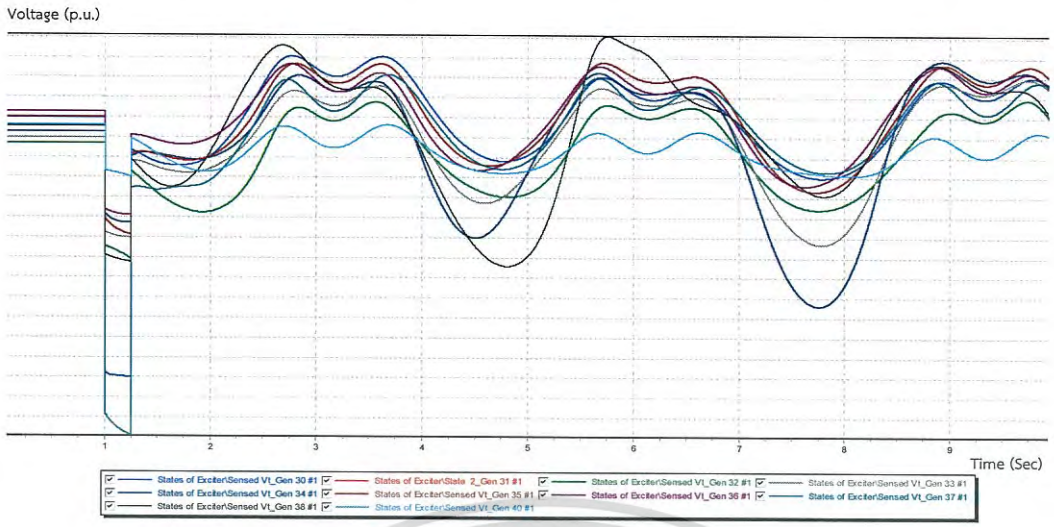

Figure 6.25 Exciter Vt Curve After Fault Clearance at CCT

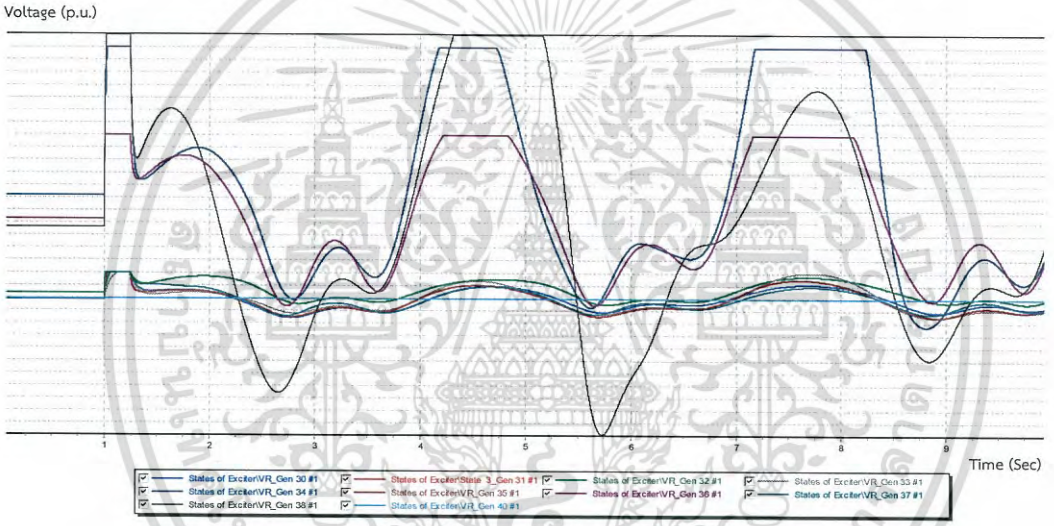

Figure 6.26 Exciter Vr Curve After Fault Clearance at CCT

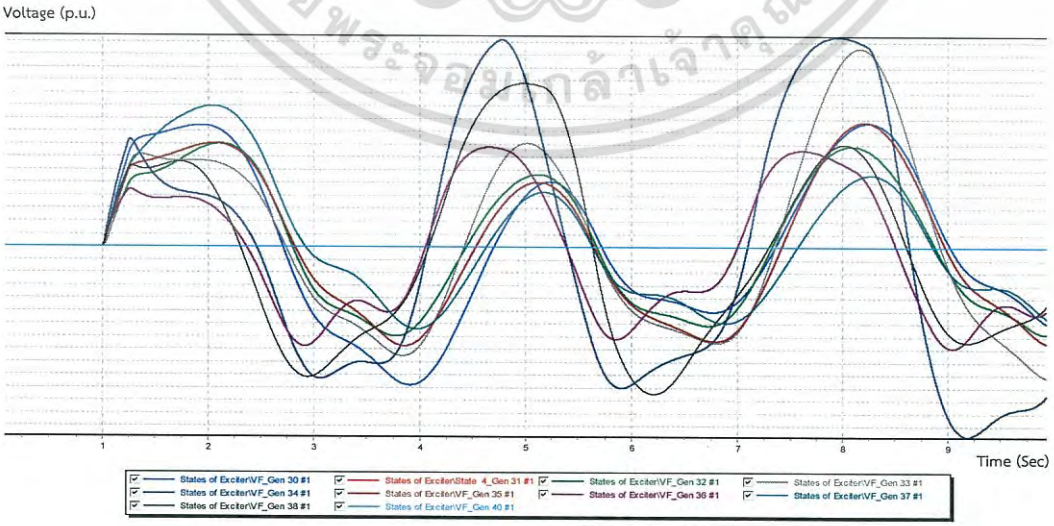

Figure 6.27 Exciter Vf Curve After Fault Clearance at CCT

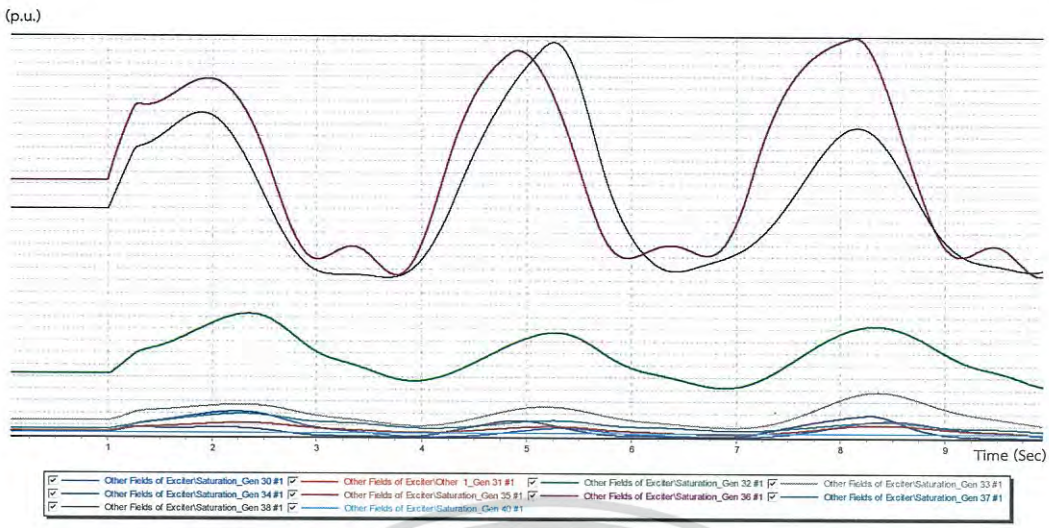

Figure 6.28 Exciter Saturation Curve After Fault Clearance at CCT

In the various cases having different loads, the 3-phase balanced fault is applied at either a transmission line or a bus in the study area at a momentary time. The transmission line happening fault is composed of 1-2, 7-8, 3-18, 19-24, and 28-29 lines. The position of the fault applied is varied along the transmission line. The fault clearance is done by isolating two nearby circuit breakers.

Table 6.4 Type of AVR model and the turbine governor model applied to the IEEE 39-bus system

Bus	Machine	Excitation	Governor
30	Two-axis model	IEEET1	GGOV1
31	Two-axis model	IEEET2	IEEEG1
32	Two-axis model	IEEET1	GGOV1
33	Two-axis model	AC8B	TGOV3
34	Two-axis model	IEEEX1	IEEEG1
35	Two-axis model	IEEET2	GGOV1
36	Two-axis model	IEEEX1	TGOV3
37	Two-axis model	AC8B	IEEEG1
38	Two-axis model	AC8B	TGOV3
39	Two-axis model	AC8B	IEEEG1

The rotor angles relative to the slack bus's angle are plotted for the first 30 seconds subject to 0.001 s of the time-step (Δt). To resolve the CCT of each

case, the fault clearing time is gradually increased with a step time of 0.001 s until the system is unstable. Figure 6.29 illustrates a base case of the stable swing curve when fault clearing time at t = 0.131 second after disturbance occurs. Figure 6.30 illustrates a base case example of the unstable swing curve when fault clearing time over the CCT at t = 0.132 second after disturbance occurs.

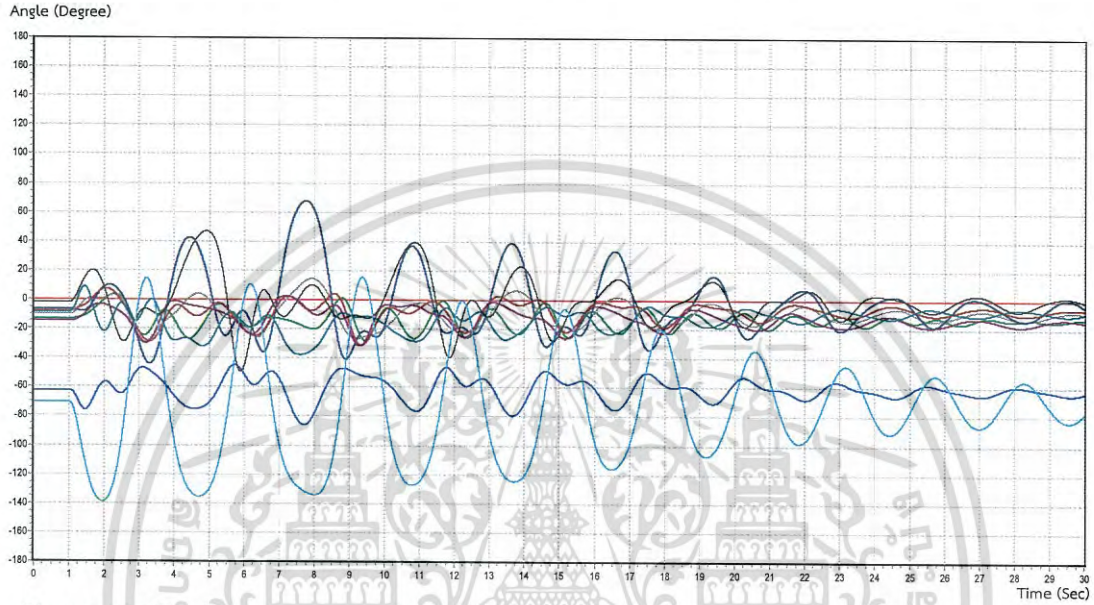

Figure 6.29 Swing curve when fault clearing time at t = 0.131 second after disturbance occurs (stable)

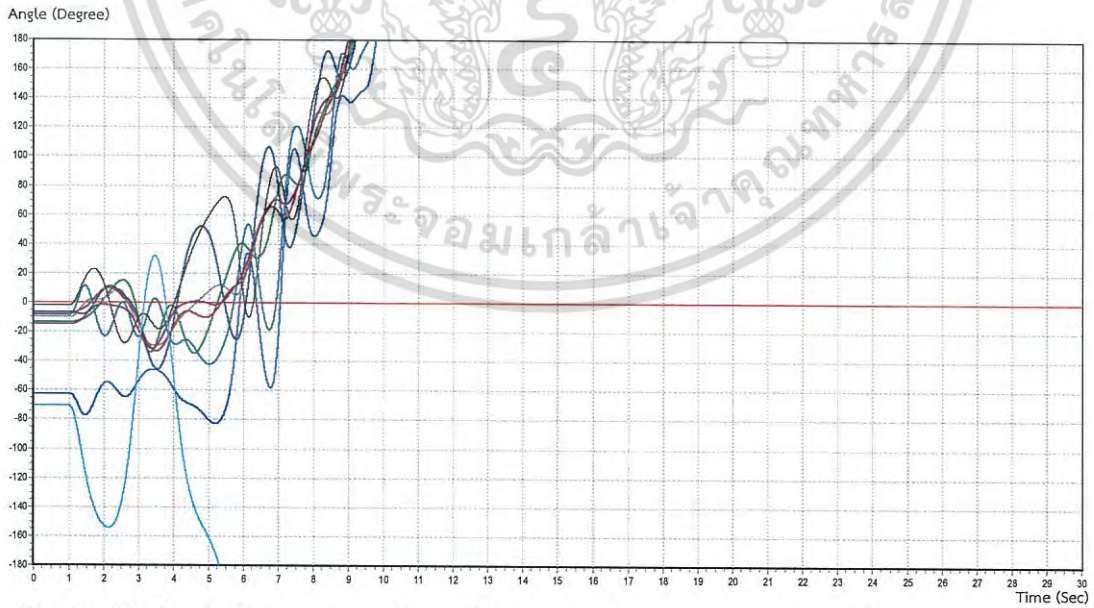

Figure 6.30 Swing curve when fault clearing time at t = 0.132 second after disturbance occurs (unstable)

There is totally 1200 sets of data produced from the simulation for ANFIS implementation. The whole sets of data produced from the simulation are random for the training sets for 90% and for the testing sets for 10%. The 1080 sets of data are used for training and 120 sets of data are used for testing. The required output of ANFIS is CCT. The variables used for ANFIS inputs are composed of:

- Active Power at PV Bus;
- Reactive Power at PV Bus;
- Faulted transmission line; and
- Position of fault.

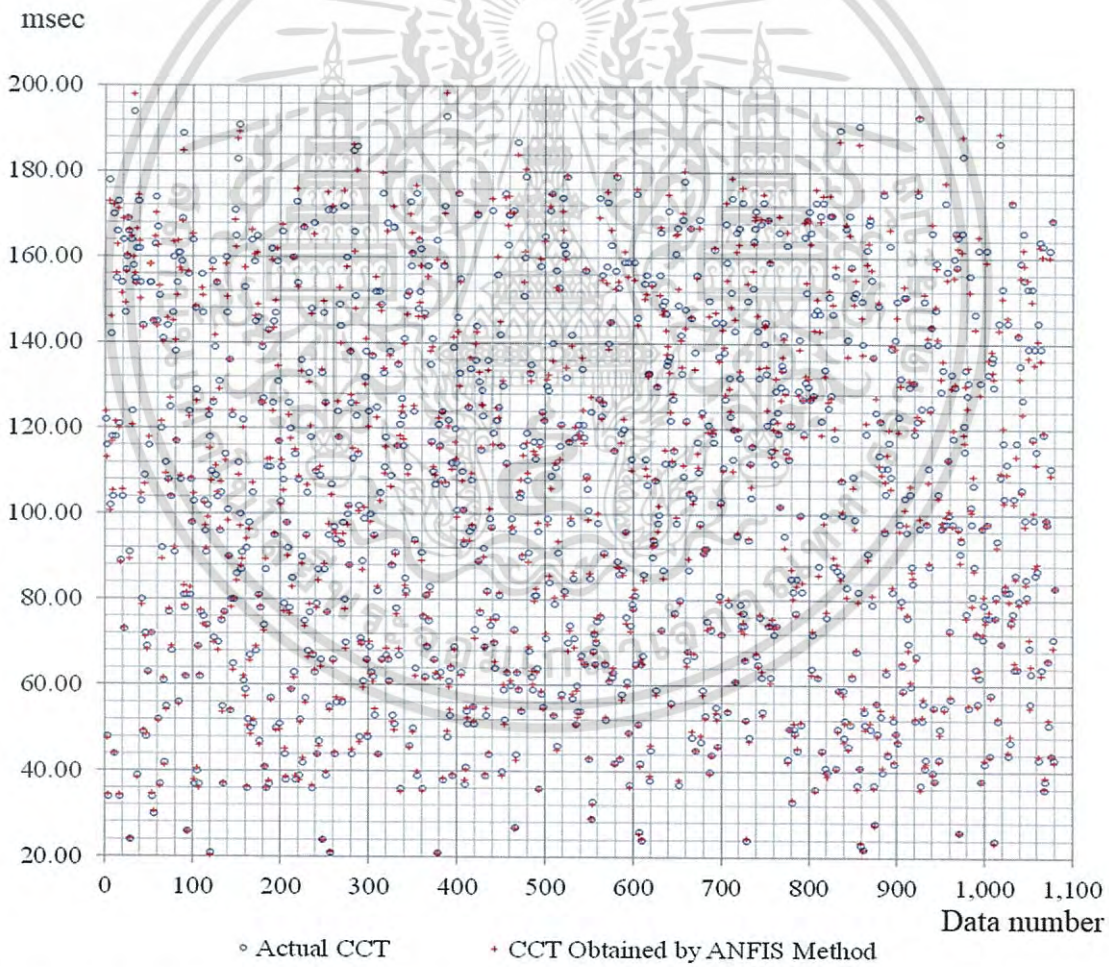

Figure 6.31 ANFIS outputs and target outputs: training data for the IEEE 39-bus system

The active power and reactive power are inputted in units of MW and MVAR, respectively. The input of the fault position on the transmission line is represented by the percentage of the transmission length between nearby buses.

Next, we need to design the ANFIS structure. Its optimal structure can be found by means of trial and error. The optimal structure is 2-2-2-2-2-2-2-2-2-2-2-2-2-2-2-2-2-2-2-2-2-2-2-2-2-2-2-2-2-2-2-2-2-2-4-3. It means that there are 2 membership functions for each active power input and each reactive power input. There are 4 membership functions for input of the faulted transmission line number and there are 3 membership functions for the position of fault. All membership functions are pi-shaped with 256 fuzzy rules set.

We obtain the RMSE of 1.579 for training. The CCT acquired by the time domain method and the predicted CCT acquired by the ANFIS method are plotted in Figure. 6.11 for the training data.

6.3 RESULT

The ANFIS performance index is assessed by the root mean square error (RMSE) between the actual CCT acquired by the time domain method and the predicted CCT acquired by the ANFIS method. The RMSE equation can be written as follows:

$$RMSE = \sqrt{\frac{\sum_{i=1}^{n}(O_i - F_i)^2}{n}} \tag{6.1a}$$

where O_i is the actual CCT, F_i is the predicted CCT acquired by the ANFIS method, and n is the number of training set

The ANFIS outputs and target outputs of testing data for IEEE 9-bus and IEEE 39-bus are plotted in Figure 6.32 and Figure 6.33 respectively.

The ANFIS results above are compared to the results of Artificial NNs (ANN), which is generally applied for the power system. The ANN structure applied with this research is multi-layer feedforward type and gets trained applying the Levenberg-Marquardt algorithm. The same 600 patterns and 1,200 patterns of training data and testing data used for the ANFIS study are applied for ANN for

the IEEE 9-bus and the IEEE 39-bus system, respectively. All variables are normalized for training and testing patterns.

The optimized structure of ANN used for the IEEE 9-bus implementation is comprised of 3 layers, comprising 1 output layer and 2 hidden layers. The 1st hidden layer has 14 neurons and the 2nd hidden layer has 13 neurons. The transfer functions in the 1st hidden layer, the 2nd hidden layer, and the output layer are log-sigmoid, log-sigmoid, and tan-sigmoid, respectively. For the IEEE 39-bus system implementation, the optimized structure of ANN is comprised of three layers, comprising 1 output layer and 2 hidden layers. The 1st hidden layer has 16 neurons the 2nd hidden layer has 15 neurons. The transfer functions in the 1st hidden layer, the 2nd hidden layer, and the output layer are log-sigmoid, tan-sigmoid, and linear, respectively

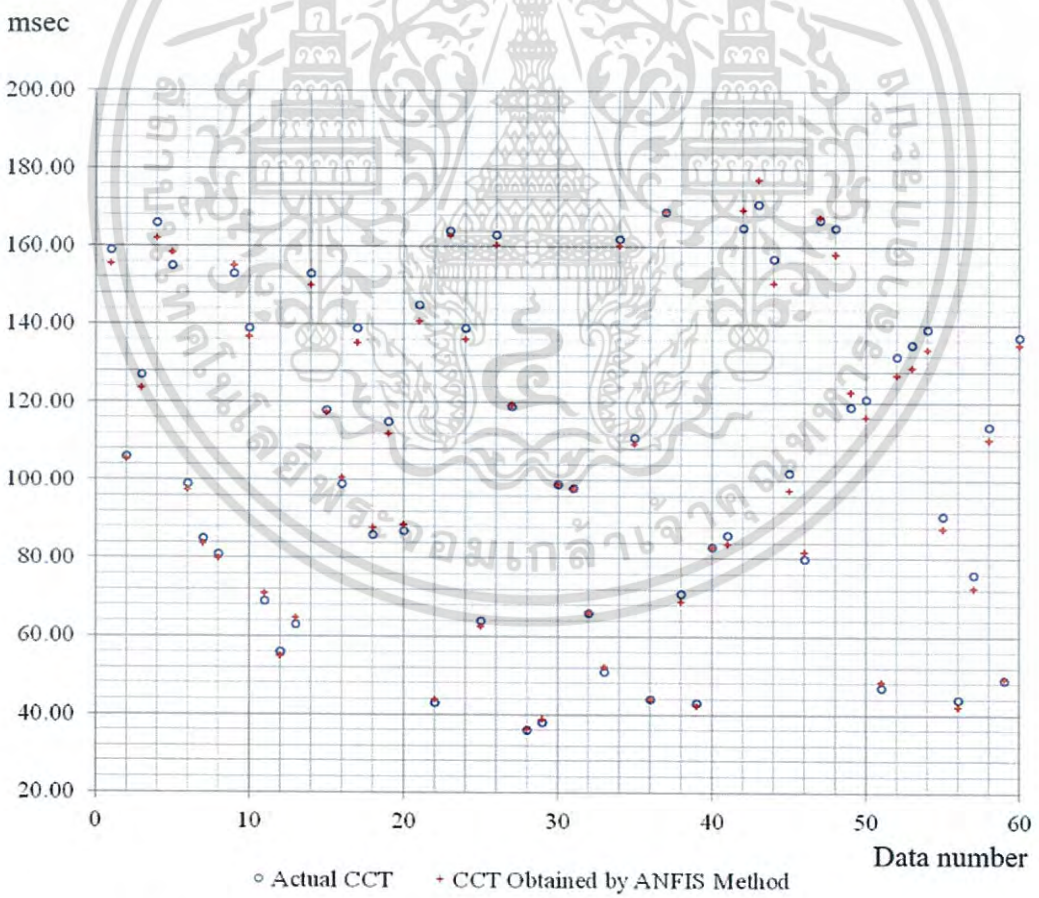

Figure 6.32 ANFIS outputs and target outputs: testing data for IEEE 9-bus

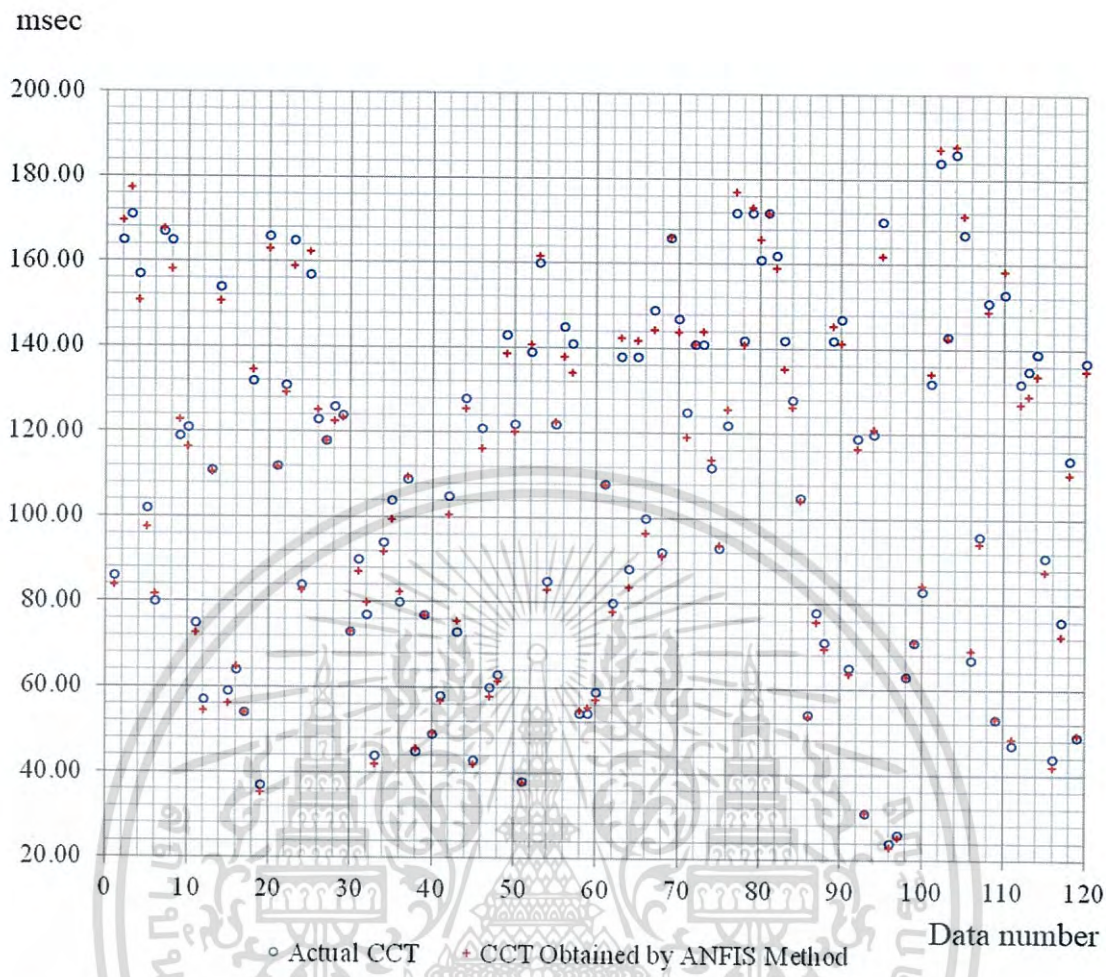

Figure 6.33 ANFIS outputs and target outputs: testing data for the IEEE 39-bus system

For IEEE 9-bus system implementation, we obtain the RMSE of 2.102 for testing. The CCT acquired by the time domain method and the predicted CCT acquired by the ANFIS method are plotted in Figure 6.32 for the testing data sets. For IEEE 39-bus system implementation, we obtain the RMSE of 2.633 for testing. The CCT acquired by the time domain method and the predicted CCT acquired by the ANFIS method are plotted in Figure 6.33 for the testing data sets. The RMSE between time domain results and the results acquired by the ANN method for the IEEE 9-bus and IEEE 39-bus system implementations are given in Table 6.5.

Table 6.5 RMSE of ANFIS and ANN testing

System	ANN Structure Data			RMSE	
	First Layer	Second Layer	Transfer Function	ANN	ANFIS
9-bus	14	13	log-log-tan	2.977	2.102
39-bus	16	15	log-tan-lin	4.121	2.633

Note: log is log-sigmoid, tan is tan-sigmoid, and lin is linear.

CHAPTER 7

CONCLUSION AND SUGGESTION

7.1 CONCLUSION

In this study, we focus on the transient stability assessment in real-time with an acceptable accurate results having an error less than 5%. The critical clearing time is used as an index for the transient stability assessment. All significant models and effects of dynamic parameters in the system are considered; not only the machine model but also the turbine governor model, AVR model, and load characteristic are taken into account in the simulation in order to have accurate results as much as possible. Moreover, other than the considered parameters mentioned, to be realistic as much as possible, we also consider the constraint of transmission line, i.e., current capability and power flow limitation. As well as the generator capability curve, i.e., stator heating limit, rotor heating limit, stability limit, zero field current limit, and core end heating limit are also considered in this study.

An approach called adaptive neuro-fuzzy inference system (ANFIS) which is an algorithm applied from neural networks and fuzzy logic principles effectively implemented is proposed in this study for the real-time estimation of CCT. Our target in this study is the estimated CCT by ANFIS proposed can be solved in real-time subject to the accuracy of result is acceptable. In order that the system can differentiate between a temporary fault and a permanent instability once the abnormal behavior of system occurs as fast as possible. Also the protective relays can be calculating the real-time CCT obtained from ANFIS for an on-line setting of its delay time to avoid any inefficient tripping. All power values in a system could be on-line transferred to ANFIS through a supervisory control and data acquisition (SCADA) system for the CCT estimation once any fault occurs in a system.

In this research, the active power and reactive power of all PV buses including the faulted transmission line and the fault position are selected to be as the inputs for the CCT prediction. We also use the sobol sequences technique for the ANFIS input random to increase the ANFIS learning effectiveness.

In the transient simulation, the models of AVR and governor applied with each generation unit are varied for each bus. However, the stabilizer and its parameter are ignored. A fault by the 3-phase short-circuit is simulated to the system and cleared by disconnection of the line having fault by isolating nearby circuit breakers at the ends of the line. In the various cases having different loads, the 3-phase balanced short-circuit is applied at either a transmission line or a bus. The position of the short-circuit applied is varied along the transmission line (0–100% of transmission length). To solve the CCT of each pattern, we use the trial and error by decrease and increase in the step-time (Δt) of fault clearing time by 0.001s and checking the plotted rotor angle curve until the system became unstable.

In this study, the modified IEEE 9-bus or IEEE 9-bus Western System Coordinating Council (WSCC) and Institute of Electrical and Electronics Engineers (IEEE) 39-bus systems are applied for implementation. We simulate the various governor models and AVR models in each system to reflect the realistic practice. The time domain method is used for the simulation in order to get the training and testing data for the ANFIS inputs and outputs. Various types of AVR model and governor model are applied in each system. Fault locations and load levels and are varied for testing. The power world simulation software version 17 is used for the load flow simulation. And we use MATLAB version 2014B for ANFIS application.

The results from ANFIS indicate that the application of ANFIS in CCT prediction considering the dynamic effects of the machine model, AVR system, turbine governor, and load characteristic is satisfied with high accuracy. Also the ANFIS results are compared to the ANN results, which are generally used; it can be seen that the ANFIS results are better.

7.2 SUGGESTION

Suggestion for next study or implementation are as follows:

7.2.1 Considering the unit commitment condition

7.2.2 Implementing the automatic adjustment of protective relay setting

REFERENCE

[1] M. Pavella, D. Ruiz-Vega and D. Ernst, "A Unified Approach to Assessment and Control," *Transient Stability of Power Systems,* 2000.

[2] P. Anderson and A. Fouad, Power System Control and Stability IEEE Series on Power Engineering, 2nd ed., 2003.

[3] I. A. Noor, Wahab, A. Mohamed and A. Hussain, "Transient Stability Assessment of a Power System Using PNN and LS-SVM Methods," *Journal of Applied Sciences,* pp. 3208-3216, 2007.

[4] A. W. I. Noor , "A new method of transient stability assessment in power systems using LS-SVM," in *Research and Development SCOReD*, 2007.

[5] S. Haykin, Neural Networks and Learning Machines, 3rd ed., Prentice-Hall, 2008.

[6] D. Sobajic and Y.-H. Pao, "Artificial neural net based dynamic security assessment for electric power systems," *IEEE Transactions on Power System,* vol. 14 (1), p. 954–960, 1989.

[7] F. Aboytes and R. Ramires, "Transient stability assesment in longitudinal power systems using artificial neural networks," *IEEE Transactions on Power Systems,* vol. 11, p. 2003–2010, 1996.

[8] S. Jiriwibhakorn, "Neural networks for constrained transient stability flows," *IEEE Power Engineering Society Winter Meeting,* vol. 2, pp. 1119-1123, 2002.

[9] S. Jiriwibhakorn, "Critical generator and maximum power limit determination using neural networks," *IEEE Power Engineering Society Summer Meeting,* 2002.

[10] A. Bettiol, A. Souza, J. Todesco and J. Tesch, "Estimation of critical clearing times using neural networks," in *Proceedings of the IEEE Conference on Power Technology*, 2003.

[11] K. Sanyal, "Transient stability assessment using artificial neural network," *Proceedings of the IEEE International Conference on Electric Utility Deregulation Restructuring and Power Technologies,* p. 633–637, 2004.

[12] C. Xiaodong and L. Yutian, "On-line learning applied to power system transient stability prediction," *IEEE International Symposium,* vol. 4, p. 3906–3909, 2005.

[13] H. Sawhney and B. Jeyasurya, " feed-forward artificial neural network with enhanced feature selection for power system transient stability assessment," *Electric Power Systems Research,* vol. 76, pp. 1047-1054, 2006.

[14] N. Wahab and A. Mohamed, "Transient stability assessment of a power system using probabilistic neural network," *American Journal of Applied Sciences,* vol. 5, p. 1225–1232, 2008.

[15] A. M. Haidar, M. Mustafa, F. A. Ibrahim and I. A. Ahmed, "Transient stability evaluation of electrical power system using generalized regression neural networks," *Applied Soft Computing,* vol. 11, pp. 3558-3570, 2011.

[16] H. A. Mohd, P. Minwon, Y. In-Keun , M. Toshiaki, J. Tamura and B. Wu, "Enhancement of transient stability by fuzzy logic-controlled SMES considering communication delay," *Electrical Power and Energy Systems,* vol. 31, pp. 402-408, 2009.

[17] P. Kundur, Power system stability and control, McGraw-Hill, 1994.

[18] P. Sauer and M. Pai, Power system dynamics and stability, New Jersey: Prentice Hall, 1998.

[19] I. Ngamroo, Dynamic and stability of power system, King Mongkut's Institute of Technology Ladkrabang, 2011.

[20] N. Hashim, N. Hamzah, P. Mohd Arsad, R. Baharom, N. N. Ismail, N. Aminudin and D. Johari, "Modeling of power system dynamic devices incorporated in dynamic computation for power systems (DCPS) for transient stability analysis," *IEEE International Electric Machines & Drives Conference (IEMDC),* pp. 647-652, 2011.

[21] A. Karami and S. Esmaili, "Transient stability assessment of power systems described with detailed models using neural networks," *Electrical Power and Energy Systems,* vol. 45, p. 279–292, 2013.

[22] S. Kyuwa, T. Yoshida, S. Yuasa, K. Omata and K. Mitamura, "Operator Training Simulator with Real-time Transient Analysis," *IEEE Transaction on Power System,* vol. 9, no. 2, pp. 721-729, 1994.

[23] R. Kuruneru and A. Bose , "Feasibility Study of transient stability analysis for operator training simulators," in *IEE Proceeding Generation Transmission Distribution*, 1997.

[24] G. Aloisio, M. Bochicchio, M. La Scala and R. Sbrizza, "A DISTRIBUTED COMPUTING APPROACH FOR REAL-TIME TRANSIENT STABILITY ANALYSIS," *IEEE Transaction on Power Systems,* vol. 12, no. 2, pp. 981-987, 1997.

[25] C.-W. Liu, S.-S. Tsay and Y.-J. Wa, "Neuro-fuzzy approach to real-time transient stability prediction based on synchronized phasor measurements," *Electric Power Systems Research,* vol. 49, p. 123–127, 1999.

[26] V. Vittal, "Consequence and Impact of Electric Utility Industry Restructuring on Transient Stability and Small-Signal Stability Analysis," in *IEEE Proceeding*, 2000.

[27] H. Sawhney and B. Jeyasurya, "A feed-forward artificial neural network with enhanced feature selection for power system transient stability assessment," *Electric Power Systems Research,* vol. 76, p. 1047–1054, 2006.

[28] Y. Li, H. Chiang, B. Choi, Y. Chen, D. Huang and M. Lauby, "Representative static load models for transient stability analysis: development and examination," in *IET Generation Transmission and Distribution*, 2007.

[29] S. Muyeen, M. Hasan Ali, R. Takahashi, T. Murata, J. Tamura, Y. Tomaki, A. Sakahara and E. Sasano, "Comparative study on transient stability analysis of wind turbine generator system using different drive train models," *IET Renewable Power Generation,* vol. 1, pp. 132-141, 2007.

[30] M. Hasan Ali, M. Park, I.-K. Yu, T. Murat, J. Tamura and B. Wu, "Enhancement of transient stability by fuzzy logic-controlled SMES considering communication delay," *Electrical Power and Energy Systems,* vol. 31, pp. 402-408, 2009.

[31] R. Khanna, G. Singh and T. Nagsarkar, "Artificial Neural Network Based SMES Unit for Transient Stability Improvement," in *IEEE Conference*, 2011.

[32] N. Hashim, N. Hamzah, P. Mohd Arsad, R. Baharom, N. Nik Ismail, N. Aminudin, D. Johari and A. Sallehhudin , "Modeling of Power System Dynamic Devices Incorporated in Dynamic Computation for Power Systems (DCPS) for

Transient Stability Analysis," in *IEEE International Electric Machines & Drives Conference (IEMDC)*, 2011.

[33] A. Marini Mohamad, N. Hashim, N. Hamzah, N. F. Nik Ismail and M. F. Abdul Latip, "Transient Stability Analysis on Sarawak's Grid using Power System Simulator for Engineering (PSS/E)," in *IEEE Symposium on Industrial Electronics and Applications*, Malaysia, 2011.

[34] S. C. Marchiori, M. d. C. G. da Silveira, A. D. P. Lotufo, C. R. Minussi and M. L. Martins Lopes, "Neural network based on adaptive resonance theory with continuous training for multi-configuration transient stability analysis of electric power systems," *Applied Soft Computing*, vol. 11, pp. 706-715, 2011.

[35] A. Karami, "Power system transient stability margin estimation using neural network," *Electrical Power and Energy Systems*, vol. 33, pp. 983-991, 2011.

[36] H. H. Al Marhoon, I. Leevongwat and P. Rastgoufard, "A Practical Method for Power Systems Transient Stability and Security Analysis," in *IEEE Conference*, 2012.

[37] L. Wang, "Techniques for High Performance Analysis of Transient Stability," in *IEEE Proceeding*, 2013.

[38] J. Astic, M. Jerosolimski and A. Bihain, "The Mixed Adams-BDF Variable Step Size Algorithm to Simulate Transient an Long Term Phenomena in Power Systems," *IEEE Transactions* , vol. 9, no. 2, 1994.

[39] M. Tomim, J. Martí and L. Wang, "Parallel solution of large power system networks using the Multi-Area Thévenin Equivalents (MATE) algorithm," *International Journal of Electrical Power & Energy System*, vol. 31, no. 9, pp. 497-503, 2009.

[40] J. Tong and L. Wang, "Design of a DSA Tool for Real Time System Operations," in *Powercon 2006*, China, 2006.

[41] L. Wang, M. Klein, S. Yirga and P. Kundur, "Dynamic Reduction of Large Power Systems For Stability Studies," *IEEE Transaction on Power Systems*, vol. 12, no. 2, pp. 889-895, 1997.

[42] L. Loud, S. Guillon, G. Vanier, J. Huang, D. Lefebvre and J. Rizzi, "Hydro-Québec's challenges and experiences in on-line DSA applications," in *IEEE PES General Meeting*, Minneapolis, 2010.

[43] H. Ahmadi, H. Ghasemi, A. Haddadi and H. Lesani, "Two approaches to transient stability-constrained optimal power flow," *Electrical Power and Energy Systems,* vol. 47, pp. 181-192, 2013.

[44] S. R. Khuntia and S. Panda, "ANFIS approach for SSSC controller design for the improvement of transient stability performance," *Mathematical and Computer Modelling,* vol. 57, pp. 289-300, 2013.

[45] Y. Oguz, S. V. Ustun, I. Yabanova, M. Yumurtaci and I. Guney, "Adaptive neuro-fuzzy inference system to improve the power quality of a split shaft microturbine power generation system," *Journal of Power Sources,* vol. 197, pp. 196-209, 2012.

[46] D. Abdellah and L. Djamel, "Power flow analysis using adaptive neuro-fuzzy inference systems," in *IEEE Renewable and Sustainable Energy Conference (IRSEC),* 2015.

[47] Y. Oguz and I. Guney, "Adaptive neuro-fuzzy inference system to improve the power quality of variable-speed wind power generation system," *Turkish Journal of Electrical Engineering & Computer Sciences,* vol. 18, pp. 625-645, 2010.

[48] A. Vani, "An adaptive neuro fuzzy inference system for fault detection in transformers by analyzing dissolved gases," *IEEE Information Technology, Computer and Electrical Engineering (ICITACEE),* 2014.

[49] O. A. Kumar and C. R. Reddy, "Hybrid neuro-fuzzy controller based adaptive neuro-fuzzy inference system approach for multi-area load frequency control of interconnected power system," *SSRG International Journal of Electrical and Electronics Engineering,* vol. 3, pp. 17-25, 2016.

[50] U. R. Babu, V. V. K. Reddy and S. T. Kalyani, "Design of power system stabilizer with neuro-fuzzy UPFC controller," *International Journal of Electrical, Computer, Energetic, Electronic and Communication Engineering,* vol. 8, pp. 1945-1948, 2014.

[51] A. Jamal and R. Syahputra, "Adaptive Neuro-Fuzzy Approach for the Power System Stabilizer Model in Multi-machine Power System," *International Journal of Electrical & Computer Sciences,* vol. 12, pp. 6-13, 2012.

[52] R. Berglund, W. Mittelstadt, M. Shelton, P. Barkan, C. Dewey and K. Skreiner, "Once-Cycle Fault Interruption at 500 kV: System Benefits and Breaker Design," *IEEE Transaction,* vol. 93, pp. 1240-1251, 1974.

[53] J. Esztergalyos, M. Yee, M. Chamia and S. Liberman, The development and operation of an ultra high speed relaying system for EHV lines, CIGRE 34-03, 1978.

[54] C. Lindsay and V. Shenoy, Reliability and selection of characteristics for EHV transformers, CIGRE 12-08, 1978.

[55] G. Breuer, H. Rustebakke, R. Gibley and H. Simmons, "The use of series capacitors to obtain maximum EHV transmission capability," *IEEE Transaction,* vol. 83, pp. 1090-1101, 1964.

[56] E. Kimbark, "Improvement of System Stabiility by Switched Series Capacitors," *IEEE Transaction,* vol. 85, pp. 180-188, 1966.

[57] IEEE Task Force Report, "A description of discrete supplmentary controls for stability," *IEEE Transaction,* vol. 97, pp. 149-165, 1978.

[58] H. Ellis, J. Hardy, A. Blythe and J. Skooglund, "Dynamic stability of the peace river transsion system," *IEEE Transaction,* vol. 85, pp. 586-600, 1966.

[59] M. Shelton, R. Winkleman, W. Mittelstadt and W. Bellerby, "Bonneviller power administration 1400 MW braking resistor," *IEEE Transaction,* vol. 94, pp. 602-611, 1975.

[60] EPRI Report EL-5859, "Technical limits to transmission system operation," Power Technologies, 1988.

[61] N. Knudsen, Single-phase switching of transmission lines using reactors for extinction of the secondary arc, CIGRE 310, 1962.

[62] A. Fakheri, The use of reactor switches in single phase switching, CIGRE 13-06, 1980.

[63] W. Suparta and K. M. Alhasa, Modeling of tropospheric delays using ANFIS, SpringerNature, 2016.

[64] S. Haykin, Neural Networks and Learning Machines, 3rd ed., Prentice Hall, 2009.

[65] M. Warren and W. Pitts, "A Logical Calculus of Ideas Immanent in Nervous Activity," *Bulletin of Mathematical Biophysics,* pp. 115-133, 1943.

[66] W. Duch and N. Jankowski, Survey of Neural Transfer Functions. Neural Computing Surveys, 1999.

[67] M. Dorofki, A. Elshafie, O. Jaafar and O. Karim, "Comparison of artificial neural network transfer functions abilities to simulate extreme runoff data," *International Proceedings of Chemical, Biological and Environmental,* pp. 39-44, 2012.

[68] A. Jain, J. Mao and K. Mohiuddin, "Artificial neural networks: a tutorial," *Computer,* pp. 31-44, 1996.

[69] Jang, Sun and Mizutani, Neuro-fuzzy and soft computing, Prentice Hall, 1997, pp. 335-368.

[70] N. Nedjah, "Adaptation of fuzzy inference system using neural learning theory and practice," *Studies in Fuzziness and Soft Computing, Springer Verlag,* pp. 53-83, 2005.

[71] S. Burhenne, D. Jacob and G. P. Henz, "Sampling Based On Sobol Sequences for Monte Carlo Techniques Applied to Building Simulations," in *Proceedings of Building Simulation*, 2011.

[72] I. Sobol, Distribution of points in a cube and approximate evaluation of integrals, U.S.S.R Comput. Maths, 1967.

[73] H. Niederreiter, "Low-Discrepancy and Low-Dispersion Sequences," *Journal of Number Theory,* vol. 30, p. 51–70, 1988.

[74] I. Antonov, and V. Saleev, "An economic method of computing LPτ-sequences," *Maths,* vol. 19, p. 252–256, 1979.

[75] Powerworld, "Powerworld Simulator Version 17".

[76] F. Milan, "An open source power system analysis toolbox," *IEEE Transaction on Power System,* p. 1199–1405, 2005.

[77] MATLAB, "MATLAB 2012a".

APPENDIX

APPENDIX A

BLOCK MODELS USED IN THIS RESEARCH

A.1 Exitation Block Model

Excitor IEEET1

IEEE Type 1 Excitation System Model

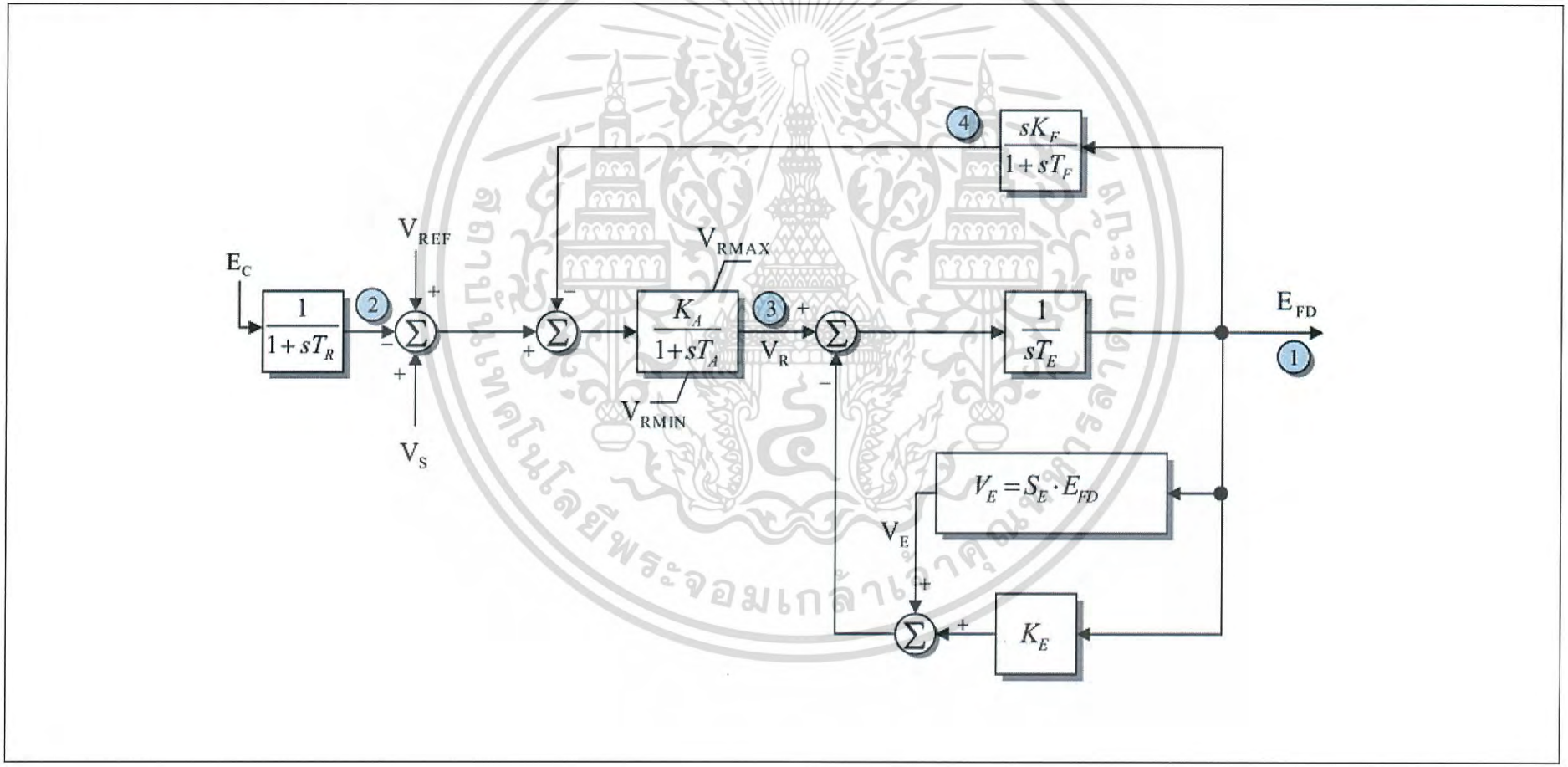

Excitor IEEET2

IEEE Type 2 Excitation System Model

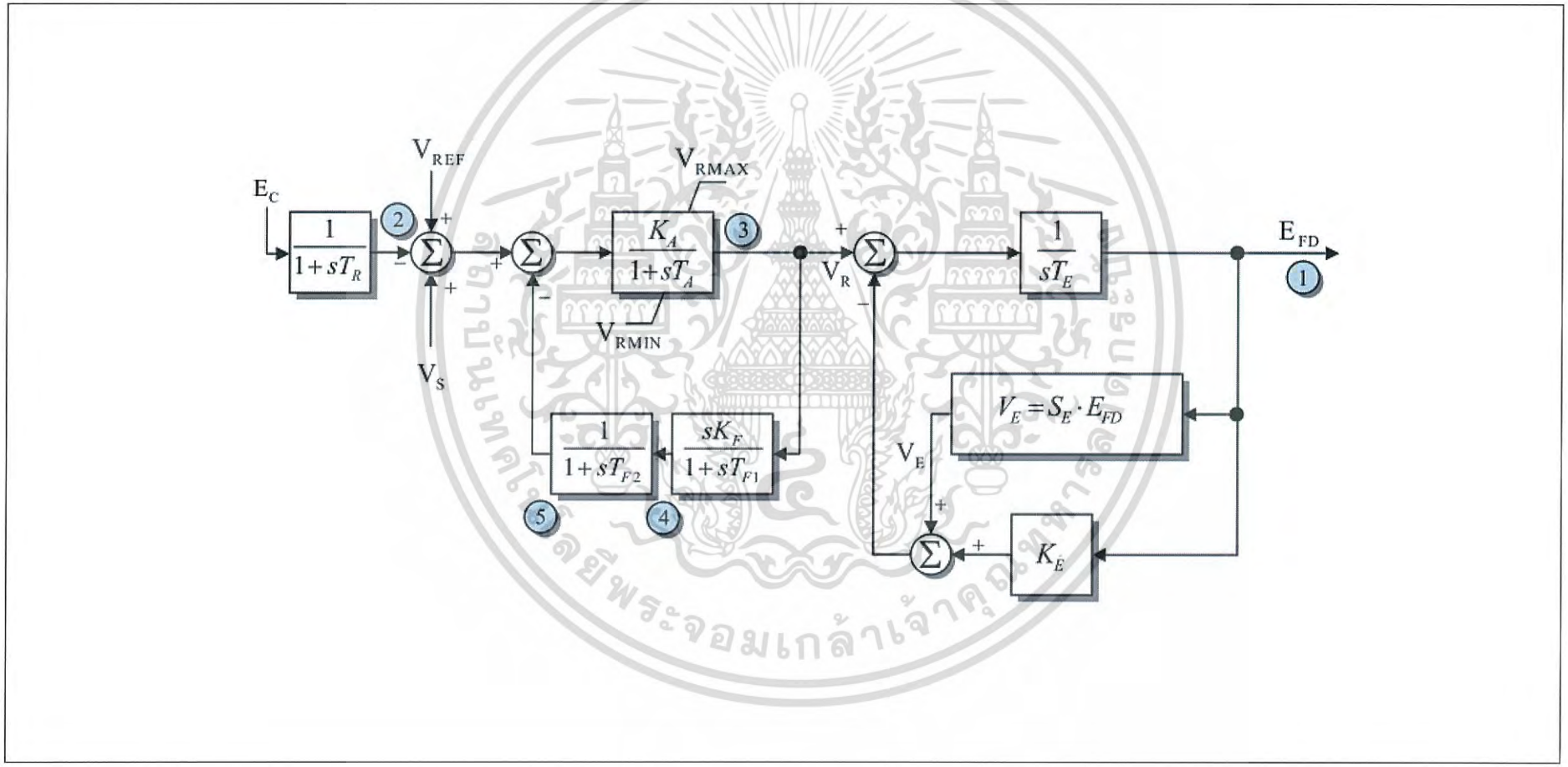

Excitor IEEEX1

IEEEX Type 1 Excitation System Model

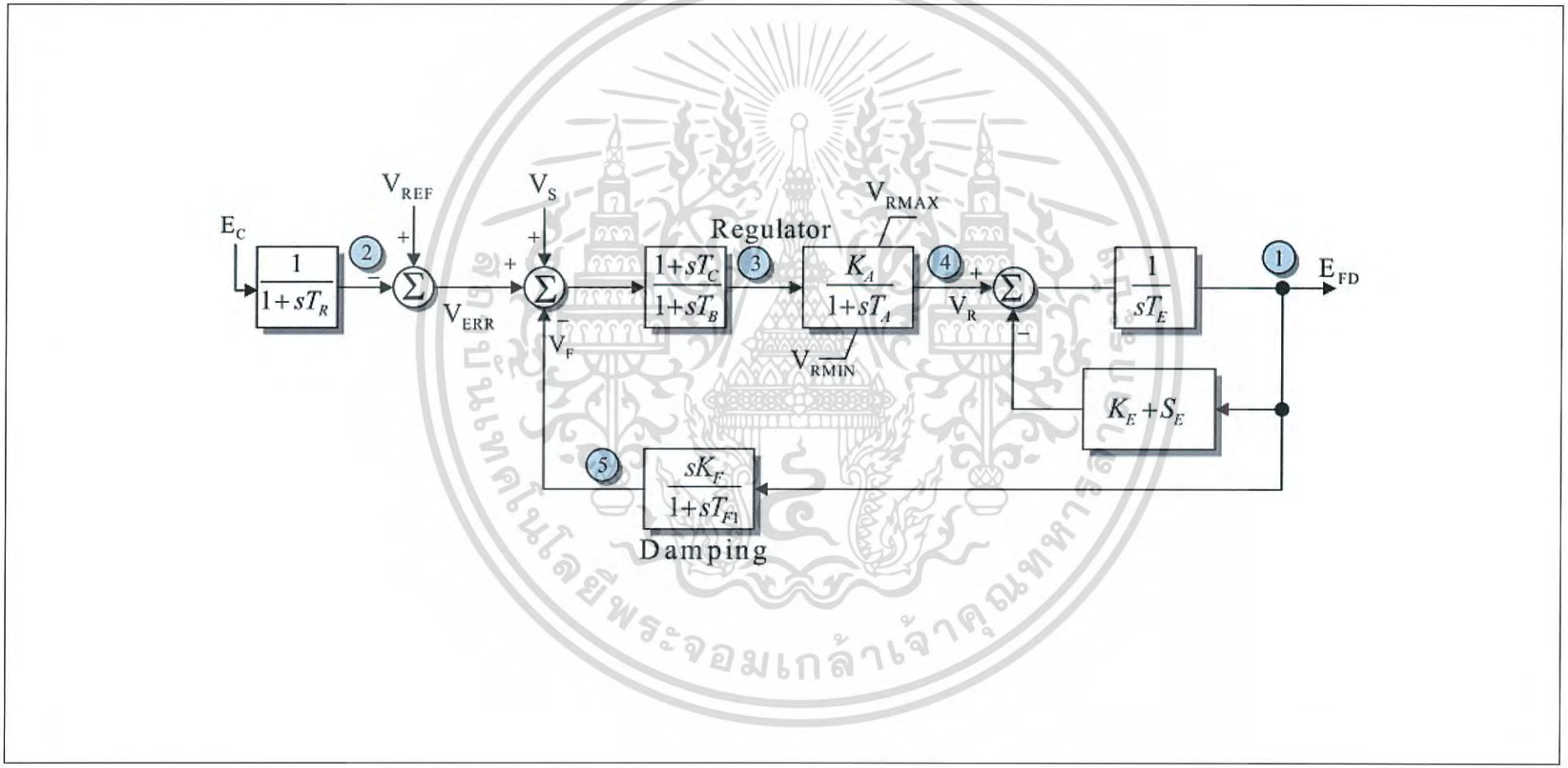

Excitor AC8B

AC8B Excitation System - IEEE 421.5 2005

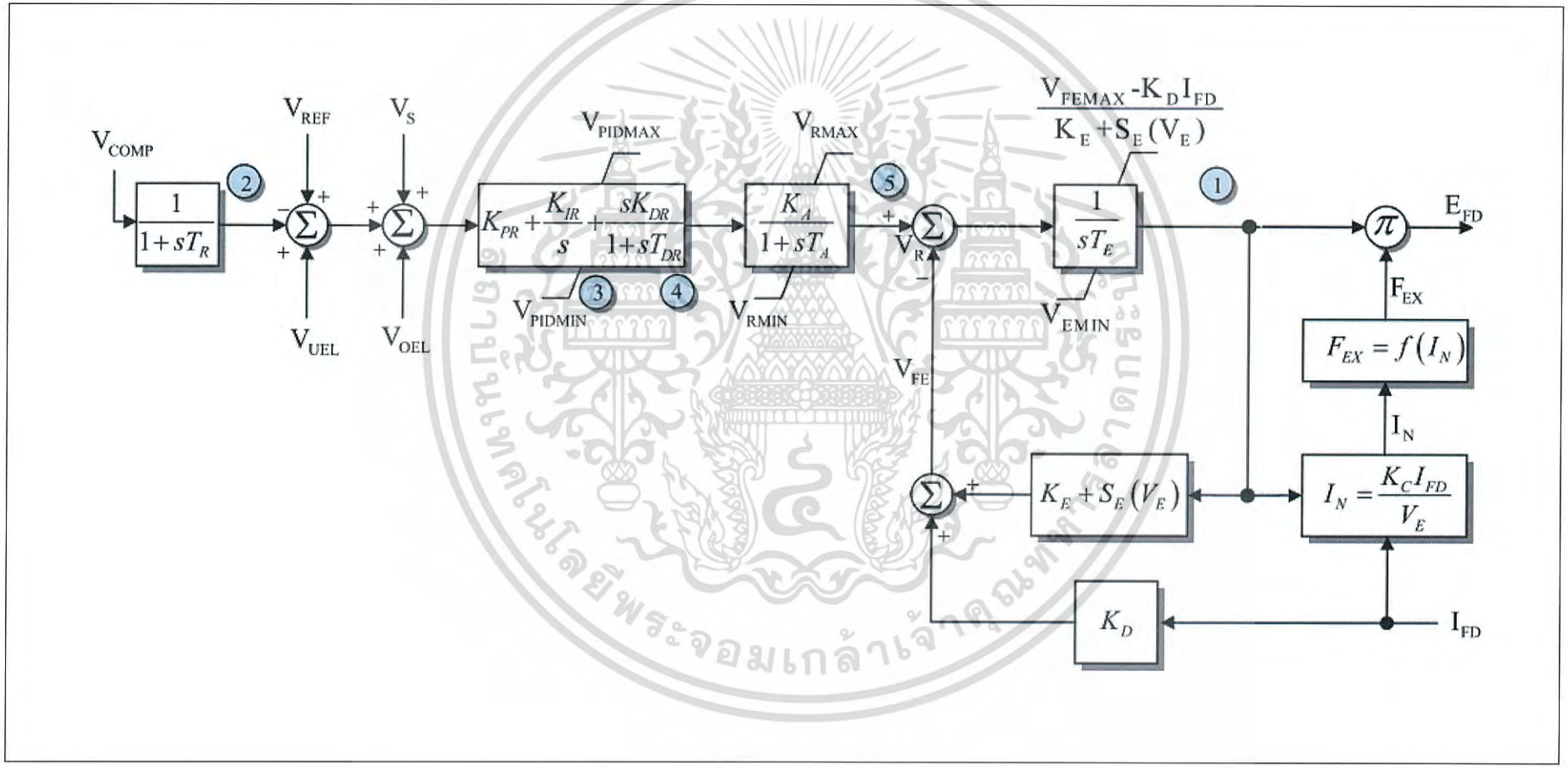

A.2 Governor Block Model

Governor IEEEG1

Governor Model - IEEE Type 1 Speed

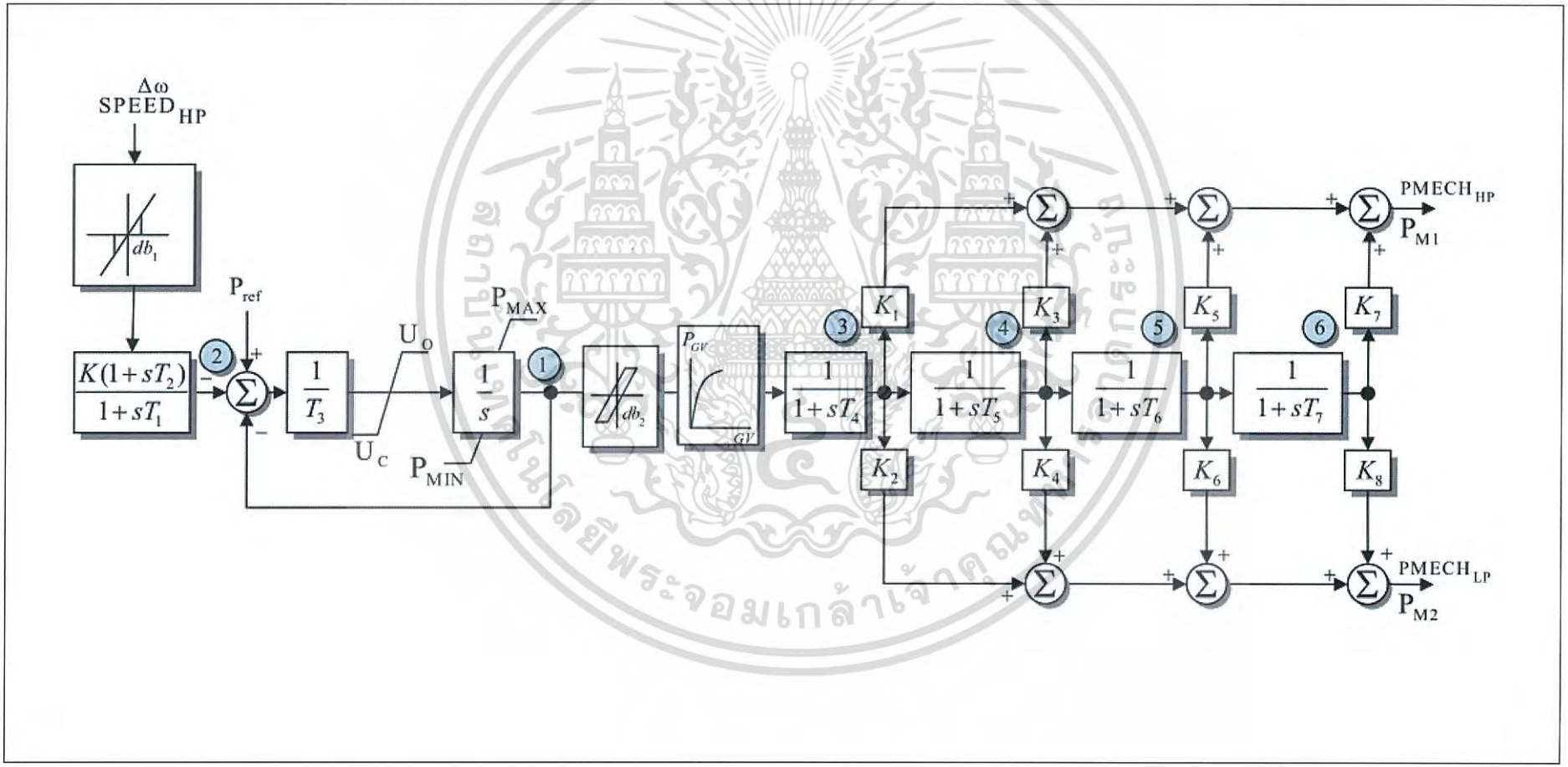

Governor GGOV1

GE General Governor - Turbine Model

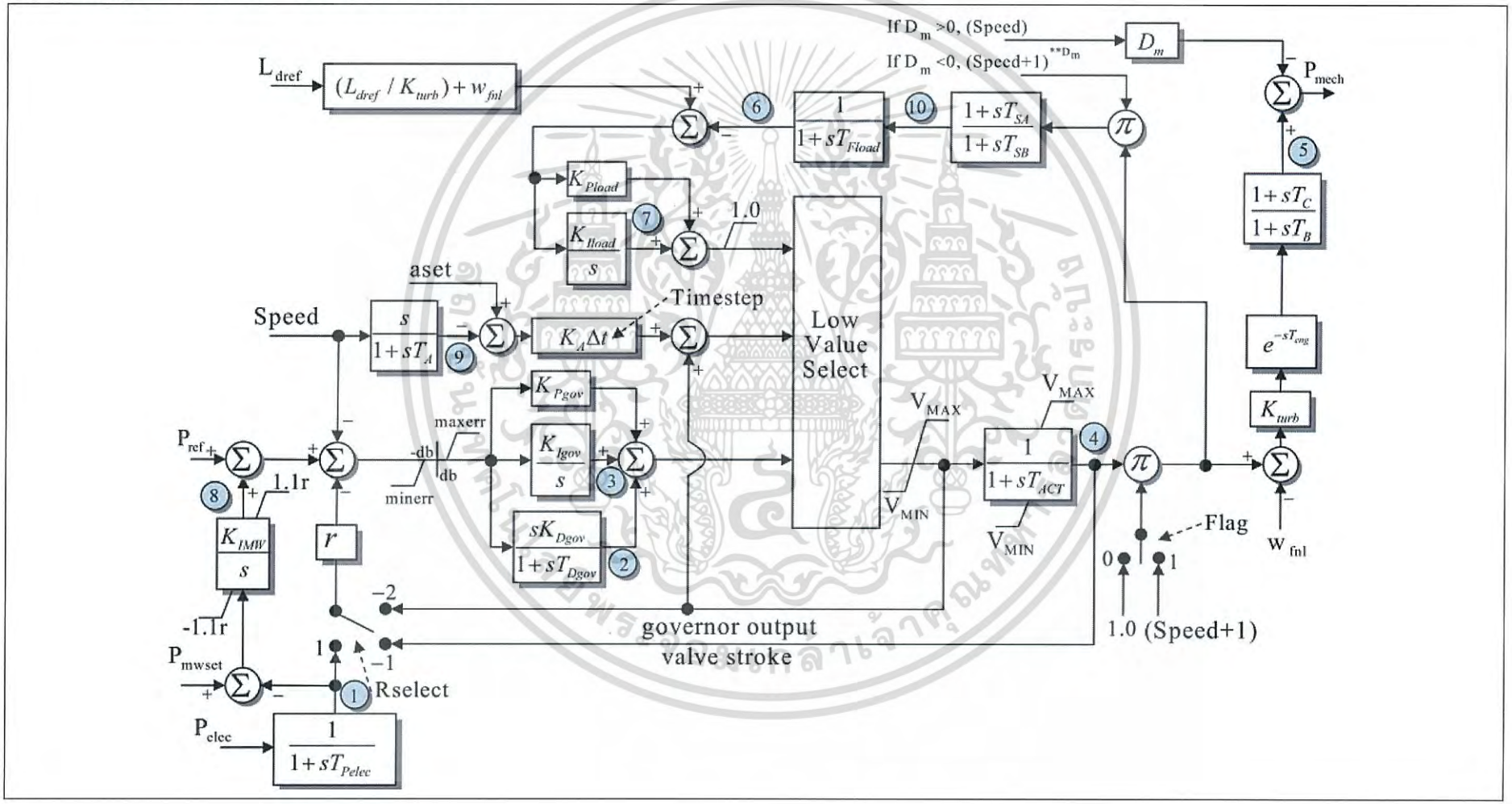

Governor TGOV3

Speed-Governor with Fast Valving Model - Modified IEEE Type 1

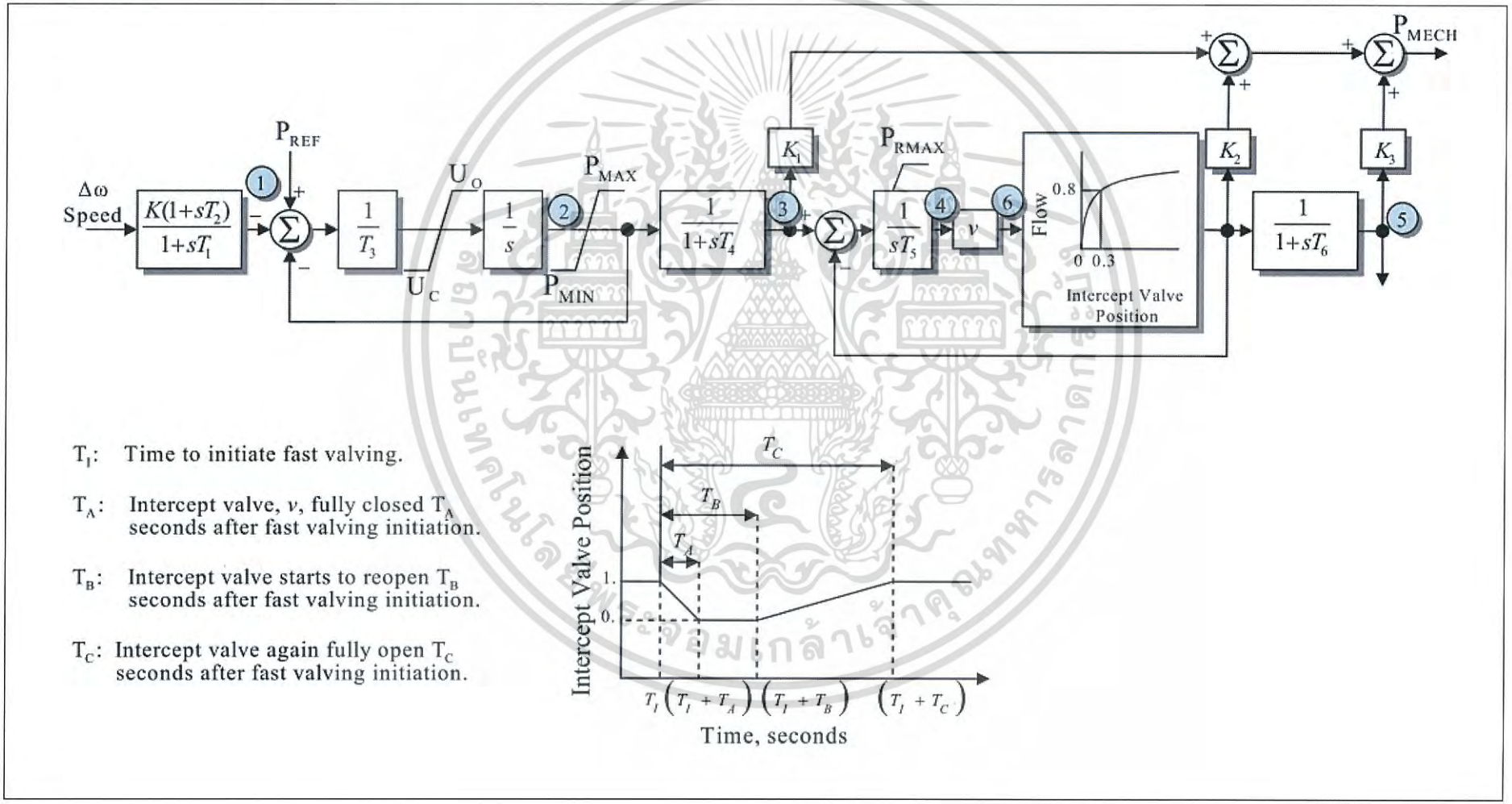

A.3 Machine Block Model

Machine Model GENCLS

Synchronous machine represented by classical modeling

Speed-Governor with Fast Valving Model - Modified IEEE Type 1

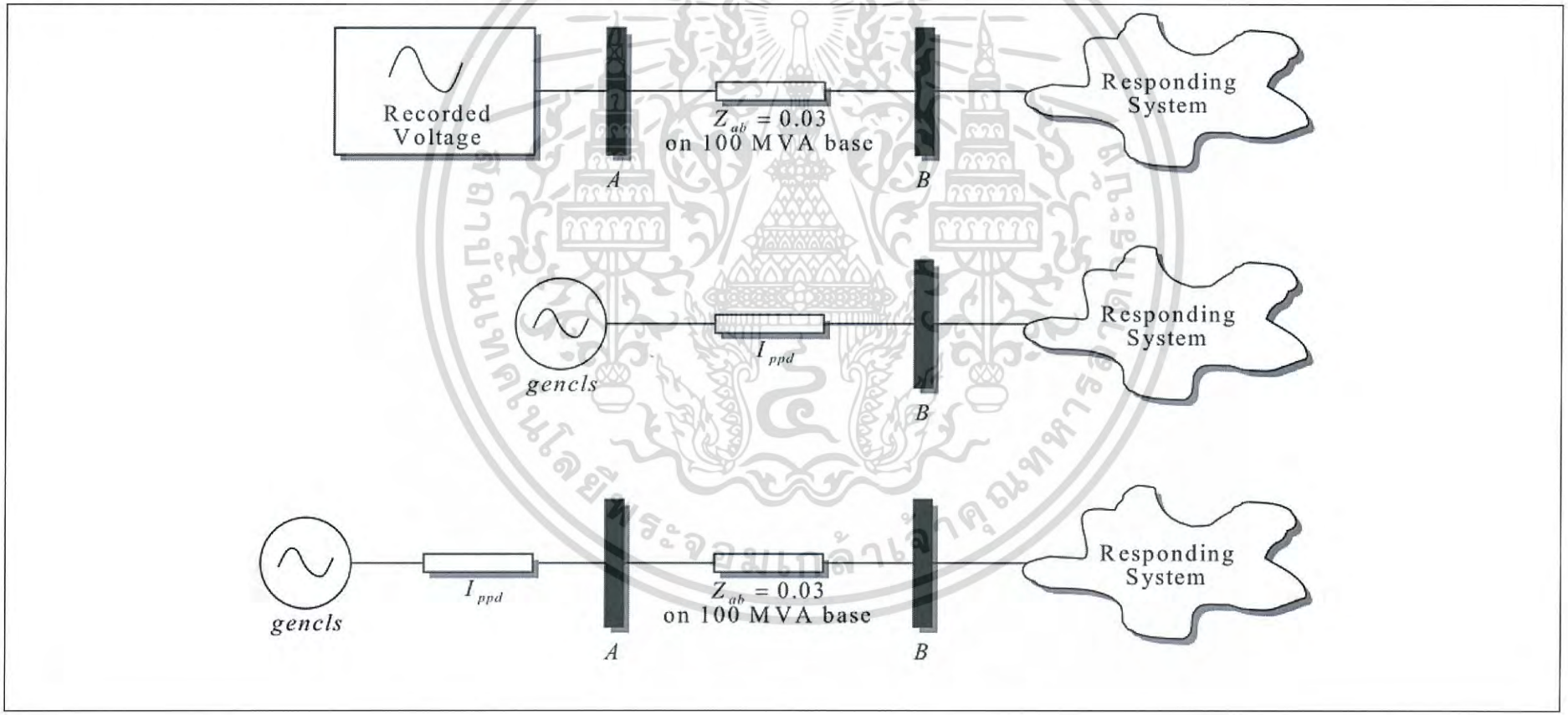

Machine Model GENROU

Solid Rotor Generator represented by equal mutual inductance rotor modeling

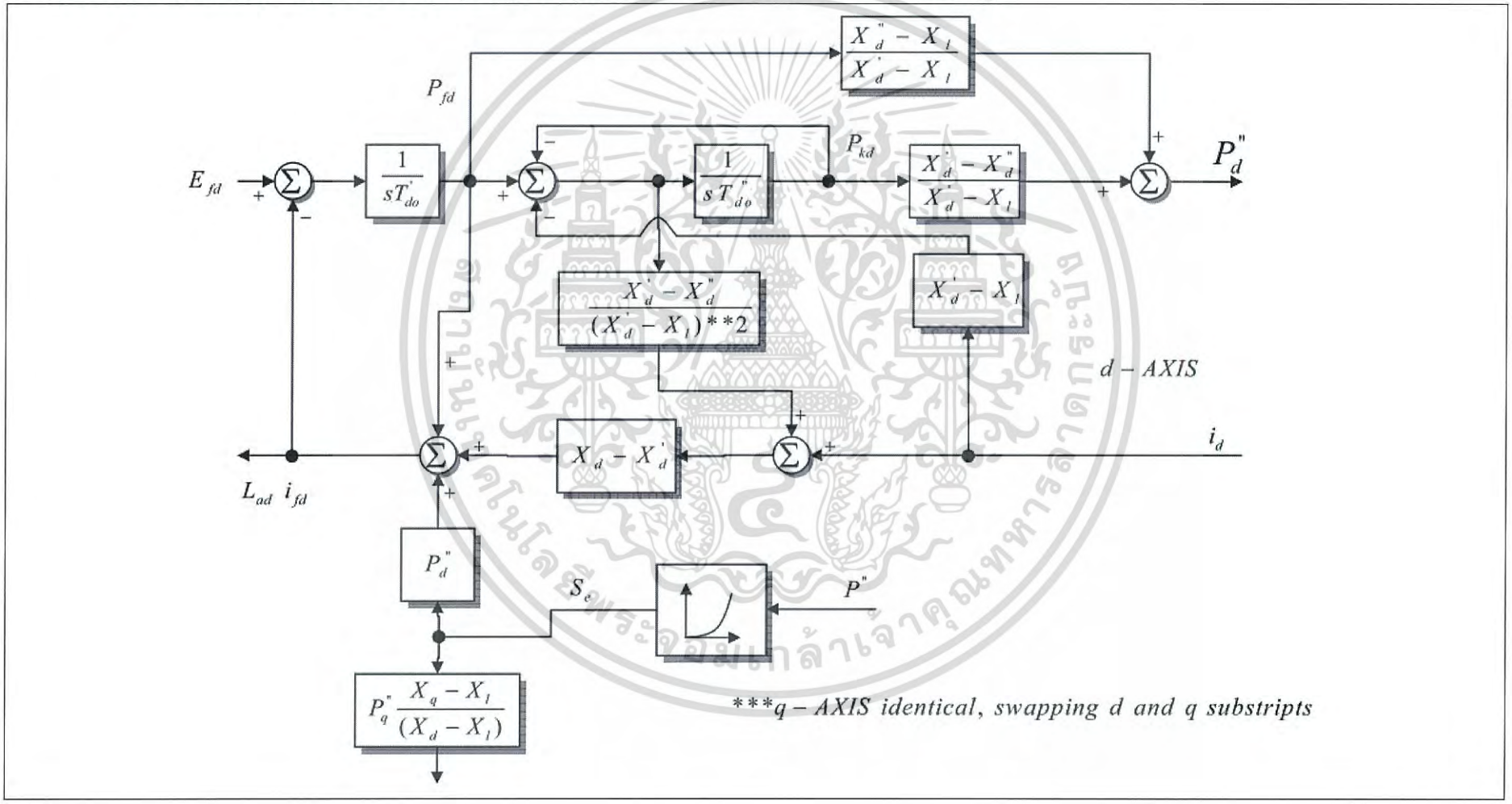

Machine Model GENSAL

Salient Pole Generator represented by equal mutual inductance rotor modeling

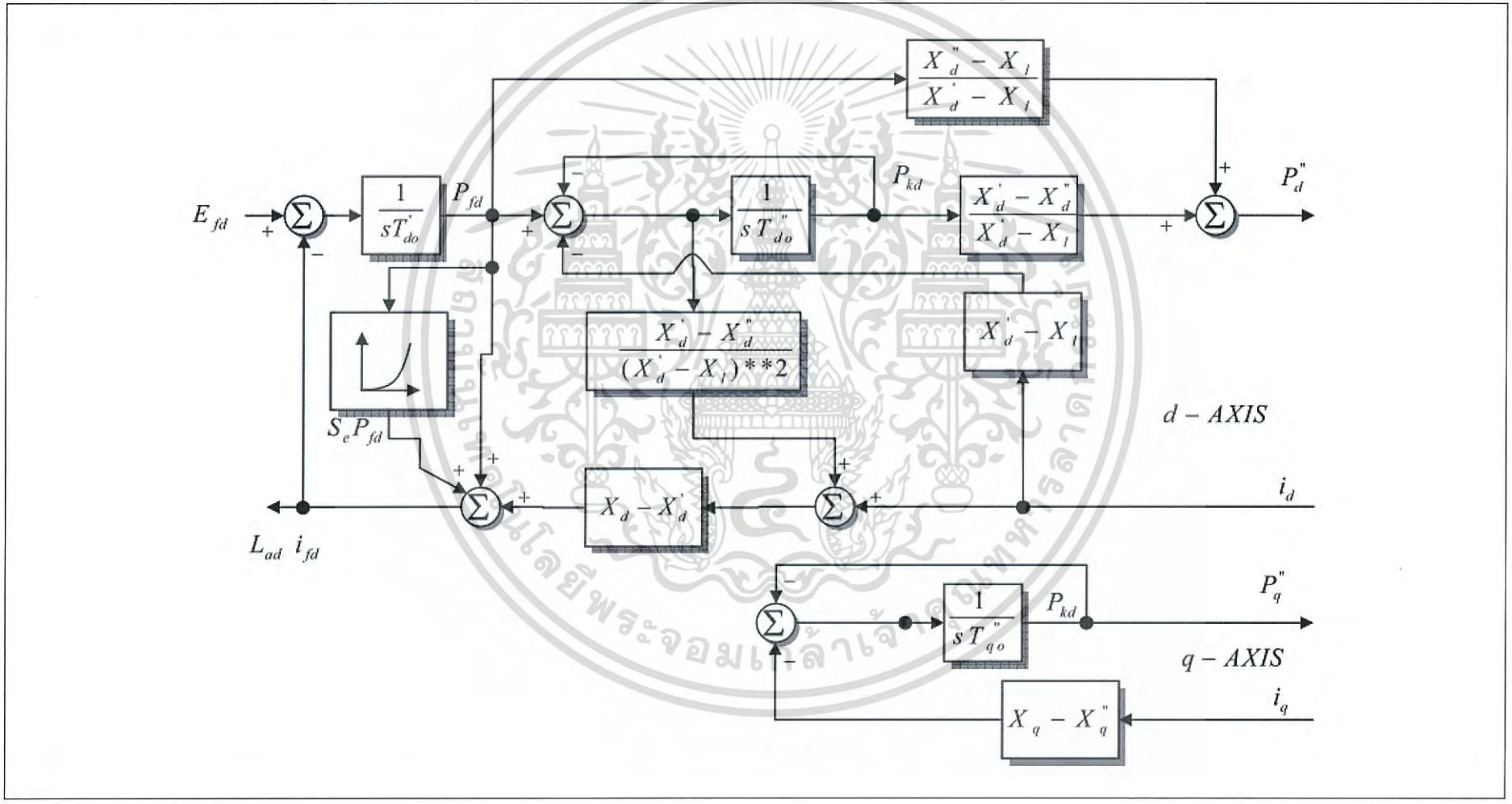

A.4 Load System

Load Characteristic CLOD

Complex Load Model

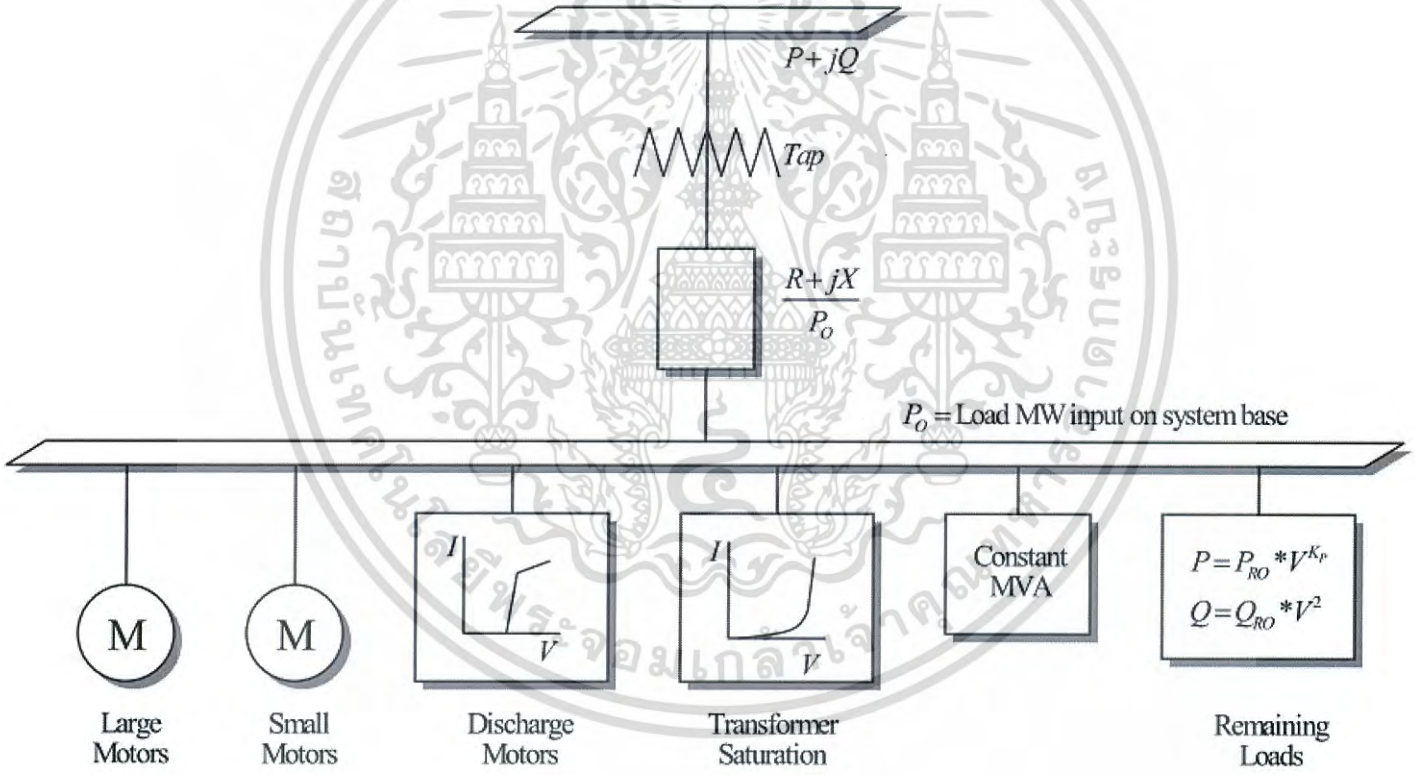

APPENDIX B

PARAMETERS USED IN THIS RESEARCH

Generator Records for Base Case

Bus	Gen MW	Gen Mvar	Set Volt	Min MW	Max MW	Min Mvar	Max Mvar
30	250	194.96	1.0475	0	350	-110.79	208.57
31	839.34	322.67	0.982	0	1200	-385.94	723.75
32	650	202.62	0.9831	0	750	-200.15	364.61
33	632	148.84	0.9972	0	800	-232.46	447.31
34	508	183.79	1.0123	0	700	-218.83	413.26
35	650	45.57	1.0493	0	800	-226.29	438.57
36	560	176.22	1.0635	0	700	-201	388
37	540	-5.02	1.0278	0	700	-207.86	397.71
38	830	33.9	1.0265	0	1000	-276.86	539.71
40	1000	172.69	1.03	0	1400	-443.14	834.29

Machine Model – Gen 2 Axis Poles Model

Bus	H	D	Xd	Xq	Xdp	Xqp	Tdop	Tqop
30	84	0.84	0.1	0.069	0.031	0.008	10.2	0.1
31	60.6	0.606	0.295	0.282	0.697	0.17	6.56	1.5
32	71.6	0.716	0.2495	0.237	0.0531	0.0876	5.7	1.5
33	50	0.5	0.262	0.258	0.0436	0.166	5.69	1.5
34	52	0.52	0.67	0.62	0.132	0.166	5.4	0.44
35	69.2	0.692	0.254	0.241	0.05	0.0814	7.3	0.4
36	52.8	0.528	0.295	0.292	0.049	0.186	5.66	1.5
37	48.6	0.486	0.29	0.28	0.057	0.0911	6.7	0.41
38	69	0.69	0.2106	0.205	0.057	0.0587	4.79	1.96
40	750	7.5	0.02	0.019	0.006	0.008	7	0.7

Exciter Model – IEEET1 Model

Bus	Ka	Ta	Vrmin	Ke	Te	Kf	Tf	SE(E1)	SE(E2)
30	5	0.06	-1	-0.0485	0.25	0.04	1	0.0063	0.0171
31	6.2	0.05	-1	-0.633	0.405	0.057	0.5	0.37	0.4916
32	5	0.06	-1	-0.0198	0.5	0.08	1	0.0249	0.0853
33	5	0.06	-1	-0.0525	0.5	0.08	1	0.0055	0.0231

Bus	Ka	Ta	Vrmin	Ke	Te	Kf	Tf	SE(E1)	SE(E2)
34	40	0.02	-10	1	0.785	0.03	1	0.0002	0.0016
						0.075	1.2		
35	5	0.02	-1	-0.0419	0.471	4	46	0.0033	0.0104
36	40	0.02	-6.5	1	0.73	0.03	1	0.2784	0.398
						0.085	1.2		
37	5	0.02	-1	-0.047	0.528	4	6	0.0043	0.0156
38	40	0.02	-10.5	1	1.4	0.03	1	0.3005	0.3754
40	0	0.06	0	-0.0485	0.25	0.04	1	0.0063	0.0171

APPENDIX C

RELATIVE PUBLISHED PAPERS

RELATIVE PUBLISHED PAPERS

1. Witsawa Phootrakornchai and Somchat Jiriwibhakorn. "**Online critical clearing time estimation using an adaptive neuro-fuzzy inference system (ANFIS).**" International Journal of Electrical Power and Energy Systems. Vol. 73. 2015. pp. 170-181.
2. Witsawa Phootrakornchai and Somchat Jiriwibhakorn. "**Transient Staiblity Analysis by Adaptive Neuro Fuzzy Inference System and Sobol Sequence.**" Conference Proceeding: ECTI International Conference (ECTI-CON). 2018.
3. Witsawa Phootrakornchai and Somchat Jiriwibhakorn. "**Real-time Critical Clearing Time Estimation By Considering Contingency Conditions.**" Conference Proceeding: ECTI International Conference (ECTI-CON). 2018.

Electrical Power and Energy Systems 73 (2015) 170–181

Contents lists available at ScienceDirect

Electrical Power and Energy Systems

journal homepage: www.elsevier.com/locate/ijepes

Online critical clearing time estimation using an adaptive neuro-fuzzy inference system (ANFIS)

Witsawa Phootrakornchai *, Somchat Jiriwibhakorn

Electrical Engineering Department, Faculty of Engineering, King Mongkut's Institute of Technology Ladkrabang, Ladkrabang District, 10520 Bangkok, Thailand

ARTICLE INFO

Article history:
Received 11 July 2014
Received in revised form 9 February 2015
Accepted 19 March 2015
Available online 16 May 2015

Keywords:
Transient stability assessment
Critical clearing time
Classical model
Detailed model
Adaptive neuro-fuzzy inference system

ABSTRACT

This paper describes an approach using an adaptive neuro-fuzzy inference system (ANFIS) for the assessment of online critical clearing time (CCT). The ANFIS can integrate neural networks and fuzzy logic principles, and has a potential to combine the advantages of both in a single framework. In this paper, the ANFIS is applied for the prediction of CCT by varying load levels and fault locations in buses and transmission lines. The IEEE 39-bus system and 9-bus western system coordinating council are tested and implemented in this study. All machines of the IEEE 39-bus system are considered as the classical model without considering any generator's exciters. While three machines in the 9-bus western system coordinating council are considered as detailed models, forth-order differential equation is described for all machines by considering the excitation system controller. CCT values obtained by the time domain simulation method using step-by-step calculation are used as the benchmark. The power world version 17 is used for transient simulation, and the ANFIS is implemented using MATLAB version 2014B. The results obtained from the ANFIS approach are quite satisfied with high accurate solutions and much lower computation time. Finally, the graphical user interface in MATLAB is applied for the online CCT estimation of two test power systems by using appropriate ANFIS models obtained from simulations.

Introduction

The recent increase in power demand has significantly influenced the stability of power systems, making them complicated. Further studies of power system stability [1] are required to maintain the power system steady with high efficiency. It helps us understand the change of parameters in power flow and synchronism capability caused by fault current, transmission system outage, generator outage, and sudden increase or decrease in load. These induce the deviation of voltage, current, power, generator shaft speed, and generator shaft torque.

Any sudden change in the power system changes the equilibrium between electrical and mechanical power, which may cause power oscillation and be unable to stabilize until a generator in the power system has to be tripped. Moreover, the sudden tripping of the generator may consequently make other generators tripped. It can take an effect of power outage largely in system.

In power systems with good stability and reliability, the system is able to sustain the power quality while being disturbed and after the disturbance is over. A frequent cause of the problem is from short circuit current. Appropriate protection for the system will eliminate the fault within CCT [1,2], otherwise the system may lead to instability and failure.

Present power systems are quite large with many PV buses and PQ buses with a complex connection of each bus. Thus, the transient stability analysis needs a computer for calculation. Majority of the CCT solutions are solved by time-domain simulation using the means of step-by-step, which are taken several times [2,3]. Many techniques are studied to be applied with the transient stability evaluation. For example, the application of fuzzy logic has been proposed for a stability controller system [4]. The approach of least square support vector machine (LS-SVM) has been applied for transient stability assessment [5]. The artificial neural networks (ANNs) has been proposed for CCT evaluation and transient stability assessment [6–8]. The feed forward multilayer perceptron with back propagation learning algorithm has been implemented to estimate CCT [9,10]. The generalized regression neural network)-based classification has been proposed for transient stability assessment via estimated CCT evaluation [11]. The direct approach based on transient energy function method without numerically solving the power system equations has been proposed to assess the transient stability [12].

In this paper, the ANFIS is proposed for the online critical clearing time estimation of power system. The ANFIS is a type of neural

* Corresponding author. Tel.: +66 81 831 4472; fax: +66 2 731 3931.
E-mail address: witsawa.p@hotmail.com (W. Phootrakornchai).

http://dx.doi.org/10.1016/j.ijepes.2015.03.024
0142-0615/

$$\frac{dV_{fi}}{dt} = \frac{1}{T_{fi}}\left[-V_{fi} - \frac{(1+S_{ei}(E_{fdi}))K_{fi}E_{fi}}{T_{ei}} + \frac{K_{fi}V_{ri}}{T_{ei}}\right], \tag{12}$$

$$S_e(E_{fd}) = A_e(e^{B_e|E_{fd}|} - 1), \tag{13}$$

where V_{ri} is the output voltage of automatic voltage regulator (AVR), V_{fi} is the output voltage of excitation system stabilizer, V_{refi} is the reference voltage of AVR, K_{ai} is the gain of AVR, K_{fi} is the gain of excitation system stabilizer, T_{ai} is the time constant of AVR, T_{ei} is the time constant of exciter, T_{fi} is the time constant of excitation system stabilizer, E_{fdi} is the voltage applied to generator field winding, S_e is the exciter saturation function. A_e and B_e are the constant values determined by the open-circuit magnetization curve.

The output voltage of AVR is limited at the lowest point by V_{rmin} and the highest point by V_{rmax}. If the AVR output value obtained from Eq. (9) is greater than the value set as V_{rmax}, the output will be V_{rmax}. However, if the AVR output value obtained from Eq. (9) is less than the value set as V_{rmin}, the output will be V_{rmin}.

Adaptive neuro-fuzzy inference system (ANFIS)

The ANFIS was developed from neural networks and fuzzy logic based on the Takagi–Sugeno fuzzy inference system, with potential to capture the benefits of both in a single framework. The NN has a capability of automatic learning but is unable to explain how to obtain the output from making decision. The fuzzy logic has an ability to generate output from fuzzy logical decision, but is not capable of self-operating learning.

The ANFIS architecture is shown in Fig. 2. The circular nodes represent fixed nodes, and the square nodes are nodes with parameters to be learnt. There are forward and backward passes for the ANFIS learning. The forward pass propagates the input vector through the network layer by layer. In the backward pass, the error is sent back through the network similar to the means of back propagation [21–23].

The inference system corresponds to a set of fuzzy IF-THEN rules with learning capability to approximate nonlinear functions. Assuming that the fuzzy inference system has two inputs x and y and one output z. The rules of first-order Sugeno fuzzy model can be described as the following:

If x is A_1 and y is B_1 THEN $f_1 = p_1x + q_1y + r_1$

If x is A_2 and y is B_2 THEN $f_2 = p_2x + q_2y + r_2$.

Layer 1, the output of each node is:

$$O_{1,i} = \mu_{A_i}(x) \quad i = 1,2, \tag{14}$$

$$O_{1,i} = \mu_{B_{i-2}}(y) \quad i = 1,2, \tag{15}$$

where x and y are the input nodes, i and A_i (or B_{i-2}) are the linguistic label associated with this node. $O_{1,i}(x)$ is the membership grade for x and y. In the IEEE 39-bus system implementation, pi-shaped function is selected, which can be explained as the equation below:

$$(x,a,b,c,d) = \begin{cases} 0, & x \leqslant a \\ 2\left(\frac{x-a}{b-a}\right)^2, & a \leqslant x \leqslant \frac{a+b}{2} \\ 1-2\left(\frac{x-b}{b-a}\right)^2, & \frac{a+b}{2} \leqslant x \leqslant b \\ 1, & b \leqslant x \leqslant c \\ 1-2\left(\frac{x-c}{d-c}\right)^2, & c \leqslant x \leqslant \frac{c+d}{2} \\ 2\left(\frac{x-d}{d-c}\right)^2, & \frac{c+d}{2} \leqslant x \leqslant b \\ 0, & x \geqslant d \end{cases}, \tag{16}$$

where a, b, c, d are parameters to be learnt. These are called the premise parameters.

Layer 2, every node in this layer is fixed. In this paper, the t-norm use 'AND' for the membership grades:

$$O_{2,i} = w_i = \mu_{A_i}(x)\mu_{B_i}(y), \quad i = 1,2. \tag{17}$$

Layer 3, contains fixed nodes that calculate the ratio of the firing strengths of the rules:

$$O_{3,i} = \overline{w}_i = \frac{w_i}{w_1 + w_2}. \tag{18}$$

In the layer 4, the nodes are adaptive and perform the consequent of the rules:

$$O_{4,i} = \overline{w}_i f_i = \overline{w}_i(p_ix + q_iy + r_i). \tag{19}$$

The parameters in this layer p_i, q_i, r_i are to be determined and referred to as the consequent parameters.

In the layer 5, there is a single node that computes the overall output:

$$O_{5,i} = \sum_i \overline{w}_i f_i = \frac{\sum_i w_i f_i}{\sum_i w_i}. \tag{20}$$

The method for ANFIS training in this paper is chosen as hybrid, which uses least-squares method to identify the consequent

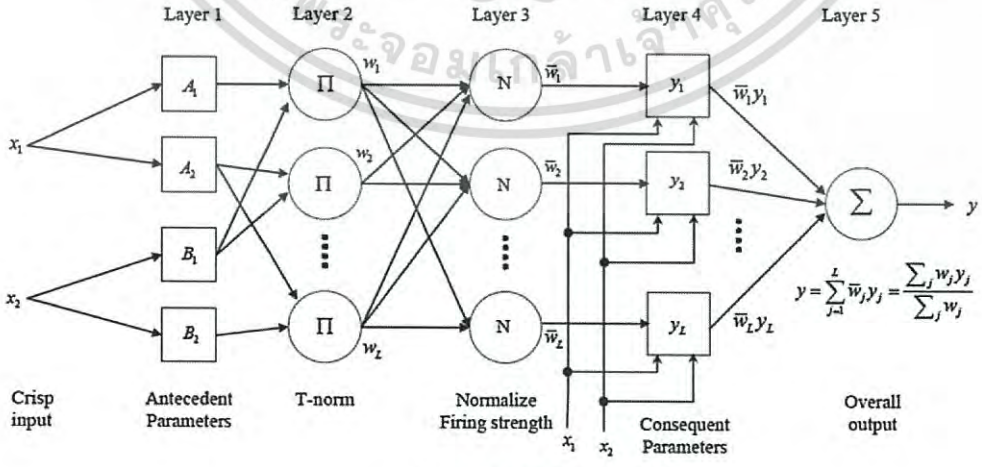

Fig. 2. ANFIS architecture.

parameters in the forward pass the algorithm. While in the backward pass the errors are propagated backward and the premise parameters are updated by the gradient descent. These are clearly explained in [22].

Implementation of ANFIS for transient stability assessment

The IEEE 39-bus system and 9-bus western system coordinating council are applied in this paper for the ANFIS implementation. The power world version 17 [13] is used for the transient simulation, and the ANFIS is implemented using MATLAB version 2014B [14].

The transient stability assessment focuses on CCT. The fault clearing time is randomly set to resolve the CCT value. If the rotor angles related to the slack bus angle are still stable or convergent after the three-phase fault has been cleared, it means that the system is stable. But if the rotor angles related to the slack bus angle are divergent, it means that the system is unstable. The different curves between the stable system and unstable system after fault cleared are shown in Figs. 3 and 4, respectively. In Fig. 3, the three-phase balanced fault occurs at $t = 1$ s and the fault is cleared at $t = 1.163$ s. In Fig. 4, the three-phase balanced fault occurs at $t = 1$ s and the fault is cleared at $t = 1.164$ s. If the time step (Δt) is considered at 0.001 s, the CCT herein will be 0.163 s after the fault occurs. It means that the fault clearing time shall be not greater than 0.163 s, otherwise the system will be unstable. Data obtained from the transient simulation are recorded for the ANFIS training and testing output.

39-bus system implementation

Parameters of machine, transformer, transmission line system, and load used for 39-bus system are given in Appendix A. The classical model is considered for all 10 machines. Due to the large system, so we select to examine some buses. In the simulation here, we intend to vary all loads and fault locations. Hence, we need to determine the study area so that the amount of input

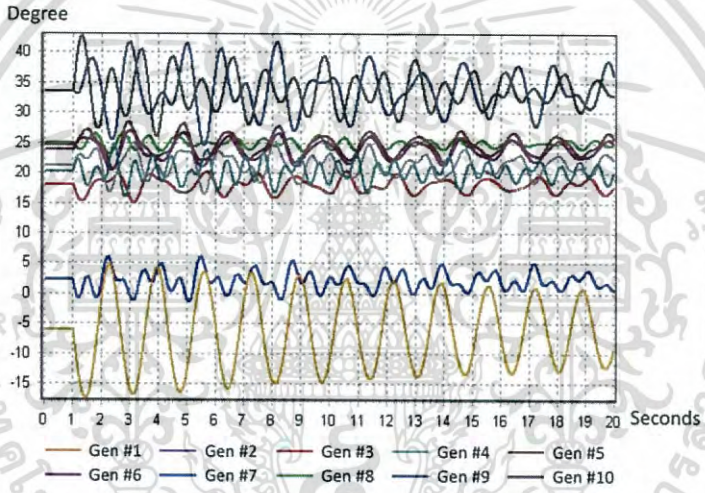

Fig. 3. Rotor angles related to the slack bus angle for a stable system after fault cleared.

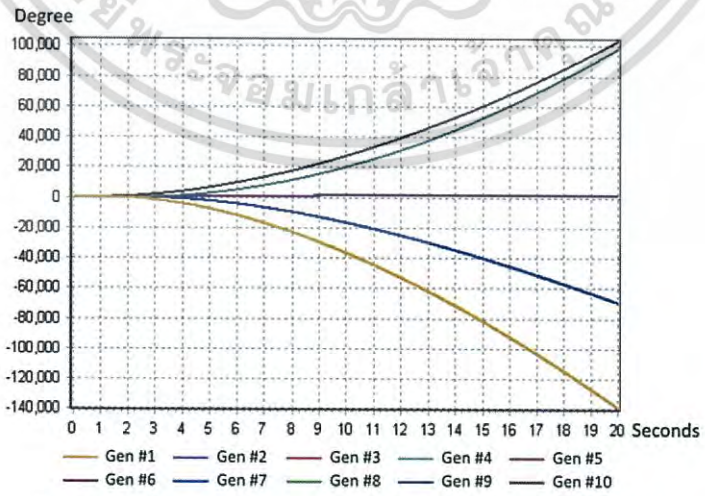

Fig. 4. Rotor angles related to the slack bus angle for an unstable system after fault cleared.

and training data could be less. The study area is in the dash line, as shown in Fig. 5. Training and testing data are generated using conventional type power world software.

The power user load simulated is varied between 0.8 and 1.2 of the values given in Appendix A. While the power factors of the load are set as constant. The power user load change is made only in the study area, including the load at buses 26, 27, 28, and 29. The contingency event chosen for simulation is three-phase balanced fault. The fault is occurred on a bus and also on a branch in the study area at a time. The fault position studied is 0.25, 0.50, and 0.75 of the whole transmission line length. The transmission line occurring the fault studied in this paper comprises 17–27, 26–27, 26–28, 26–29, and 28–29 lines. The data sets used for the simulation are randomly generated by MATLAB program.

The simulation runs for 20 s with 0.001 s of the time step (Δt). There are 400 sets of data generated from the simulation by power world software. The data set are divided into two sets, one is for training and the other is for testing. In this paper, 80% data of the data set is chosen for training and 20% of the data set is chosen for testing.

The ANFIS structure is designed as a pi-shaped membership function. The pi-shaped equation is described in Eq. (16). The variables used for ANFIS inputs comprise the power user loads and fault position. The training and testing outputs selected of ANFIS are CCT values. There is one CCT output and five inputs comprising four power user load inputs and one fault position input. The fault location and the fault position of transmission line are merged into one input. For example: if a fault occurs at 26–28 line and the position is at 75% of line length from the bus 26, the numerical input will be set as 262,875. The examples for inputs and output of ANFIS training patterns for IEEE 39-bus system are shown in Appendix B.

The amount of node in the layer 1 is 2-2-2-2-4, as shown in Fig. 6; it can be explained that there are 2 membership functions for the bus 26 load input, 2 membership functions for the bus 27 load input, 2 membership functions for the bus 28 load input, 2 membership functions for the bus 29 load input, and 4 membership functions for the fault position input. Moreover, there are 64 fuzzy rules set for ANFIS logical operation. Before ANFIS training, all data used for input and output have been normalized to zero mean and unity variance.

The flow chart of implementation steps in this paper is shown in Fig. 7.

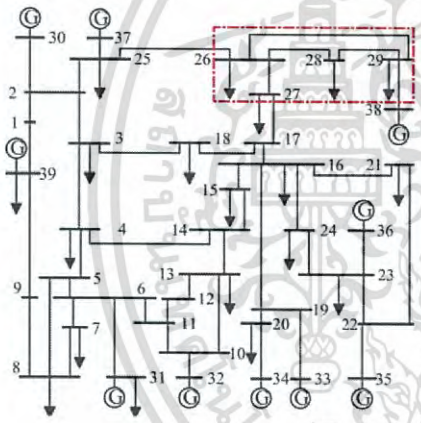

Fig. 5. IEEE 39-bus system.

9-bus western system coordinating council implementation

In this section the 9-bus western system coordinating council implementation is briefly described since the approach is similar to the 39-bus system implementation. Parameters of machine, excitation system, transformer, transmission system, and load used for 9-bus western system coordinating council shown in Fig. 8 are given in Appendix C. The 3 machines in the system are considered as a detailed mode. Training and testing data are generated by using power world software. The time domain method is chosen to solve the detailed model transient simulation because it is the most accurate method.

The power user loads simulated are varied between 0.8 and 1.2 of the values given in Appendix C. While the power factors of the load are set as constant. The contingency event chosen for the simulation is three-phase balanced fault. The fault positions studied are only 0.25, 0.50, and 0.75 of the whole transmission line length and at the bus. The above data are randomly generated by MATLAB program.

The simulation runs for twenty seconds with 0.001 s of the time step (Δt). There are 300 sets of data generated from the simulation

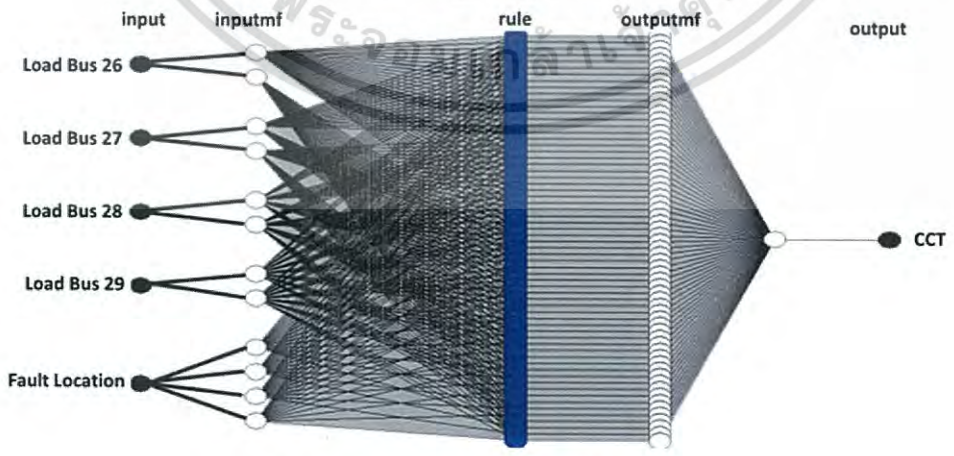

Fig. 6. ANFIS structure for 39-bus system implementation.

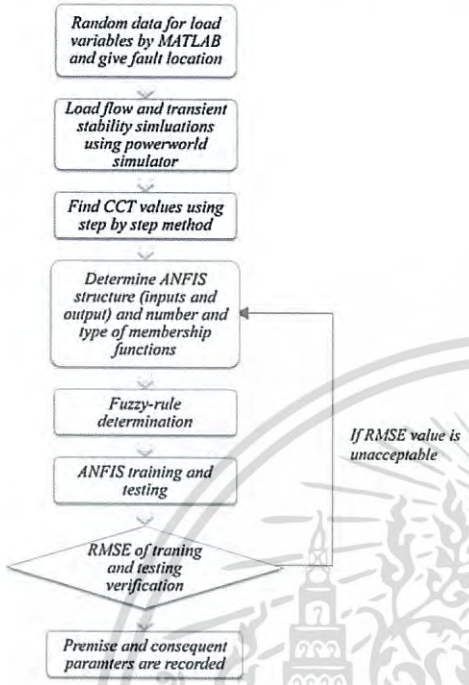

Fig. 7. Flow chart of implementation steps.

by power world software. The data set are divided into two sets, one is for training and another one is for testing. In this paper, 80% of the data from the data set are chosen for training and 20% of data from the data set are chosen for testing.

The ANFIS structure is designed by using the triangular-shaped membership function. The triangular-shaped membership function can be represented by the following equation:

$$f(x,a,b,c) = \begin{cases} 0, & x \leqslant a \\ \frac{x-a}{b-a}, & a \leqslant x \leqslant b \\ \frac{c-x}{c-b}, & b \leqslant x \leqslant c \\ 0, & c \leqslant x \end{cases} \quad (21)$$

where a, b, c are the premise parameters to be learnt.

The ANFIS architecture is shown in Fig. 9. The variables used for ANFIS inputs comprise the power user loads and fault position of transmission lines. While the training and testing output of ANFIS use the CCT values solved by using the step-by-step method mentioned above. There is one CCT output and there are four inputs comprising 3 power user load inputs and 1 fault position input. Moreover, there are 56 fuzzy rules set for ANFIS logical operation. The fault location and the fault position of transmission line are merged into one input, as described in the 39-bus system implementation subject.

All data used for the inputs and output have been normalized to zero mean and unity variance in the same manner as the 39-bus system implementation.

Results

The performance index of the proposed ANFIS is evaluated by root mean square error (RMSE) between the actual CCT obtained by power world simulation and estimated CCT obtained by the trained ANFIS method. The RMSE can be described in the following equation:

$$\text{RMSE} = \sqrt{\frac{\sum_{i=1}^{n}(O_i - F_i)^2}{n}}, \quad (22)$$

where O_i is actual CCT, F_i is estimated CCT obtained by ANFIS method, and n is number of training or testing data

39-bus system implementation results

As the ANFIS testing with 320 sets of training data and 80 sets of testing data, the appropriated ANFIS structure is found via trial and error means, as shown in Table 1. The 3-3-3-3-4 structure for the first layer with 324 fuzzy rules has the lowest RMSE for training

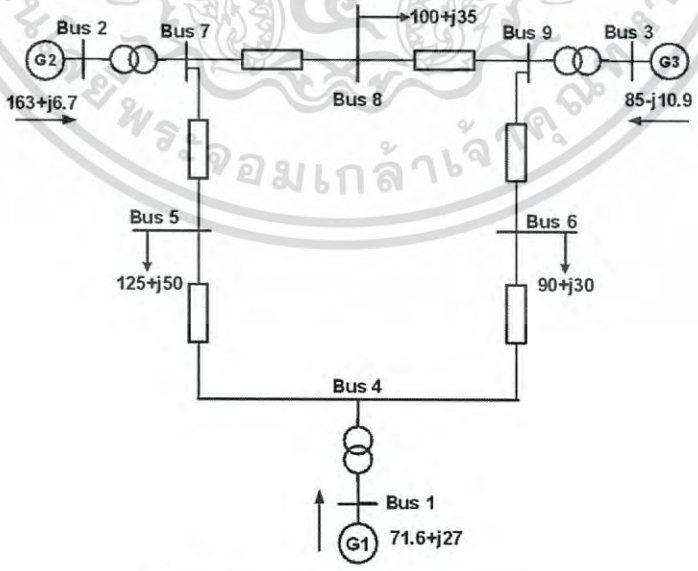

Fig. 8. 9-bus western system coordinating council.

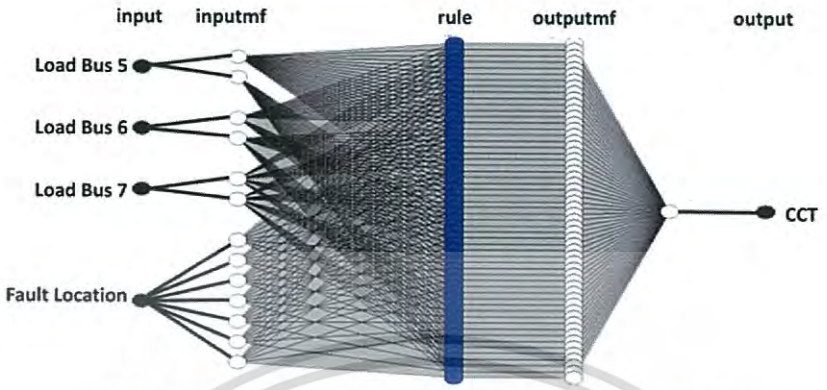

Fig. 9. ANFIS structure for 9-bus western system coordinating council implementation.

Table 1
Root mean square error in each structure for 39-bus system implementation.

Amount of node in Layer 1						(RMSE)	
Bus 26	Bus 27	Bus 28	Bus 29	Fault pos.	Rule	Error training	Error testing
2	2	2	2	2	32	0.0139	0.0165
2	2	2	2	3	48	0.0123	0.016
2	*2*	*2*	*2*	*4*	*64*	*0.009*	*0.0128*
3	3	3	3	2	162	0.01	0.3
3	3	3	3	3	243	0.00815	0.4473
3	3	3	3	4	324	0.0038	0.801

The italics indicate the most suitable structures which have the lowest RMSE for error testing.

but the highest RMSE for testing. While the 2-2-2-2-4 structure gives the lowest RMSE for testing and acceptable low RMSE for training. In this case, the 2-2-2-2-4 structure for the first layer is found as the most suitable structure with the RMSE of 0.009 for training and 0.0128 for testing. The parameters of each membership function obtained by the 2-2-2-2-4 ANFIS training are shown in Fig. 10.

The actual CCT obtained by power world simulation and estimated CCT obtained by the trained ANFIS method are plot, as shown in Fig. 11, for the training data set. In addition, the actual CCT obtained by power world simulation and estimated CCT obtained by the trained ANFIS method are plot as shown in Fig. 12 for the testing data set.

9-bus western system coordinating council implementation Result

From the ANFIS testing with 240 sets of training data and 60 sets of testing data, the appropriated ANFIS structure is found via trial and error, as shown in Table 2. The 2-2-2-7 structure for the first layer with 196 fuzzy rules has lowest RMSE for training, but the highest RMSE for testing. While the 2-2-2-7 structure gives the lowest RMSE for testing and acceptable low RMSE for training. In this case, the 2-2-2-7 structure for the first layer is found as the most suitable structure with the RMSE of 0.0195 for training and 0.018 for testing. The parameters of each membership function obtained by the 2-2-2-7 ANFIS training are shown in Fig. 13.

Result comparison

The results obtained by ANFIS above are compared with results obtained from ANN, which is an efficient method and frequently used for power system implementation. The structure of ANN used

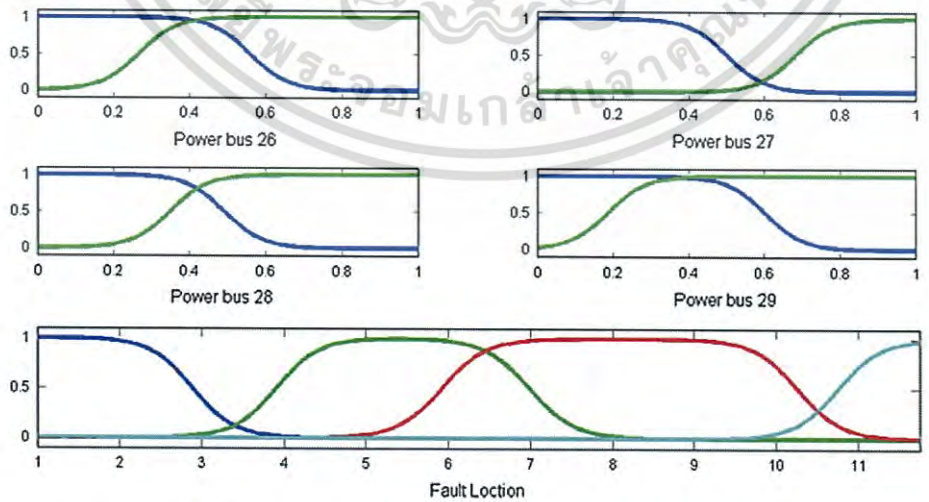

Fig. 10. Membership function obtained by 2-2-2-2-4 ANFIS training for 39-bus system.

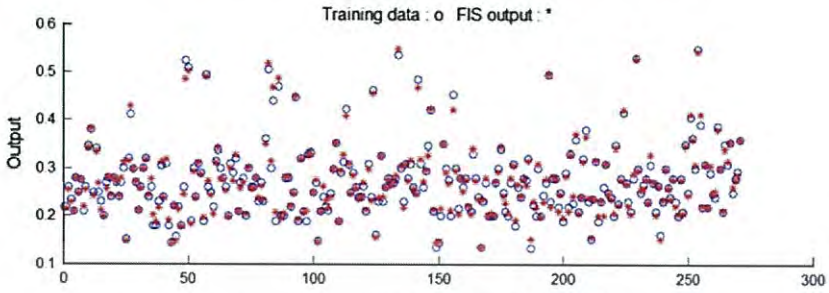

Fig. 11. Target output and estimated output obtained by ANFIS for training data.

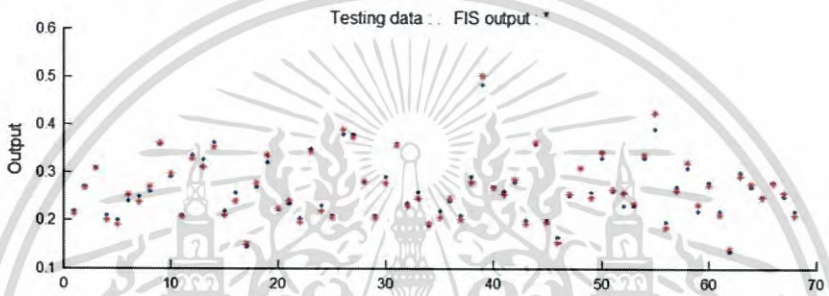

Fig. 12. Target output and estimated output obtained by ANFIS for testing data.

Table 2
Root mean square error (RMSE) in each structure for 9-bus western system coordinating council implementation.

Amount of node in Layer 1					(RMSE)	
Bus 5	Bus 6	Bus 8	Fault pos.	Rule	Error training	Error testing
2	2	2	2	16	0.0394	0.04
3	2	2	2	24	0.039	0.041
2	3	2	2	24	0.038	0.041
2	2	3	2	24	0.039	0.04
2	2	2	3	24	0.037	0.0395
3	3	3	3	81	0.0333	0.0531
7	2	2	2	56	0.036	0.048
2	2	2	5	40	0.031	0.036
2	*2*	*2*	*7*	*56*	*0.0195*	*0.018*
2	2	5	7	140	0.0151	0.18
2	2	7	7	196	0.0128	0.1677
2	2	2	2	16	0.0394	0.04

The italics indicate the most suitable structures which have the lowest RMSE for error testing.

in this paper is multilayer feed-forward type. It is trained using the back-propagation method using the Levenberg–Marquardt algorithm [6,8].

For the IEEE 39-bus system, the same 400 patterns of training and testing data generated for ANFIS testing are used for the ANN simulation. The optimized structure of ANN comprises three layers, including two hidden layers and one output layer. There are 15 neurons in the first hidden layer and 14 neurons in the second hidden layer. The optimized transfer functions for the first hidden layer, second hidden layer, and output layer are hyperbolic-tangent, log-sigmoid, and linear, respectively. The RMSE between testing data and estimated output obtained by ANN method are given in Table 3.

For the 9-bus western system, the same 300 patterns of training and testing data used for ANFIS testing are taken for ANN. The optimized structure of ANN comprises three layers, including two hidden layers and one output layer. There are 12 neurons in the first hidden layer and 11 neurons in the second hidden layer. The

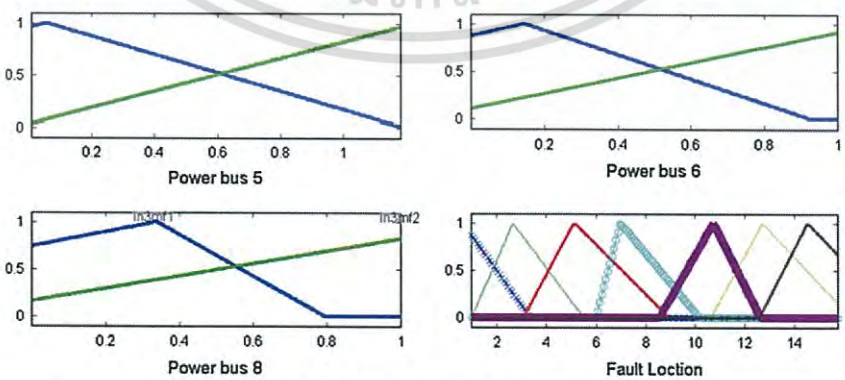

Fig. 13. Membership function obtained by 2-2-2-7 ANFIS training for 9-bus western system coordinating council.

Table 3
RMSE obtained by ANN and ANFIS testing for 39-bus system and 9-bus western system coordinating council.

System	ANN structure data			RMSE	
	1st Layer Neurons	2nd Layer Neurons	Transfer function	ANN	ANFIS
39-Bus	15	14	Tan-Log-Linear	0.0335	0.0128
9-Bus	12	11	Tan-Log-Tan	0.0778	0.018

transfer functions used for the first hidden layer, second hidden layer, and output layer are hyperbolic-tangent, log-sigmoid, and hyperbolic-tangent, respectively. The RMSE between testing data and estimated output obtained by ANN method is given in Table 3.

Conclusions

The transient stability assessment proposed in this paper is the estimation of CCT values through ANFIS approach. The sample IEEE 39-bus system and 9-bus western system coordinating council are used in this paper for the ANFIS implementation. The machines of IEEE 39-bus system and the 9-bus western system coordinating councils are modeled as the classical model and detailed model, respectively. The output training data and testing data are generated by time domain method of power world simulator program. The results obtained from ANFIS are compared with the results obtained from ANN, which is widely used; the ANFIS results look slightly better.

The results show that the ANFIS technique can estimate the CCT quickly with satisfied accuracy under varying load levels and fault locations in buses and transmission lines. It can be used to assess online transient stability approximation. For example for the online CCT approximation, all real-time values of load quantity are sent to ANFIS via SCADA system. And in case of system fault, the fault location detected by other protection relays will be sent to ANFIS for CCT calculation which the computation time is quite quick. So the estimated CCT can be used for real-time setting of the delay time of relays in order to avoid inefficient tripping.

In addition, we have developed the CCT estimation by the ANFIS method with a graphical user interface, as shown in Appendix D for the IEEE 39-bus system.

Acknowledgement

The authors would like to thank the research fund of the year 2013–2014 from King Mongkut's Institute of Technology Ladkrabang.

Appendix A

Gen	H	R_a	X'_d	X'_q	X_d	X_q	T'_{do}	T'_{qo}	X_l
1	500	0	0.006	0.008	0.02	0.019	7.0	0.7	0.003
2	30.3	0	0.0697	0.17	0.295	0.282	6.56	1.5	0.035
3	35.8	0	0.0531	0.0876	0.2495	0.237	5.7	1.5	0.0304
4	28.6	0	0.0436	0.166	0.262	0.258	5.69	1.5	0.0295
5	26	0	0.132	0.166	0.67	0.62	5.4	0.44	0.054
6	34.8	0	0.05	0.0814	0.254	0.241	7.3	0.4	0.0224
7	26.4	0	0.049	0.186	0.295	0.292	5.66	1.5	0.0322
8	24.3	0	0.057	0.0911	0.290	0.280	6.7	0.41	0.028
9	34.5	0	0.057	0.0587	0.2106	0.205	4.79	1.96	0.0298
10	42	0	0.031	0.008	0.1	0.069	10.2	0.0	0.0125

Line data					Transformer tap	
From	To	R	X	B	Magnitude	Angle
1	2	0.0035	0.0411	0.6987	0.000	0.00
1	39	0.0010	0.0250	0.7500	0.000	0.00
2	3	0.0013	0.0151	0.2572	0.000	0.00
2	25	0.0070	0.0086	0.1460	0.000	0.00
3	4	0.0013	0.0213	0.2214	0.000	0.00
3	18	0.0011	0.0133	0.2138	0.000	0.00
4	5	0.0008	0.0128	0.1342	0.000	0.00
4	14	0.0008	0.0129	0.1382	0.000	0.00
5	6	0.0002	0.0026	0.0434	0.000	0.00
5	8	0.0008	0.0112	0.1476	0.000	0.00
6	7	0.0006	0.0092	0.1130	0.000	0.00
6	11	0.0007	0.0082	0.1389	0.000	0.00
7	8	0.0004	0.0046	0.0780	0.000	0.00
8	9	0.0023	0.0363	0.3804	0.000	0.00
9	39	0.0010	0.0250	1.2000	0.000	0.00
10	11	0.0004	0.0043	0.0729	0.000	0.00
10	13	0.0004	0.0043	0.0729	0.000	0.00
13	14	0.0009	0.0101	0.1723	0.000	0.00
14	15	0.0018	0.0217	0.3660	0.000	0.00

Appendix A (*continued*)

Line data					Transformer tap	
From	To	*R*	*X*	*B*	Magnitude	Angle
15	16	0.0009	0.0094	0.1710	0.000	0.00
16	17	0.0007	0.0089	0.1342	0.000	0.00
16	19	0.0016	0.0195	0.3040	0.000	0.00
16	21	0.0008	0.0135	0.2548	0.000	0.00
16	24	0.0003	0.0059	0.0680	0.000	0.00
17	18	0.0007	0.0082	0.1319	0.000	0.00
17	27	0.0013	0.0173	0.3216	0.000	0.00
21	22	0.0008	0.0140	0.2565	0.000	0.00
22	23	0.0006	0.0096	0.1846	0.000	0.00
23	24	0.0022	0.0350	0.3610	0.000	0.00
25	26	0.0032	0.0323	0.5130	0.000	0.00
26	27	0.0014	0.0147	0.2396	0.000	0.00
26	28	0.0043	0.0474	0.7802	0.000	0.00
26	29	0.0057	0.0625	1.0290	0.000	0.00
28	29	0.0014	0.0151	0.2490	0.000	0.00
12	11	0.0016	0.0435	0.0000	1.006	0.00
12	13	0.0016	0.0435	0.0000	1.006	0.00
6	31	0.0000	0.0250	0.0000	1.070	0.00
10	32	0.0000	0.0200	0.0000	1.070	0.00
19	33	0.0007	0.0142	0.0000	1.070	0.00
20	34	0.0009	0.0180	0.0000	1.009	0.00
22	35	0.0000	0.0143	0.0000	1.025	0.00
23	36	0.0005	0.0272	0.0000	1.000	0.00
25	37	0.0006	0.0232	0.0000	1.025	0.00
2	30	0.0000	0.0181	0.0000	1.025	0.00
29	38	0.0008	0.0156	0.0000	1.025	0.00
19	20	0.0007	0.0138	0.0000	1.060	0.00

Bus	Type	Voltage [PU]	Load		Generator		
			MW	MVar	MW	MVar	Unit no
1	PQ	–	0.0	0.0	0.0	0.0	
2	PQ	–	0.0	0.0	0.0	0.0	
3	PQ	–	322.0	2.4	0.0	0.0	
4	PQ	–	500.0	184.0	0.0	0.0	
5	PQ	–	0.0	0.0	0.0	0.0	
6	PQ	–	0.0	0.0	0.0	0.0	
7	PQ	–	233.8	84.0	0.0	0.0	
8	PQ	–	522.0	176.0	0.0	0.0	
9	PQ	–	0.0	0.0	0.0	0.0	
10	PQ	–	0.0	0.0	0.0	0.0	
11	PQ	–	0.0	0.0	0.0	0.0	
12	PQ	–	7.5	88.0	0.0	0.0	
13	PQ	–	0.0	0.0	0.0	0.0	
14	PQ	–	0.0	0.0	0.0	0.0	
15	PQ	–	320.0	153.0	0.0	0.0	
16	PQ	–	329.0	32.3	0.0	0.0	
17	PQ	–	0.0	0.0	0.0	0.0	
18	PQ	–	158.0	30.0	0.0	0.0	
19	PQ	–	0.0	0.0	0.0	0.0	
20	PQ	–	628.0	103.0	0.0	0.0	
21	PQ	–	274.0	115.0	0.0	0.0	
22	PQ	–	0.0	0.0	0.0	0.0	
23	PQ	–	247.5	84.6	0.0	0.0	
24	PQ	–	308.6	−92.0	0.0	0.0	
25	PQ	–	224.0	47.2	0.0	0.0	
26	PQ	–	139.0	17.0	0.0	0.0	
27	PQ	–	281.0	75.5	0.0	0.0	

(*continued on next page*)

Appendix A (*continued*)

Bus	Type	Voltage [PU]	Load		Generator		
			MW	MVar	MW	MVar	Unit no
28	PQ	–	206.0	27.6	0.0	0.0	
29	PQ	–	283.5	26.9	0.0	0.0	
30	PV	1.0475	0.0	0.0	250.0	–	Gen10
31	PV	0.9820	9.2	4.6	–	–	Gen2
32	PV	0.9831	0.0	0.0	650.0	–	Gen3
33	PV	0.9972	0.0	0.0	632.0	–	Gen4
34	PV	1.0123	0.0	0.0	508.0	–	Gen5
35	PV	1.0493	0.0	0.0	650.0	–	Gen6
36	PV	1.0635	0.0	0.0	560.0	–	Gen7
37	PV	1.0278	0.0	0.0	540.0	–	Gen8
38	PV	1.0265	0.0	0.0	830.0	–	Gen9
39	PV	1.0300	1104.0	250.0	1000.0	–	Gen1

Appendix B

Bus 26 (MW)	Bus 27 (MW)	Bus 28 (MW)	Bus 29 (MW)	Fault location	CCT (s)
152.1349	306.1713	183.0703	249.1096	292,900	0.133
152.1349	306.1713	183.0703	249.1096	262,775	0.193
152.1349	306.1713	183.0703	249.1096	262,850	0.173
152.1932	268.1402	214.3084	262.6349	262,600	0.156
152.1932	268.1402	214.3084	262.6349	262,850	0.176
152.1932	268.1402	214.3084	262.6349	262,600	0.156
152.1932	268.1402	214.3084	262.6349	262,850	0.176
152.1932	268.1402	214.3084	262.6349	262,950	0.175
152.1932	268.1402	214.3084	262.6349	282,925	0.152
152.3406	320.2677	177.6634	229.4522	171,700	0.18
152.3406	320.2677	177.6634	229.4522	262,725	0.164
152.5308	263.4504	183.0716	257.1676	282,975	0.1395
152.5308	263.4504	183.0716	257.1676	282,950	0.1454
152.5308	263.4504	183.0716	257.1676	262,600	0.1533
152.5308	263.4504	183.0716	257.1676	172,725	0.1995

Appendix C

Gen	H	R_a	X'_d	X'_q	X_d	X_q	T'_{do}	T'_{qo}	X_l
1	4.72	0	0.304	0.484	0.730	4.484	8.96	0.31	0.15
2	2.56	0	0.299	0.492	2.23	2.16	6.00	0.53	0.15
3	3.01	0	0.181	0.25	1.31	1.25	5.89	0.60	0.12

From	To	R	X	B
4	6	0.017	0.092	0.158
4	5	0.010	0.085	0.176
5	7	0.032	0.161	0.306
6	9	0.039	0.17	0.358
7	8	0.0085	0.072	0.149
8	9	0.0119	0.1008	0.209
1	4	0	0.0576	0
2	7	0	0.0625	0
3	9	0	0.0586	0

Bus	Load		Generator		
	MW	MVar	MW	MVar	Unit no.
1	0	0	72	27	Gen1
2	0	0	163	0	Gen2
3	0	0	85	0	Gen3
4	0	0	0	0	–
5	125	50	0	0	–
6	90	30	0	0	–
7	0	0	0	0	–
8	100	35	0	0	–
9	0	0	0	0	–

Appendix D

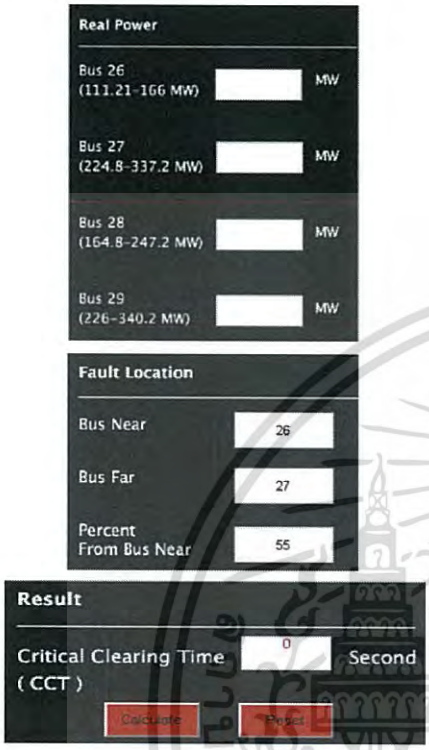

References

[1] Issarachai N. Dynamic and stability of power system. King Mongkut's Institute of Technology Ladkrabang; 2011.

[2] Pessanha JEO, Saavedra OR, Buzar JCR, Paz AA, Poma CP. Power system stability reinforcement based on network expansion: a practical case. J Electr Power Syst Res 2007:208–16.

[3] Padilha A, Denis EF. Transient stability indices from a hybrid approach. In: Proceeding of the IEEE Porto power tech conference, Porto, Portugal; 2001. p. 1–5.

[4] Ramos RA. Stability analysis of power systems considering AVR and PSS output limiters. J Electr Power Energy Syst 2009;31(4):153–9.

[5] Noor Izzri AW. A new method of transient stability assessment in power systems using LS-SVM. In: Research and development SCOReD 5th student conference; 2007. p. 1–6.

[6] Jiriwibhakorn S. Neural networks for constrained transient stability flows. In: IEEE Power engineering society winter meeting, vol. 2; 2002. p. 1119–23.

[7] Xiaodong C, Yutian L. On-line learning applied to power system transient stability prediction. In: IEEE international symposium, vol. 4; 2005. p. 3906–9.

[8] Jiriwibhakorn S. Critical generator and maximum power limit determination using neural networks. In: IEEE power engineering society summer meeting; 2002.

[9] Bettiol AL, Souza A, Todesco JL, Tesch JR. Estimation of critical clearing times using neural networks. In: Proceedings of the IEEE conference on power technology; 2003. p. 1–6.

[10] Sanyal KK. Transient stability assessment using artificial neural network. In: Proceedings of the IEEE international conference on electric utility deregulation restructuring and power technologies; 2004. p. 633–7.

[11] Haidar Ahmed MA, Mustafa MW, Ibrahim Faisal AF, Ahmed Ibrahim A. Transient stability evaluation of electrical power system using generalized regression neural networks. Appl Soft Comput 2011;11:3558–70.

[12] Al Marhoon H. A practical method for power systems transient stability and security analysis. In: Transmission and distribution conference and exposition (T&D); 2012. p. 1–6.

[13] Powerworld Simulator version 17. <http://www.powerworld.com>.

[14] MATLAB 2012a, The MathWorks. Inc., <http://www.mathworks.com>.

[15] Wahab NIA, Mohamed A. Transient stability assessment of a power system using probabilistic neural network. Am J Appl Sci 2008;5(9):1225–32.

[16] Liu CW, Su MC, Tsay SS, Wang YJ. Application of a novel fuzzy neural network to real-time transient stability swings prediction based on synchronized phasor measurements. IEEE Trans Power Syst 1999;14(2):685–92.

[17] Kundur P. Power system stability and control. McGraw-Hill; 1994.

[18] Sauer P, Pai M. Power system dynamics and stability. New Jersey: Prentice Hall; 1998.

[19] Karami A, Esmaili SZ. Transient stability assessment of power systems described with detailed models using neural networks. Electr Power Energy Syst 2013;45:279–92.

[20] Milano F. An open source power system analysis toolbox. IEEE Trans Power Syst 2005:1199–405.

[21] Nedjah N. Adaptation of fuzzy inference system using neural learning theory and practice. In: Studies in fuzziness and soft computing. Springer Verlag; 2005. p. 53–83.

[22] Jang, Sun, Mizutani. Neuro-fuzzy and soft computing. Prentice Hall; 1997. p. 335–68.

[23] Mohd Hasan Ali, Minwon Park, In-Keun Yu, Toshiaki Murata, Junji Tamura, Bin Wu. Enhancement of transient stability by fuzzy logic-controlled SMES considering communication delay. Electr Power Energy Syst 2009;31:402–8.

Transient Staiblity Analysis by Adaptive Neuro Fuzzy Inference System and Sobol Sequence

Witsawa Phootrakornchai
Electrical Engineering Department, Faculty of Engineering
King Mongkut's Institute of Technology Ladkrabang
Ladkrabang, Bangkok, Thailand
witsawa.p@hotmail.com

Somchat Jiriwibhakorn
Electrical Engineering Department, Faculty of Engineering
King Mongkut's Institute of Technology Ladkrabang
Ladkrabang, Bangkok, Thailand
somchat_j@yahoo.com

***Abstract*—It is known that the time domain is the most accurate method used for the assessment of transient stability and critical clearing time for any power systems. However, the time domain method normally takes a long time for the calculation due to many differential and non-linear equations, thus it may not be appropriate to apply with the real-time analysis, especially the large power system. We try to find any approaches to minimize the computation time and maximize the accuracy of results as much as possible. This paper therefore proposes an approach using adaptive neuro fuzzy inference system and sobol sequence for solving the critical clearing time. The approach proves that it can give us the satisfactory estimation of critical clearing time even for a large power system. The results are also compared to the results obtained by means of artificial neural network being generally used for the power system analysis.**

Keywords—critical clearing time; classical model; sobol sequence; adaptive neuro fuzzy inference system; artificial neural networks

I. Introduction

Nowadays the power systems are larger and more complicated. It is not easy to do the assessment of system stability in real-time. Other than the time domain approach used for transient stability assessment [1], there are a number of various techniques proposed for the assessment, for example, fuzzy logic [2], least square support vector machine (LS-SVM) [3], artificial neural networks (ANN) [4-6], feed forward multilayer perceptron (MLP) with back propagation learning algorithm [7,8], generalized regression neural network (GRNN) based classification [9], and direct approach based on transient energy function method [10].

In this paper, the adaptive neuro fuzzy inference system (ANFIS) [11-15] are proposed for the estimation of critical clearing time (CCT) [16,17]. As we know, the accuracy of result obtained from artificial intelligence (AI) computation depends on the quality and quantity of the training data. Thus, we propose the sobol sequence technique [18-20] to generate quasi-random inputs of ANFIS, it is able to provide a good distribution within a specified range.

The time domain simulation is used to generate the training and testing data for the CCT outputs. We use the IEEE 39-bus system for the study in this research. All machines in the system are considered as classical model [21,22].

This paper is organized as follows: the mathematical model is described in Section 2. The ANFIS principle is described in Section 3. The sobol sequence technique used for generating ANFIS inputs is described in Section 4. The power system simulation and ANFIS implementation are described in Section 5. The results from the ANFIS implementation using the sobol sequence approach are shown in Section 6. And the conclusion is summarized in Section 7.

II. Mathematical Modelling

Some assumptions are made to represent a synchronous machine mathematically by the classical model. The assumptions are:

- The exciter dynamics are not considered and the field current is assumed to be constant.
- The effect of damper windings, present on the rotor of the synchronous generators, is neglected.
- The input mechanical power to the generator is assumed to be constant during the period of study.
- The saliency of the generator is neglected, that is the generator is assumed to be of cylindrical type rotor.

The dynamic behavior of machines subject to the assumptions abovementioned can be explained using the following equations [22]:

$$\frac{d\omega}{dt} = \frac{d^2\delta}{dt^2} \tag{1}$$

$$M\frac{d^2\delta}{dt^2} = P_m - P_e \tag{2}$$

Where, δ_i is rotor angle of machine, ω_i is rotor speed of machine, M_i is moment of inertia of the machine, P_{mi} is machine mechanical power input, P_{ei} is electrical mechanical power input, and θ_i is machine angle.

978-1-4673-9749-0/16/$31.00 ©2016 IEEE

III. Adaptive Neuro Fuzzy Inference System

The ANFIS is used as a prime tool in this work. The ANFIS is a neuro fuzzy technique where the fusion is made between the neural network and the fuzzy inference system. The architecture of ANFIS can be presented as Fig. 1 [13].

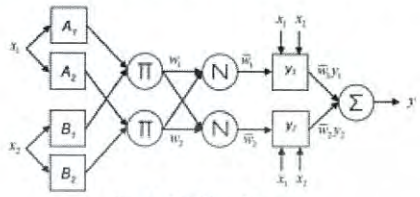

Fig. 1. ANFIS architecture.

In the Layer 1, every node i in this layer is adaptive with a node function [11-15].

$$O_{1,i} = \mu_{A_i}(x_1) \tag{3}$$

$$O_{1,i} = \mu_{B_i}(x_2) \tag{4}$$

where x and y are nodes of input. A_i and B_i are the labels relative to this node function. $O_{1,i}$ is the membership function of A_i and it specifies the level to which the given x makes the acceptable quantity A_i.

Layer 2, each node in this layer is fixed node. The output of each node called firing strength is the product of all the incoming signals to it as the following equation.

$$w_i = \mu_{A_i}(x)\mu_{B_i}(y). \tag{5}$$

Layer 3, every node in this layer is also fixed. The i node calculates the ratio of the i rule's output of layer 2 to the sum of all rules' outputs of layer 2. The output from the i node is the normalized firing strength given by the following equation:

$$O_{3,i} = \overline{w_i} = \frac{w_i}{\sum w_i}. \tag{6}$$

In Layer 4, every node in this layer is an adaptive node with a node function as the following equation:

$$O_{4,i} = \overline{w_i} f_i = \overline{w_i}(p_i x + q_i y + r_i). \tag{7}$$

The parameters in this layer p_i, q_i, r_i called consequent parameter are to be determined.

In Layer 5, this layer comprises of only one fixed node that calculates the overall output as the summation of all incoming signals:

$$O_{5,i} = \sum_i \overline{w_i} f_i = \frac{\sum_i w_i f_i}{\sum_i w_i} \tag{8}$$

In the forward pass of the learning algorithm, the parameters in the layer 4 are identified by the least squares estimate. In the backward pass, the error signals, which are the derivatives of the squared error with respect to each node output, propagate backward from the output layer to the input layer. In this backward pass, the parameters in the layer 2 are updated by the gradient descent algorithm [23-25].

IV. Sobol Sequence

Generally, a random sample can be generated by a pseudo-random number generator which is available in many software packages [26]. A sample is randomly distributed in a defined interval according to some distribution. For some sampling, the samples may contain gaps and clusters as shown in Fig. 2. on the line 'a'. Regions with gaps are not taken into account in the statistical analyses for any uncertainty or sensitivity analysis and function values in the regions with clusters are overemphasized in the calculations. The sample on the line 'b' was drawn using the same pseudo-random number generator but shows a better coverage of the interval.

Fig. 2. Sampling with a pseudorandom number generator

With a three-dimensional plot, it is a more difficult task to check if the parameter space is explored in a proper way. Fig. 3 shows the variables x, y, and z plotted against each other in two dimensional plots. The plots for random sampling show clusters and gaps.

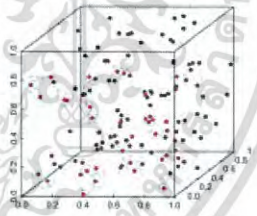

Fig. 3. Three-dimensional plot of the pseudo-randomly sampled points in the parameter space

The sobol sequences are designed to generate a sample that is uniformly distributed over the unit hypercube [18-20]. The sobol sequence belongs to the family of quasi-random sequences which are designed to generate samples of multiple parameters as uniformly as possible over the multi-dimensional parameter space. The biggest difference to pseudo-random numbers is that the sample values are chosen under consideration of the previously sampled points and thus avoiding the occurrence of clusters and gaps.

The sampling based on sobol sequences is designed to generate samples with low discrepancy. The points produced by a sampling based on sobol sequences are more evenly

distributed than the points produced with the other sampling techniques as shown in Fig. 4. The discrepancy in the exploration of the multi-dimensional parameter space is lower compared to the other sampling techniques. The mean and variance can be calculated in the same way as for the other sampling techniques.

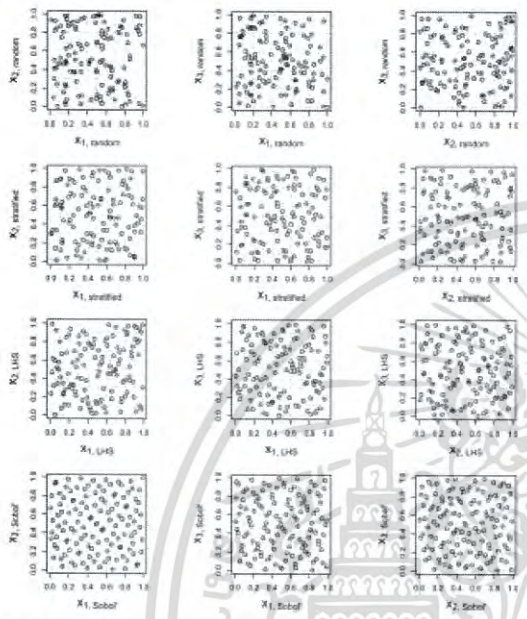

Fig. 4. Scatterplot of a two-dimensional stratified sampling. The position of the points within each cell is chosen randomly.

V. Implementation

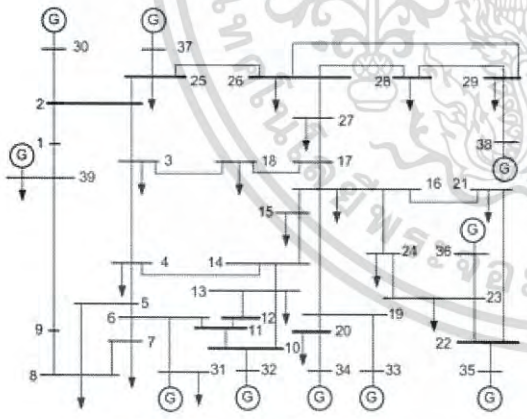

Fig. 5. Modified IEEE 39 Bus System.

The IEEE 39 bus system is used for the study [27]. We assume that there are three levels of voltage in the system. The voltage at all generators' terminal is 13.8 kV. Others are 115 kV and 345 kV in compliance with each connected transformer. However, we can see that the generator at slack bus in the standard IEEE 39 bus system is directly connected to the 345 kV bus without any transformer but in fact, it is not practical for such the big generator. We therefore add a 13.8/345 kV transformer having low reactance (0.000001 p.u.) between the 13.8 kV generator and 345 kV bus in accordance with the real practice. Now there are totally 40 buses for the system as Fig. 5. The voltage levels of 13.8 kV, 115 kV, and 345 kV are shown as black, green, and blue respectively.

Power World Simulation software [28] is used for simulation of dynamic system including CCT resolution. The simulation is subject to means of time domain. The exciter parameters are set as zero. The bus 1 is determined as the slack bus. All loads are assumed that the impedances are constant all the time.

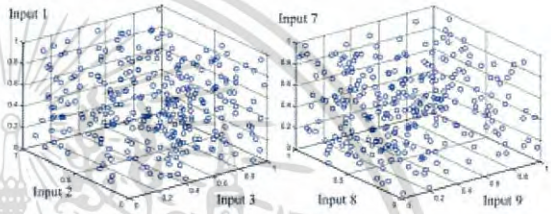

Fig. 6. Example of Distribution of Training Input Obtaining from Sobol Sequence

Values of active power (MW) and reactive power (MVar) of all buses are selected for the ANFIS input. The output we need to resolve is the CCT value (msec). We apply the sobol sequence for the input selection. The distribution of inputs we obtain is quite good as Fig. 6. The selected inputs are used for the dynamic simulation by time domain method to get the CCT values. The three-phase balance fault to ground is simulated at the middle of transmission line between bus 25 and bus 31.

The ANFIS is implemented using MATLAB [29]. All training and testing data are normalized before the ANFIS training. We have 110 sets of training data and 20 sets of testing data. Each set comprises 20 inputs (i.e. 10 active power and 10 reactive power) and 1 output (i.e. CCT). There are 10 membership functions and 10 logical fuzzy rules for the ANFIS operation. The training method is hybrid. The selected membership function for the IEEE 39-bus system is bell shaped, its equation can be written as follows:

$$\mu_{A_i}(x) = \exp\left\{-\left(\frac{x-c_i}{a_i}\right)^2\right\} \tag{9}$$

where a and c are the variables to be adjusted from learning.

VI. Result

We take 4.2 seconds for the ANFIS training subject to the 110 sets of training data. The ANFIS result errors are shown

as Fig. 6. We also implement the artificial neural network (ANN) [4-6] for comparison of result accuracy and computation time. Subject to the same condition, the ANN approach takes 9.3 seconds for the training and its MAPE is more than ANFIS's result.

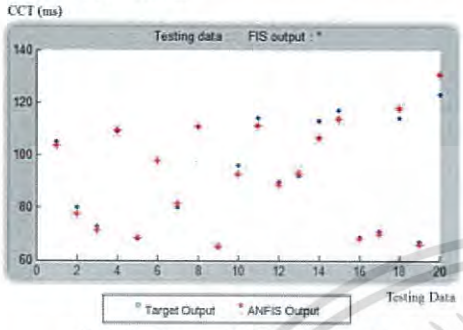

Fig. 6. Results from ANFIS Implementation

The mean absolute percentage error (MAPE) of ANFIS output is 2.591% but ANN's is 4.786%. The MAPE can be described as the following equation:

$$MAPE = \frac{1}{n}\sum_{i=1}^{n}\left|\frac{output_{target\,(i)} - output_i}{output_{target\,(i)}}\right| \times 100\% \quad (10)$$

In addition, we apply the various numbers of training data set for each implementation. As the Table 1, we can see that the MAPE is less if the number of training data is greater, based on the same amount of testing data.

TABLE I MEAN ABSOLUTE PERCENTAGE ERROR OF ANFIS AND ANNS

No.	Training Data (Set)	ANFIS Min (%)	ANFIS MAPE (%)	ANFIS Max (%)	ANNs Min (%)	ANNs MAPE (%)	ANNs Max (%)
1	30	1.769	4.254	7.652	2.582	7.892	9.935
2	60	0.913	3.088	5.911	1.367	6.045	9.214
3	110	0.101	2.591	5.864	0.409	4.786	6.163

*'Min' is the minimum absolute error in percentage and 'Max' is the maximum absolute error in percentage.

VII. CONCLUSION

This paper presents an approach to solve the CCT of the large power system by ANFIS approach using sobol sequence for the input quasi-random. For the IEEE 39-bus system we study, it shows that the ANFIS with sobol sequence can give us the better prediction of critical clearing time than the ANN approach, both of accuracy and computation time. It can be improved for more real use.

REFERENCES

[1] Sauer PW, Pai MA. Power system dynamics and stability. New Jersey, Prentice-Hall, 1998.

[2] R.A. Ramos, "Stability analysis of power systems considering AVR and PSS output limiters," Journal of Electrical Power and Energy Systems 31 (4), 2009, pp. 153–159.

[3] A. W. Noor Izzri, "A new method of transient stability assessment in power systems using LS-SVM," Research and Development SCOReD 5th Student Conference, 2007, pp. 1–6.

[4] S. Jiriwibhakorn, "Neural networks for constrained transient stability flows," IEEE Power Engineering Society Winter Meeting Vol. 2, 2002, pp. 1119-1123.

[5] C. Xiaodong, L. Yutian, "On-line learning applied to power system transient stability prediction," IEEE International Symposium Vol. 4, 2005, pp. 3906–3909.

[6] S. Jiriwibhakorn, "Critical generator and maximum power limit determination using neural networks," IEEE Power Engineering Society Summer Meeting; 2002.

[7] A.L. Bettiol, A. Souza, J.L. Todesco, J.R. Tesch, "Estimation of critical clearing times using neural networks," Proceedings of the IEEE Conference on Power Technology, 2003, pp. 1–6.

[8] K.K. Sanyal, "Transient stability assessment using artificial neural network," Proceedings of the IEEE International Conference on Electric Utility Deregulation Restructuring and Power Technologies, 2004, pp. 633–637.

[9] Ahmed M.A. Haidar, M.W. Mustafa, Faisal A.F. Ibrahim, Ibrahim A. Ahmed, "Transient stability evaluation of electrical power system using generalized regression neural networks," Applied Soft Computing 11, 2011, pp. 3558-3570.

[10] H. Al Marhoon, "A practical method for power systems transient stability and security analysis," Transmission and Distribution Conference and Exposition (T&D), 2012, pp. 1–6.

[11] C.W. Liu, M.C. Su, S.S. Tsay, Y.J. Wang, "Application of a novel fuzzy neural network to real-time transient stability swings prediction based on synchronized phasor measurements," IEEE Transaction on Power System 14 (2), 1999, pp. 685–692.

[12] N. Nedjah, "Adaptation of fuzzy inference system using neural learning theory and practice," Studies in Fuzziness and Soft Computing, Springer Verlag, 2005, pp. 53-83.

[13] Jang, Sun, Mizutani, "Neuro-fuzzy and soft computing. Prentice Hall," 1997, pp. 335-368.

[14] J.S.R. Jang, C.T. Sun, and E. Mizutani, "Neuro-Fuzzy and Soft Computing", A Computational Approach to Learning and Machine Intelligence, Prentice Hall Inc., 1997.

[15] J.S.R. Jang, "ANFIS: Adaptive-network-based fuzzy inference systems," IEEE Trans. on Syst., Man and Cybern., vol. 23, no. 3, pp. 665–684, May/June 1993.

[16] N. Issarachai, "Dynamic and stability of power system," King Mongkut's Institute of Technology Ladkrabang, 2011.

[17] J.E.O. Pessanha, O.R. Saavedra, J.C.R. Buzar, A.A. Paz, C.P. "Poma. Power system stability reinforcement based on network expansion," a practical case, Journal of Electric Power Systems Research, 2007, pp. 208–216.

[18] Sobol, I.M., "Dstribution of points in a cube and approximate evaluation of integrals," U.S.S.R Comput. Maths. Math. Phys. 7, 1967, pp. 86–112.

[19] Niederreiter, H., "Low-Discrepancy and Low-Dispersion Sequences," Journal of Number Theory 30, 1988, pp. 51–70.

[20] Antonov, I.A. and Saleev, V.M., "An economic method of computing LPτ-sequences," U.S.S.R. Comput. Maths. Math. Phys. 19, 1979, pp. 252–256.

[21] E.W. Kimbark, "Power System Stability," Volume I, Elements of Stability Calculations, John Wiley (New York), 1948.

[22] S.B. Crary, "Power System Stability Volume I: Steady State stability," John Wiley, New York, 1945.

[23] S. Haykin, "Neural Networks - A Comprehensive Foundation," 4th ed. Pearson Education (Singapore) Pvt. Ltd., Indian Branch, 2003.

[24] J. M. Zurada, "Introduction to Artificial Neural Systems," Jaico Publishing House 121, Mumbai, 1999.

[25] M. T. Hagan, H. B. Demuth, and M. H. Beale, "Neural Network Design," 2nd ed. PWS Publishing, Boston, MA, USA, 1996.

[26] Sebastian Burhenne, Dirk Jacob, and Gregor P. Henze, "Sampling Based On Sobol Sequences for Monte Carlo Techniques Applied to Building Simulations," Proceedings of Building Simulation, 2011, pp. 1816-1823.

[27] A. Karami, S.Z. Esmaili, "Transient stability assessment of power systems described with detailed models using neural networks," Electrical Power and Energy Systems, 45, 2013, pp. 279-292.

[28] Powerworld Simulator version 17, http://www.powerworld.com.

[29] MATLAB 2012a. The MathWorks, Inc., http://www.mathworks.com.

Real-time Critical Clearing Time Estimation By Considering Contingency Conditions

Witsawa Phootrakornchai
Electrical Engineering Department, Faculty of Engineering
King Mongkut's Institute of Technology Ladkrabang
Ladkrabang, Bangkok, Thailand
witsawa.p@hotmail.com

Somchat Jiriwibhakorn
Electrical Engineering Department, Faculty of Engineering
King Mongkut's Institute of Technology Ladkrabang
Ladkrabang, Bangkok, Thailand
somchat_j@yahoo.com

***Abstract*—This paper presents an approach called adaptive neuro-fuzzy inference system for the transient stability assessment by considering contingency conditions of networks. The contingency condition herein means a case of transmission outage and network configuration change. In addition, in this study all significant dynamic parameters of a power system (e.g. machine models, excitation systems, turbine governors, and load characteristic etc.) are considered for the estimation. We use the critical clearing time for the transient stability index. The 9-bus IEEE is applied for the power dynamic simulation. Finally, this study shows that the adaptive neuro-fuzzy inference system can be applied with the real-time critical clearing time estimation subject to contingency conditions and some parameters affecting the system's dynamic behavior are taken into account.**

Keywords—critical clearing time; machine model; automatic voltage regulator model; governor model; load characteristic; adaptive neuro fuzzy inference system

I. INTRODUCTION

Generally, the power system network for transient stability analysis can be presented by a nodal admittance matrix or a nodal impedance matrix [1-3]. But in fact the power systems involves more thousand nodes, any method for the transient stability analysis therefore takes significant influence on computation time. Moreover, if all dynamic parameters are considered in the model, the computation will take time very much as a number of non-linear equations [4-8]. The real-time assessment can help us to make a decision quickly during the power system is being operated (e.g. decrease in generation, switching load, etc.). It can be also used as an input for automatic equipment operation (e.g. load shading equipment, protective relay, etc.) This is a reason that techniques for enhancement of computational efficiency for transient stability assessment have been extensively employed [9-17]. In this paper, we proposes an approach called adaptive neuro-fuzzy inference system for the transient stability assessment [18-22]. The contingency conditions, transmission line outage and new network configuration, during the assessment are considered. The dynamic parameters of machine model, excitation system, turbine governor, and load characteristic are taken into account. The 9-bus IEEE is applied for the dynamic simulation.

In this study, we focus that whether the adaptive neuro-fuzzy inference system can apply with the real-time estimation of critical clearing time [23-24] subject to the consideration of many dynamic parameters and various contingency conditions or not.

This paper is organized as follows: Section 2 describes the models used for the simulation. Section 3 describes the ANFIS principle. Section 4 explains the ANFIS implementation. Section 5 shows the result obtained from the implementation. And Section 6 summarize the conclusion of the study.

II. MODELLING

We use the two-axis model for all machines in the 9-bus IEEE systems. The equations can be written as follows:

$$\frac{d\delta_i}{dt} = \omega_i - \omega_s \tag{1}$$

$$\frac{d\omega_i}{dt} = \frac{1}{M_i}[P_{mi} - (E'_{qi} - X'_{di}I_{di})I_{qi} - (E'_{di} + X'_{qi}I_{qi})I_{di} - D_i(\frac{d\delta_i}{dt})] \tag{2}$$

$$\frac{dE'_{qi}}{dt} = \frac{1}{T'_{doi}}[E_{fdi} - E'_{qi} - (X_{di} + X'_{di})I_{di}] \tag{3}$$

$$\frac{dE'_{di}}{dt} = \frac{1}{T'_{qoi}}[-E_{fdi} + (X_{qi} + X'_{qi})I_{qi}] \tag{4}$$

$$E'_{qi} = V_i\cos(\delta_i - \theta_i) + R_{si}I_{qi} + X'_{di}I_{di} \tag{5}$$

$$E'_{di} = V_i\cos(\delta_i - \theta_i) + R_{si}I_{di} - X'_{qi}I_{qi}, \tag{6}$$

where, δ_i is rotor angle of machine, ω_i is rotor speed of machine, ω_s is rotor synchronous speed of machine, M_i is moment of inertia of the machine, P_{mi} is machine mechanical power input, P_{ei} is machine electrical power input, V_i is machine terminal voltage, θ_i is machine angle, R_{si} is machine armature resistance, E'_{qi} is q-axis transient voltage, E'_{di} is d-axis transient voltage, I'_{qi} is q-axis transient current, I'_{di} is d-axis transient current, X_{qi} is q-axis synchronous reactance, X_{di} is d-axis synchronous reactance, X'_{qi} is q-axis transient reactance, X'_{di} is d-axis transient reactance, T'_{qoi} is q-axis open-circuit time constant, and T'_{doi} is d-axis open-circuit time constant.

For the excitation system, we apply the 421.5 2005 AC8B model that is generally used in the real system. The control

978-1-4673-9749-0/16/$31.00 ©2016 IEEE

model is shown in Fig. 1 [25].

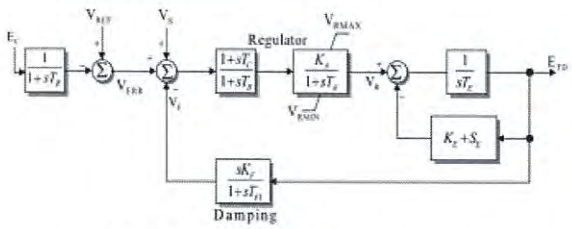

Fig. 1. IEEE 421.5 2005 AC8B excitation system model.

For the governors, we apply the TGOV3 model as it is generally used in thermal power plants. The control model is shown in Fig. 2 [25].

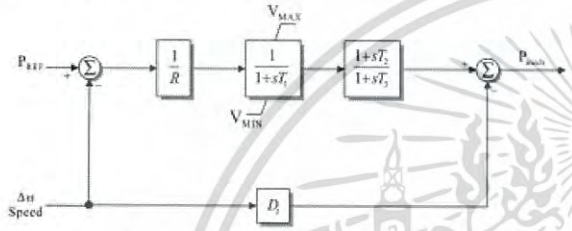

Fig. 2. TGOV3 steam turbine governor with fast valving model.

For the loads, we use the complex load model (CLOD) comprising a load consisting of lighting, transformers, induction motors, and other types of load, that represents a mixture of static and dynamic models for the load characteristics as Fig. 3 [25].

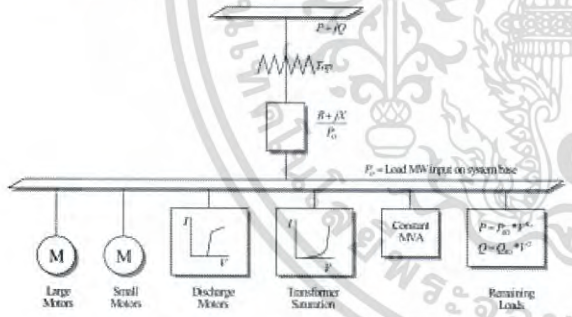

Fig. 3. CLOD complex load model.

We can see that the equations used for the detail models and the control systems are quite complicated. If there are many nodes in a system, it is not easy to calculate it real-time.

III. Adaptive Neuro Fuzzy Inference System

The ANFIS is a neuro fuzzy technique which its methodology comprises a hybrid system of fuzzy logic and neural network technique. The ANFIS architecture is shown as Fig. 4 [18].

The fuzzy logic is capable of considering the imprecision and uncertainty of the system being modeled while the neural network gives it a sense of adaptability only. The square boxes are the nodes that have parameters to be learnt for some adjustment. The circles represent the fixed nodes that no parameter needs to be learnt and adjusted. An initial fuzzy model along with its input variables are derived with the rules extracted from the input and output data of the system. The neural network is used to fine tune the rules of the initial fuzzy model to produce the final ANFIS model of the system.

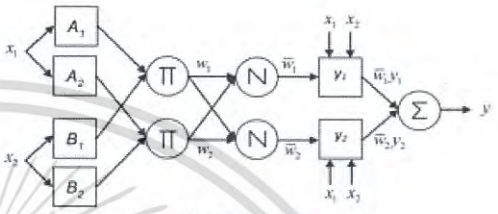

Fig. 4. ANFIS architecture.

In the Layer 1, all nodes in this layer is adaptive node like a node function. It can be written as the equations below.

$$O_{1,i} = \mu_{A_i}(x) \tag{7}$$

$$O_{1,i} = \mu_{B_{i-2}}(y) \tag{8}$$

where x and y are nodes of input, A_i and B_{i-2} are the labels relative to this node function. $O_{1,i}(x)$ is the membership function of A_i.

Layer 2, the output of each node is the product of all the incoming signals to it as the following equation.

$$w_i = \mu_{A_i}(x)\mu_{B_i}(y). \tag{9}$$

Layer 3, the output is the ratio of the i rule's output of layer 2 to the sum of all rules' outputs of layer 2, it can be written as the following equation:

$$O_{3,i} = \overline{w}_i = \frac{w_i}{w_1 + w_2}. \tag{10}$$

In Layer 4, nodes in this layer is an adaptive node with a node function as the following equation:

$$O_{4,i} = \overline{w}_i f_i = \overline{w}_i (p_i x + q_i y + r_i). \tag{11}$$

The parameters p_i, q_i, r_i are called consequent parameter. They are to be determined.

In Layer 5, this layer has only one node to calculate the overall output as the summation of all signals coming from the output of Layer 4:

$$O_{5,i} = \sum_i \overline{w_i} f_i = \frac{\sum_i w_i f_i}{\sum_i w_i} \quad (12)$$

IV. Implementation

The 9-bus IEEE system as Fig. 5 is used for the study [25]. The two-axis model is used for the machines at bus 1, 2, and 3. The models 'IEEE 421.5 2005 AC8B' is applied to the generation unit at bus 1, 2, and 3. The models 'TGOV3' is applied to the generation unit at bus 1, 2, and 3. The CLOD complex load model is applied with the load characteristic at bus 5, 6, and 8.

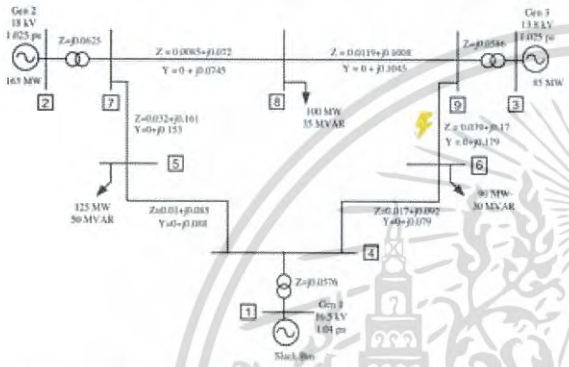

Fig. 5. 9-bus IEEE system

The CCT values used for the training and testing output of ANFIS are obtained from the time domain simulation. We use the Power World software [26] for the power dynamic simulation. In the simulation, we apply a three-phase balanced fault at the transmission line between bus 6 and bus 9. The position of the fault applied is fixed at 50% of the transmission length. Then we can clear the fault by opening two nearby circuit breakers.

Each set of ANFIS inputs comprises all active generator outputs, all reactive generator outputs, all active loads, all reactive loads, and type of network configuration. The input of network configuration is represented by the integer number. We suppose there are 3 possible contingency conditions as follows:

- The transmission line between bus 7 and bus 8 is out of service, the ANFIS integer input for this case is 1
- The transmission line between bus 4 and bus 6 is out of service, the ANFIS integer input for this case is 2
- There is installation of double circuit between bus 8 and bus 9 further, the ANFIS integer input for this case is 3

We generate 800 numbers of CCT value from various input patterns by time domain means. We use 700 sets of the data for training and 100 sets for testing. MATLAB [27] is used for ANFIS training and testing. The training use the hybrid method [18].

V. Result

The actual CCT obtained by the time domain method and the estimated CCT by the ANFIS for the training data and testing data are plotted in Fig. 6 and Fig. 7 respectively. From the plots, we can see that the results from ANFIS are not deviate from the actual results.

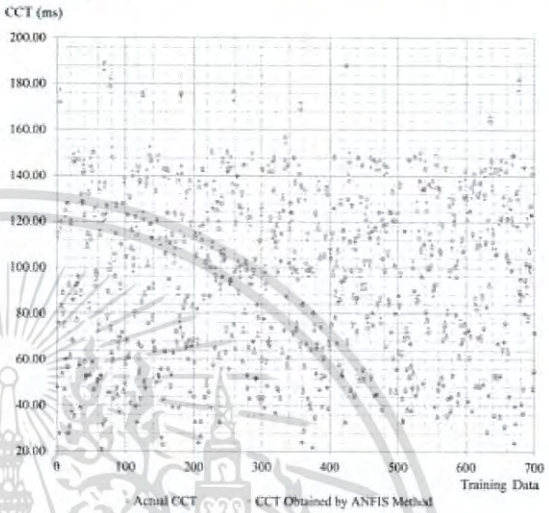

Fig. 6. ANFIS outputs and target outputs for training data.

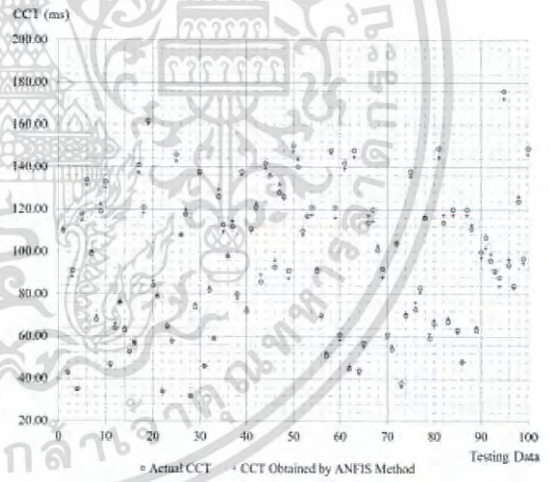

Fig. 7. ANFIS outputs and target outputs for testing data.

The ANFIS performance index is assessed by mean absolute percentage error (MAPE) between the actual CCT acquired by the time domain method and the estimated CCT acquired by the ANFIS. The MAPE can be described as the following follow [28]:

$$MAPE = \frac{1}{n}\sum_{i=1}^{n}\left|\frac{output_{target(i)} - output_i}{output_{target(i)}}\right| \times 100\% \quad (13)$$

The MAPE of ANFIS training output is 2.411%. And the MAPE of ANFIS testing output is 2.784%. The accuracy is quite good.

VI. Conclusion

We propose an approach using an ANFIS to solve CCT by considering the contingency conditions, i.e. transmission outage and network configuration change. All significant effects of dynamics are taken into account as the detail model. The 9-bus IEEE systems are used for implementation in this study. It proves that the CCT results obtained by ANFIS can be used for the real-time estimation.

References

[1] A. W. Noor Izzri, "A new method of transient stability assessment in power systems using LS-SVM," Research and Development SCOReD," 5th Student Conference, 2007, pp. 1–6.

[2] Noor Izzri Abdul, Wahab, Azah Mohamed, Aini Hussain, "Transient Stability Assessment of a Power System Using PNN and LS-SVM Methods," Journal of Applied Sciences, 2007, pp. 3208-3216.

[3] Sauer PW, Pai MA, Power system dynamics and stability, New Jersey, Prentice-Hall, 1998.

[4] P. Kundur, Power system stability and control, McGraw-Hill, 1994.

[5] N. Issarachai, Dynamic and stability of power system, King Mongkut's Institute of Technology Ladkrabang, 2011.

[6] P. Sauer and M. Pai, Power system dynamics and stability, New Jersey, Prentice Hall, 1998.

[7] A. Karami, S.Z. Esmaili, "Transient stability assessment of power systems described with detailed models using neural networks", Electrical Power and Energy Systems, Vol. 45, 2013, pp. 279–292.

[8] N. Hashim, N.R. Hamzah, P. Mohd Arsad, R. Baharom, N.F. Nik Ismail, N. Aminudin, D. Johari, "Modeling of power system dynamic devices incorporated in dynamic computation for power systems (DCPS) for transient stability analysis," IEEE International Electric Machines & Drives Conference (IEMDC), 2011, pp. 647-652.

[9] R.A. Ramos, "Stability analysis of power systems considering AVR and PSS output limiters," Journal of Electrical Power and Energy Systems 31 (4), 2009, pp. 153–159.

[10] A. W. Noor Izzri, "A new method of transient stability assessment in power systems using LS-SVM," Research and Development SCOReD 5th Student Conference, 2007, pp. 1–6.

[11] S. Jiriwibhakorn, "Neural networks for constrained transient stability flows," IEEE Power Engineering Society Winter Meeting Vol. 2, 2002, pp. 1119-1123.

[12] C. Xiaodong, L. Yutian, "On-line learning applied to power system transient stability prediction," IEEE International Symposium Vol. 4, 2005, pp. 3906–3909.

[13] S. Jiriwibhakorn, "Critical generator and maximum power limit determination using neural networks," IEEE Power Engineering Society Summer Meeting; 2002.

[14] A.L. Bettiol, A. Souza, J.L. Todesco, J.R. Tesch, "Estimation of critical clearing times using neural networks," Proceedings of the IEEE Conference on Power Technology, 2003, pp. 1–6.

[15] K.K. Sanyal, "Transient stability assessment using artificial neural network," Proceedings of the IEEE International Conference on Electric Utility Deregulation Restructuring and Power Technologies, 2004, pp. 633–637.

[16] Ahmed M.A. Haidar, M.W. Mustafa, Faisal A.F. Ibrahim, Ibrahim A. Ahmed, "Transient stability evaluation of electrical power system using generalized regression neural networks," Applied Soft Computing 11, 2011, pp. 3558-3570.

[17] H. Al Marhoon, "A practical method for power systems transient stability and security analysis," Transmission and Distribution Conference and Exposition (T&D), 2012, pp. 1–6.

[18] Jang, Sun, Mizutani, "Neuro-fuzzy and soft computing. Prentice Hall," 1997, pp. 335-368.

[19] J.S.R. Jang, "ANFIS: Adaptive-network-based fuzzy inference systems," IEEE Trans. on Syst., Man and Cybern., vol. 23, no. 3, pp. 665–684, May/June 1993.

[20] N. Nedjah, "Adaptation of fuzzy inference system using neural learning theory and practice," Studies in Fuzziness and Soft Computing, Springer Verlag, 2005, pp. 53-83.

[21] J.S.R. Jang, C.T. Sun, and E. Mizutani, "Neuro-Fuzzy and Soft Computing", A Computational Approach to Learning and Machine Intelligence, Prentice Hall Inc., 1997.

[22] C.W. Liu, M.C. Su, S.S. Tsay, Y.J. Wang, "Application of a novel fuzzy neural network to real-time transient stability swings prediction based on synchronized phasor measurements," IEEE Transaction on Power System 14 (2), 1999, pp. 685–692.

[23] N. Issarachai, "Dynamic and stability of power system," King Mongkut's Institute of Technology Ladkrabang, 2011.

[24] J.E.O. Pessanha, O.R. Saavedra, J.C.R. Buzar, A.A. Paz, C.P, "Poma. Power system stability reinforcement based on network expansion," a practical case, Journal of Electric Power Systems Research, 2007, pp. 208–216.

[25] D. Prasad Wadduwage, Christine Qiong Wu, U.D. Annakkage, "Power system transient stability analysis via the concept of Lyapunov Exponents," Electric Power Systems Research, Vol. 104, 2013, pp. 183-192.

[26] Powerworld Simulator version 17, http://www.powerworld.com.

[27] MATLAB 2012a. The MathWorks. Inc., http://www.mathworks.com.

[28] Tofallis, "A Better Measure of Relative Prediction Accuracy for Model Selection and Model Estimation," Journal of the Operational Research Society, 66(8), 2015, pp.1352-1362.

BIOGRAPHY

Name Mr. Witsawa Phootrakornchai

Birthday 30 December 1982, Bangkok, Thailand

Education

- 2000, Seconday Scool, Bodindecha (Sing Singhaseni) School
- 2004, Bachelor's Degree in Electrical Engineering, Mahidol University
- 2008, Master's Degree in Electrical Power Engineering, King Mongkut's Institute of Technology Ladkrabang (KMITL)
- 2010, Master's Degree in Business Administration (MBA), Finance, National Institute of Development Administration (NIDA)
- 2012, Pursuing Doctor's Degree in Electrical Power Engineering, King Mongkut's Institute of Technology Ladkrabang (KMITL)

Experience

- 2004-2005, Site Engineer, Mechanical and Electrical Department, E2 Engineering Co., Ltd.
- 2005-2006, Electrical Project Engineer, Electrical Department, Syntec Kurihara (Thailand) Co., Ltd.
- 2006-2009, Budget and Contract Management Engineer, Project Development Department, ATT Consultants Co., Ltd.
- 2009-2018, Assistant Vice President, Project and Business Development Department, B.Grimm Power Limited.